MSc Thesis, 30 ECTS
ISRN LUTVDG / (TVTG-5154) / 1 - 50 /(2017)

Application of ERT and IP for localisation of chlorinated hydrocarbons at a former dry-cleaning facility

A study investigating the geology, man-made structures and contamination of PCE at Hagforstvätten

Hedda Jönsson and Anna Wiberg
Engineering Geology
Faculty of Engineering
Lund University

MIRACHL

Thesis work for Master of Science 30 ECTS
Environmental Engineering

Application of ERT and IP for localisation of chlorinated hydrocarbons at a former dry-cleaning facility
- A study investigating geology, man-made structures and contamination of PCE at Hagforstvätten

Tillämpning av ERT och IP för lokalisering av klorerade kolväten vid en nedlagd kemtvätt
- Undersökning av geologi, antropogena strukturer och förorening av PCE vid Hagforstvätten

Hedda Jönsson and Anna Wiberg
Engineering Geology / Teknisk Geologi
Faculty of Engineering / Lunds Tekniska Högskola
Lund University / Lunds Universitet

Lund 2017

Supervisors / Handledare:
Torleif Dahlin, Engineering Geology
Matteo Rossi, Engineering Geology

Examiner / Examinator
Gerhard Barmen, Engineering Geology

Authors:
Hedda Jönsson
Anna Wiberg

Title:
Application of ERT and IP for localisation of chlorinated hydrocarbons at a former dry-cleaning facility
- A study investigating geology, man-made structures and contamination of PCE at Hagforstvätten

Titel:
Tillämpning av ERT och IP för lokalisering av klorerade kolväten vid en nedlagd kemtvätt
- Undersökning av geologi, antropogena strukturer och förorening av PCE vid Hagforstvätten

Front page photo:
Jönsson and Wiberg, Hagfors, April 2017

50 pages + 8 appendices (33 pages)
41 figures
3 tables

Abstract

At Hagforstvätten a dry-cleaning facility operated 1970 – 1993 and leached huge amounts of tetrachloroethene (PCE) to soil and groundwater. The severely contaminated site is situated in the center of Hagfors, Sweden, and covers an area of approximately 400×400 m^2. The former laundry facility lies upon an esker where the subsurface has a large heterogeneity of unconsolidated sediments that consists of glaciofluvial deposits mixed with embedded postglacial silt and clay bodies.

Today, there are two known sources of contaminants at Hagforstvätten: the main source underneath the dry-cleaning facility and a secondary source located south of the facility. This study focuses on applying the geophysical methods Electrical Resistivity Tomography (ERT) and Induced Polarization (IP) to investigate if it is possible to locate the secondary source, degradation zones and groundwater plumes of PCE. ERT and IP measure the resistivity and chargeability of the subsurface by injecting current into the ground using electrodes. In this study, drillings and chemical samplings were used as a complement to ERT and IP measurements to validate and strengthen the interpretation of resistivity and IP as caused by geology, PCE or man-mad disturbances.

To investigate the geology and potential disturbances for the upcoming ERT and IP measurements a background survey was conducted including ground penetrating radar (GPR), magnetic gradiometer and the electromagnetic equipment DUALEM which measures the conductivity. The background survey together with ERT and IP concluded that the site is very inhomogeneous with local variations in geology and man-made conductive objects. The shallow subsurface is considered to have been altered when a former railway was constructed at the site in the early 20th century.

Compared to previously performed traditional methods with drilling and chemical sampling, the ERT and IP measurements could in more detail describe the extension of previously detected local clay and silt-rich bodies. It is of high importance to know the extent and location of these bodies since they can sustain high groundwater concentrations of PCE due to back-diffusion. ERT also reviled an undiscovered depression or fracture in the bedrock east of the secondary source that could act as a sink releasing PCE during a long-time perspective.

The ERT and IP succeeded to locate the secondary source as a natural occurring degradation zone. However, the expected groundwater plume with PCE from the secondary source was not detected. Either the concentrations were too low to affect the ERT and IP measurements, or the inhomogeneous geology made it difficult to identify an anomaly as caused by the PCE plume. Downstream the main source an ERT and IP anomaly was detected and interpreted as either a PCE plume containing degradation products or as a clay and silt-rich body. The interpretation of resistivity and chargeability as caused by pollutants or geology was complicated due to the large heterogeneity at the site.

It is our opinion that it is a challenge to locate pollutants by using ERT and IP at inhomogeneous or less well-known subsurfaces. Even though the interpretation is difficult at inhomogeneous sites, ERT and IP are good complements to drilling and chemical sampling since they increase the understanding of the area and how the pollutants can be spread or stored in the subsurface. Since the methods provide continuous data sampling they can detect areas of interest that otherwise might have been missed with pointwise measurements. We believe that Hagforstvätten has potential for applying ERT and IP measurements in the future, especially for monitoring how the high concentrations of PCE at the secondary source changes with time during a future remediation.

Sammanfattning

Hagforstvätten är en nedlagd kemtvätt som under sin verksamhetstid 1970 – 1993 orsakade stora utsläpp av det klorerade kolvätet tetrakloroeten (PCE) till jord och grundvatten. Det idag kraftigt förorenade området är beläget i de centrala delarna av Hagfors i Värmland och täcker en yta på cirka $400 \times 400\ m^2$. Den före detta kemtvätten ligger ovanpå en rullstensås och den geologiska bildningen är av mycket varierande natur bestående av grus, sand och inbäddade silt- och lerkroppar.

På området bedöms det idag finnas två källområden med mycket höga PCE-halter: en huvudkälla belägen under kemtvätten och en sekundär källa strax söder om tvätten orsakad av en läckande dagvattenledning. Detta mastersarbete fokuserar på att utreda om det är möjligt att lokalisera den sekundära källan, eventuella nedbrytningszoner samt grundvattenplymer av PCE från källområdena med hjälp av att tillämpa de geofysiska mätmetoderna Elektrisk Resistivitets Tomografi (ERT) och Inducerad Polarisation (IP). ERT och IP mäter resistiviteten och uppladdningsförmågan hos marken genom att inducera ström via elektroder förankrade i jorden. I denna studie har data från tidigare utförda borrkärnor och kemiska analyser använts för att urskilja resultat från ERT och IP som orsakade av geologi, PCE eller mänskliga störningskällor.

För att undersöka geologin och potentiella störningskällor för ERT och IP-mätningarna utfördes kompletterande undersökningar med markradar (GPR), magnetisk gradiometer och DUALEM som mäter markens konduktivitet. Dessa mätningar visade i enighet med resultatet från ERT- och IP-mätningarna att geologin på det förorenade området är mycket heterogen med många lokala variationer. Den mänsklig påverkan på jordlagret bedömdes även vara stor vilket förmodligen uppstått av att det under tidiga 1900-talet fanns en järnväg på området.

I jämförelse med borrning och kemisk provtagning som tidigare utförts på området kunde ERT och IP-mätningarna visa en mer detaljerad utbredning av tidigare påvisade silt- och lerkroppar. Det är viktigt med bra kännedom om ler- och siltkroppars utbredning då PCE som lagras i de finkorniga sedimenten kan åter-diffundera till grundvattnet och bidra till höga PCE-halter. Vidare avslöjade ERT-resultaten en oupptäckt djuphåla eller spricka i berggrunden öster om den sekundära källan. Det är möjligt att detta är samma sänka som har påvisats vid den sekundära källan (SWECO, 2013). Denna djuphåla kan fungera som en sänka som frigör PCE och därmed bibehålls höga koncentrationer av PCE i grundvattnet under längre tid.

ERT- och IP-mätningen lokaliserade den sekundära källan som en naturlig nedbrytningszon av PCE. Däremot kunde inte ERT och IP-mätningarna påvisa den förväntade grundvattenplymen med PCE från den sekundära källan. Antingen var koncentrationerna av föroreningarna för låga för att påverka ERT och IP, eller så är geologin i området för inhomogen för att kunna avgöra om en avvikelse i resistivitet och IP är orsakat naturligt eller av PCE plymen. Nedströms huvudkällan detekterades en anomali i ERT och IP som tolkades som en plym av PCE och nedbrytningsprodukter eller en ler- och siltkropp. Arbetet med att tolka resistivitets och IP-svaren som orsakade av geologi eller förorening försvårades av att området är väldigt heterogent.

Vi anser att det är en utmaning att lokalisera föroreningar med ERT och IP för områden där geologin är väldigt inhomogen eller mindre känd. Fastän tolkningen av ERT och IP data är svår är dessa mätningar bra komplement till punktvisa borrningar och kemiska provtagningar eftersom de ökar förståelsen området och på så sätt även hur föroreningar kan utbreda sig. ERT och IP kan även upptäcka information som har missats i punktvisa provtagningar. Vår uppfattning är att ERT och IP har potential för att användas vid Hagforstvätten, särskilt för att en framtida in-situ sanering av de höga koncentrationerna av PCE vid den sekundära källan.

Acknowledgements

During the work with our master's thesis we have encountered many inspiring personalities with great passion for their topic and a strong driving force for improving things to the better. First of all, we would like to show our appreciation to our supervisors Torleif Dahlin and Matteo Rossi for good supervision and for involving us in the MIRACHL project. We would also like to thank Simon Rejkjær and Aris Nivorlis at the department of Engineering Geology for good cooperation during our field work in Hagfors. We would also like to express our gratitude to Sweco, Englöv et al., Johansson et al. and Olsson et al. for giving us permission to publish their illustrations and to NIRAS, Sofia Åkesson and Robin Jansson for sharing their unpublished data.

Table of content

1. Introduction

1.1 Working towards a non-toxic environment – a national environmental goal

Chlorinated hydrocarbons have been used worldwide because of their properties as solvents. During the 20th century chlorinated hydrocarbons were often used within the dry-cleaning industry without sufficient knowledge regarding their toxicity for humans and the environment. Today, old sins from the past are buried in the ground and it is the responsibility for present generations to treat these heavily polluted sites. Dealing with extremely polluted soil and groundwater in Hagfors, this master thesis is a small contribution to this enormous and highly important work.

One of the 16 national environmental goals in Sweden is to have a non-toxic environment until 2020. Meanwhile 1000 sites in the country are classified as severely contaminated and 7500 sites are regarded to be potentially severely contaminated but have not yet been examined (Naturvårdsverket, 2017). A large effort awaits to reach the goal with a non-toxic environment, and development of new techniques able to detect the spreading of pollutants would facilitate the work.

1.2 Motivation for usage of geophysical methods at contaminated sites

Two geophysical methods that are regarded as promising techniques for detecting chlorinated hydrocarbons and other non-aqueous phase liquids are resistivity and induced polarization (IP) (Johansson, et al., 2015). The main reason for this is that chlorinated hydrocarbons act as electrical insulators, hence they will change the electrical properties of the subsurface if they displace the pore water. On the other hand, if degradation proceeds chlorinated hydrocarbons will release chloride ions which increase the conductivity in the pore water and likely increase the IP-response.

Today it is common to use drilling and chemical sampling for defining and locating the pollutants. One drawback with these traditional methods is that drilling might cause an unwanted spreading and exposure of the pollutants (Johansson et al., 2015). Additionally, drilling results in point information and the number of samples is often restricted by the large expenses that comes with drilling. In contrast, geophysical methods obtain dense measurements which results in continuous images of the subsurface. With geophysical methods, operators can cover large areas within a shorter amount of time. The geophysical investigation can be used as a pre-study to point out interesting or ambiguous areas where drilling and sampling can verify the results. This combination is a more cost and time efficient use of drilling. Measurements of resistivity and induced polarization (IP) only requires electrodes to be pushed down into the top layers of the soil (upper decimetres), hence reducing the risk with vertical spreading of pollutants.

One reason for developing the applicability of geophysical methods at contaminated sites is to eventually use these techniques for continuous monitoring of degradation and migration of pollutants. In this way, it would be possible to follow how an in-situ remediation develops with time. Resistivity and IP measurements are suitable methods for mapping geological structures. They are also considered as promising techniques for mapping degradation status for pollutants (Sparrenbom, et al., 2016). Today the main challenge with applying IP and resistivity to detect chlorinated hydrocarbons is however to interpret the results. How to correlate IP and resistivity data with the presence of chlorinated hydrocarbons is a discussed topic with divergent results (Johansson et al., 2015).

1.3 Characterisation and Monitoring of In-situ RemediAtion of CHLorinated hydrocarbon contamination (MIRACHL)

The master's thesis is a part of a larger national project named MIRACHL. MIRACHL develops techniques for continuously monitoring of in-situ remediation of chlorinated hydrocarbons at three contaminated sites in Sweden, where one of them is Hagfors. The project works towards SEPAs[1] recommendations of using in-situ remediation instead of the common "dig and treat approach" where the contaminated material is excavated and treated separately at a controlled site. By developing techniques for monitoring in-situ remediation MIRACHL is a contribution for reaching the Swedish environmental objective of a non-toxic environment until 2020.

1.4 Introduction to Hagforstvätten

This master's thesis focuses on a site situated at Hagfors in Sweden where a dry-cleaning facility operated between 1970 and 1993. As a solvent, the industry used tetrachloroethene (PCE) which today is known for being carcinogenic and toxic for humans even at very low doses if the exposure proceeds over a longer time. The spill of PCE to soil and groundwater at Hagfors was huge, and today at least 20 – 30 tons of PCE is estimated to rest in the ground at the laundry facility (SWECO, 2013). The groundwater flowing underneath the contaminated site discharges in two nearby streams that receive high loads of PCE each year (SWECO, 2013). There are two known PCE sources at the site: one main source situated underneath the former dry-cleaning facility and one secondary source south of the dry-cleaning caused by spill from a stormwater pipe that carried water contaminated with PCE from the facility (SWECO, 2013).

The work with locating and delimiting the PCE spreading in the subsurface is complicated due to the heterogenous geology of the site. The facility is situated on an esker consisting of glaciofluvial deposits (mainly sand and gravel) with embedded bodies of silt and clay (see more details in chapter 2). Therefore, traditional methods such as drilling and chemical sampling might contribute with too sparse information in order to detect small local variations. Geophysial survey can contribute with denser and more continuous data sampling.

1.5 Objectives and approach

The main objective is to use the geophysical methods electrical resistivity tomography (ERT) and induced polarization (IP) to identify geological features and man-made structures and also to determine the spatial distribution of PCE (source, degradation zones and groundwater plume) at Hagforstvätten.

To interpret the resistivity and IP-response as caused by pollutants and not by the geology, it is highly important to have a good understanding of the geology. Therefore, the measurements will be compared with geological borehole data. Effort will be spent to interpret the IP and resistivity response to locate PCE, which today is a divergent topic (Johansson, et al., 2015). The results from resistivity and IP-measurements will be validated with previous surveys from Sweco and NIRAS that have used traditional methods for detecting PCE and determining the hydrogeology. Since the site is very heterogeneous it is of interest to test if electrical methods can detect local changes in geology or PCE that otherwise might have been missed by more sparse drilling and chemical sampling. Conclusions from previous studies within the topic will be used to interpret the data for locating the PCE and potential degradation zones (e.g. Johansson et.al, 2015).

Furthermore, complementary methods with ground penetrating radar (GPR), DUALEM and magnetic gradiometer will also be used to characterize the hydrogeological situation and

[1] SEPA = Naturvårdsverket (Swedish Environmental Protection Agency)

detect potential man-made disturbances for the ERT and IP-measurements.

1.6 Problem formulation

1. Is it possible to locate the secondary contaminant source, degradation zones and groundwater plumes of PCE at Hagforstvätten by applying ERT and IP measurements?
2. Do ERT and IP measurements contribute to a better understanding of the pollutant situation and geology at Hagforstvätten compared to previously performed traditional methods with drilling and chemical sampling?
3. Based on the outcome from the survey, are resistivity and IP measurements considered as alternative methods for future investigations at Hagforstvätten? For example, would it be possible to install permanent electrodes for continuous monitoring of PCE degradation and migration at the site?

1.7 Limitations

This master thesis focuses on describing the geology and locating PCE-contaminants at Hagforstvätten. The project should give answers to the questions mentioned under section 1.6 *Problem formulation.* The scope of the project is restricted by the following:

1. Since the time dedicated to field investigation is limited, a 3D or 4D model (with time as one dimension) from resistivity and IP measurements will not be created. Depending on the outcome of the study, this could be an interesting task for the future.

2. Which remediation techniques that are suitable for the site will not be discussed or investigated.

3. Based on the outcome from a previous study by SWECO (Sweco, 2013) this thesis will focus on the secondary source at well B19 at Hagforstvätten caused by a leaking stormwater pipe connected to the dry-cleaning facility. According to Sweco the secondary source is a heavily contaminated area and yet not remediated. The vertical depth of the survey will be approximately 25 meters from ground surface.

2. Background to Hagforstvätten

This chapter starts with a short description of the studied site and which investigations that previously have been conducted in the area. This is followed by information concerning infrastructure and conclusions from previous surveys of the geology, hydrogeology and pollutant situation.

2.1 Site description

The former dry-cleaning facility called Hagforstvätten was located in the small municipality of Hagfors in Värmland, Sweden (figure 2.1A). It was operated between 1970 and 1993 and is situated in the centre of the village, surrounded by forest, industry and residential areas. There is a small creek called Örbäcken that flows through the contaminated area (figure 2.1B).

While operated Hagforstvätten leaked huge amounts of PCE to the soil and groundwater. During this time, the dry-cleaning facility was operated by three different owners: the state-owned FFV (Förenade Fabriksverken), a private company and Värmland county (SWECO, 2013). There are two known PCE sources at the site: the main source where the dry-cleaning facility that used PCE was situated and the secondary source close to well B19 (figure 2.1B). The secondary source was caused by a leaking storm water pipe connected to the dry-cleaning facility. The storm water pipe was located about 100 meters south of the main building.

The contaminated site has been partially remediated during the years but it is estimated that 20-30 tons of estimated PCE in the ground. After the dry-cleaning was closed the contaminated soil underneath the main building was partially removed to protect the workers in the building. In total 7 tons of PCE was removed (SWECO, 2013).

2.2 Previous investigations

Today, the Geological Survey of Sweden (SGU) has the main responsibility of the polluted site. On request from SGU, the Swedish consulting-firm Sweco has summarized old survey's and performed several new surveys of the geology, hydrogeology and the pollutant situation of the investigated area from 1993-2013 (SWECO, 2013).

Additional unpublished data sampled at the site by the consulting-firm NIRAS and S. Åkesson at Lund University have also been studied during this thesis. NIRAS has contributed with geological borehole data with

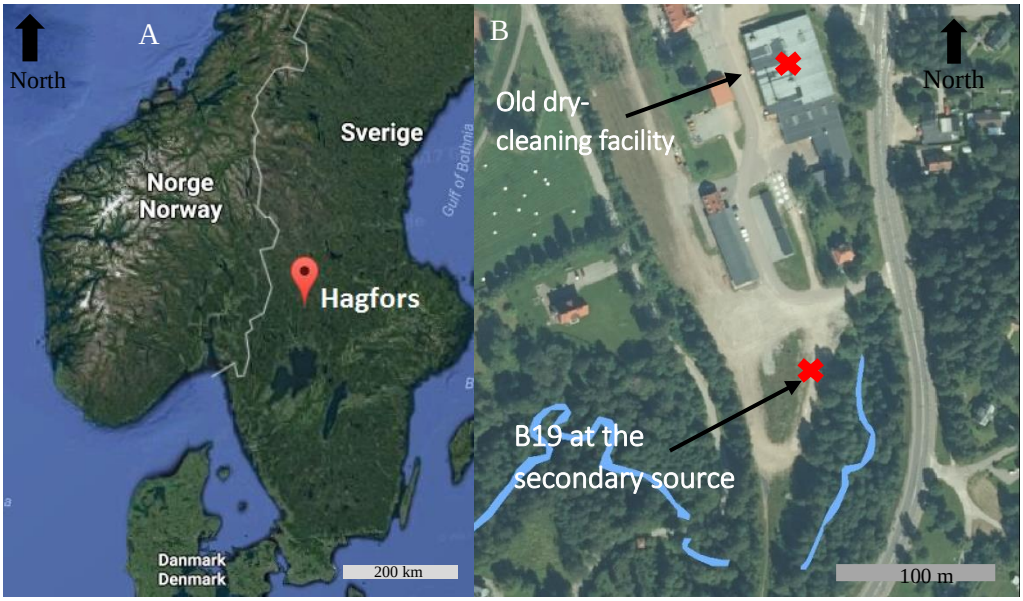

Figure 2.1. A) A Swedish map and the location of Hagfors municipality (Googlemaps, 2017). B) A zoom-in of the contaminated area Hagforstvätten. Modified verision of (Lantmäteriet, 2015)

soil types (sampled 2013-2016) and depth to bedrock (sampled 1994-2015) together with chemical sampling of PCE and its degradation products (sampled 2007-2016). Chemical groundwater sampling performed by S. Åkesson in 2017 has also been considered (see Appendix B).

2.3 Geology

According to Lundegård, et.al., (1992) the bedrock underneath the investigated area mostly consists of granite. Additionally, in the surroundings of the site there are smaller zones of gabbro and diorite.

As seen in figure 2.2 (next page) the study area at Hagforstvätten is located right at the edge of an esker where areas of glaciofluvial deposits, glacial clay and postglacial sand and clay interfere (SGU, 2017). Due to this, the site is expected to have a large heterogeneity in the subsurface. The esker stretches in northeast - southwest direction and northeast of the study area the esker is outcropped, while at the southwest side the esker is overlain by clay sediments and an area with peat.

A general conceptual model of the subsurface has been achieved by studying maps of the surrounding unconsolidated materials (SGU, 2017) together with cores from sonic drillings performed at Hagforstvätten by NIRAS (Nilsson, 2017, unpublished data) and previous conclusions from Sweco (Sweco, 2013). The esker in the proximity of Hagforstvätten is situated in a valley where lake Värmullen and river Hagälven are located (figure 2.3). At the slopes of the valley the bedrock is overlain by till and at higher altitudes the bedrock is outcropped. In the surrounding of Värmullen and Hagälven a calmer environment has made it possible for finer sediments such as postglacial silt and sand to settle above an expected layer of till. Occasionally calmer conditions at the river bank might have created the local areas rich in clay and silt that have been detected by previous investigations at Hagforstvätten (Nilsson, 2017, unpublished data). It is also possible that clay and silt bodies found deeper down in the till are created by kettle pots from the glacier (Sweco, 2013). From the general conceptual model, the subsurface below Hagforstvätten is expected to consist of till or sandy gravel in deeper parts, while sand becomes more abundant closer to the ground surface.

A few hundred meters north of the studied site a large steel industry has been located since 1876 (Stads- och kommunhistoriska institutet, 2008). When the industry was constructed it was built on filling material and probably covered parts of lake Värmullen. The steel industry also required a railway, and this was constructed at the site where the remains of Hagforstvätten is situated today. How much of the site that have been altered by human activities during the 19th and 20th century is not known today. However, the top layer of the soil at the plateau consists of backfilling material, probably dense packed sand and gravel (Månsson, 2016). This was most likely added as a filling material when the railway was constructed on the site in the late 19th century (figure 2.2).

Figure 2.2. White and black lines mark the former railway tracks crossing the studied site (Lantmäteriet, 2017)

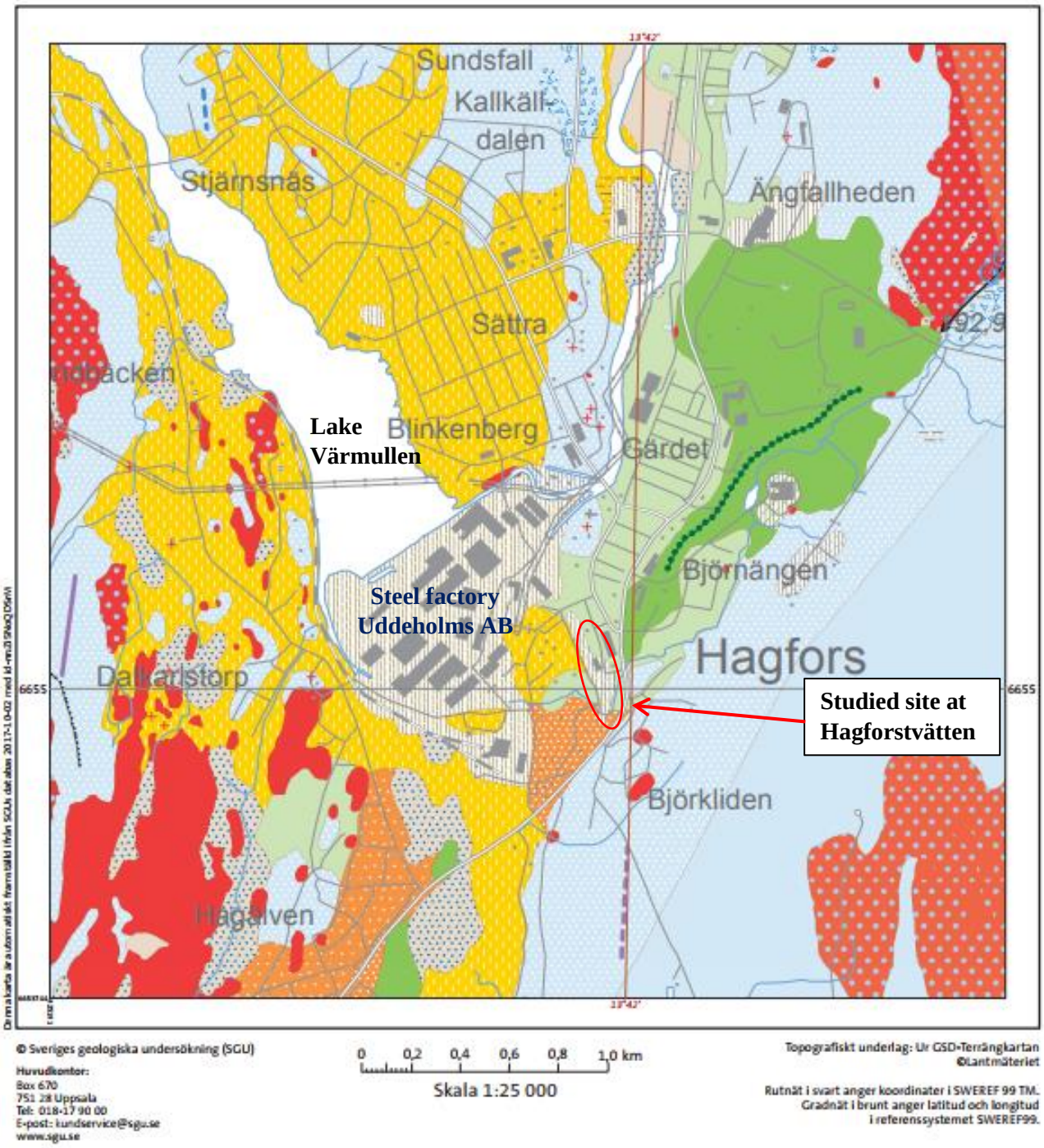

Figure 2.3. Map of unconsolidated materials in the proximity of Hagfors and the studied site (SGU, 2017).

2.3.1 Geology at the main source

At the main PCE source underneath the dry-cleaning facility there is a mix of two geological environments: 1) sand and gravel with high to moderate heterogeneity and high permeability and 2) clay and silt with low heterogeneity and low hydraulic conductivity. Underneath the main building there is a large fine-grained body above and below the groundwater table with a maximum depth of about 20 meters.

2.3.2 Geology at the secondary source

At the secondary source at well B19 the unconsolidated materials consist of mostly sand in the top and gravel down to the bedrock (SWECO, 2013). Silt and clay bodies are considered to be less abundant and situated more above the ground water table compared to the situation at the main source. A conceptual model taken along the esker (NE to SW) at the secondary source is seen in figure 2.4. The exact location of the cross-section is marked in appendix A. Indications of a depression and fractures in the bedrock has been seen close to B19 (SWECO, 2013). As seen in figure 2.4 the well B19 is situated on a plateau with steep slopes at sides. The plateau is approximately 10 meters above Örbäcken in the east and west creek.

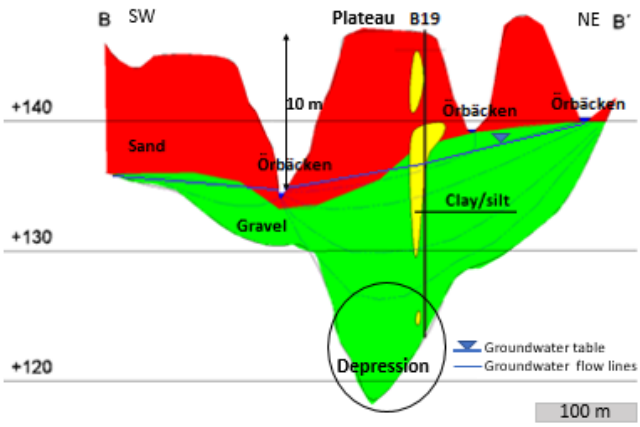

Figure 2.4. Conceptual hydrogeological profile of the esker at the secondary source. The secondary source (well B19) is situated on a plateau about 10 meters above the surroundings. The geological material is glaciofluvial deposits with embedded silt and clay bodies. The groundwater flow direction is southwest towards stream Örbäcken. The horizontal distance from B19 downstream to Örbäcken is about 100 meters. (SWECO, 2013)

2.4 Hydrogeology

According to groundwater table measurements acquired in April 2017 the levels on the plateau close to B19 are about 10 - 16 meters below ground level and 0.6 - 6 meters in the creek on the west side of the plateau (Jansson, 2017, unpublished data). The direction of the groundwater flow and pollutant plumes is illustrated in figure 2.5 which derives from Sweco (2013). The groundwater flows in southwest direction towards Örbäcken (see figure 2.5). The groundwater plume from the main source discharge in Örbäcken close to well Kb4, while the main outflow of groundwater from the secondary source is close to well Kb1 (see figure 2.5) Örbäcken is situated about 300 meters downstream of the laundry facility and 100 meters downstream the secondary source. Part of the groundwater passes stream Örbäcken and flows towards Hagälven situated about 850 meters downstream from the dry-cleaning facility.

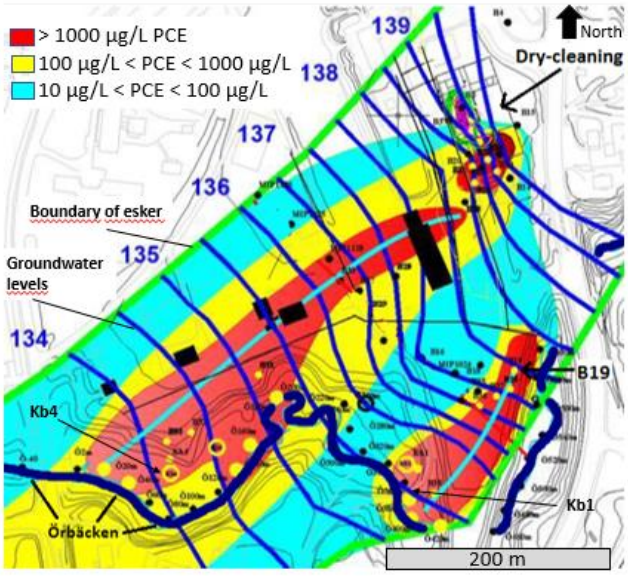

Figure 2.5. Horizontal mapping of PCE plumes in the groundwater from the dry-cleaning facility (top) and the secondary source at B19 (bottom). The groundwater flow direction from the main source and the secondary source, indicated by light blue lines, is south-west towards stream Örbäcken (SWECO, 2013).

2.5 Pollutant situation

The soil and groundwater contamination is severe at the site. An illustration of the PCE spreading in groundwater based on chemical sampling by Sweco (2013) at Hagforstvätten is shown in figure 2.5. Underneath the dry-cleaning facility an estimate of 20 - 30 ton PCE is buried that forms a large groundwater plume towards stream Örbäcken. The PCE source from the secondary source is today around 10 tons or more. This forms a large PCE plume towards stream Örbäcken.

High loads of PCE have leaked to stream Örbäcken from the years when the laundry was open until today. Sweco (2013) have estimated the current leakage of PCE to Örbäcken to 120-130 kg/year. It has also been estimated that 5 tons of PCE have leached to Örbäcken since the start of the dry-cleaner.

2.5.1 Pollutant situation at the main source

The main source is located below the laundry building, where the washing machines using PCE as solvent have leaked water contaminated with PCE to the soil. A large part of the free phase PCE (characterised by high concentrations) from the main source has diffused into the silt and clay body that exists both above and below ground water table. The fine-grained material might acts as low permeable layers that adsorb PCE through diffusion mechanisms. If the flux of PCE from the source is decreasing, the diffusion is instead reversed and PCE will migrate from silt bodies with high concentrations to the surroundings. This phenomenon, known as back diffusion, could give high and constant concentrations of PCE for a long time after free phase PCE has been transported away (SWECO, 2013). This hypothesis is strengthened by studies made by Parker et.al 2008 that observed that even relatively thin clay bodies can extend the survival of a plume with chlorinated hydrocarbon for several years or decades after the isolation of the main source (Parker, et al., 2008) From both the PCE source and the plume the pollutant is partly removed as gas.

Previous performed chemical sampling show degradation compounds and very high levels of PCE in the soil (5600 mg/kg dry soil) underneath the main source (Nilsson, 2017, unpublished data). The results from chemical soil sampling of PCE and TCE by (Nilsson, 2017, unpublished data) are seen in figure 2.7 and figure 2.8. As seen in the figures, there exist sparse chemical samplings in the expected groundwater flow from the main source to stream Örbäcken. The few drilling samples show no or low levels of PCE and degradation products such as trichloroethene (TCE) in the direction of the expected groundwater plume. Measured groundwater concentrations of PCE and TCE sampled by Sweco (2013) and Åkesson (2017, unpublished data) are seen in appendix B.

2.5.2 Pollutant situation at the secondary source

The exact location and extent of PCE at the secondary source is uncertain. The main focus of this thesis is dedicated to this area since it is heavily contaminated and yet not remediated. Additionally, the secondary source is not buried underneath buildings which facilitate the procedure of fieldwork.

The secondary source is caused by leakages and discharge from an old storm water pipe that was connected to the laundry building. The pipe discharged PCE upstream well B19 and PCE have probably sunk below the groundwater table and might have been trapped in the suspected bedrock depression close to B19 as mentioned above (figure 2.6).

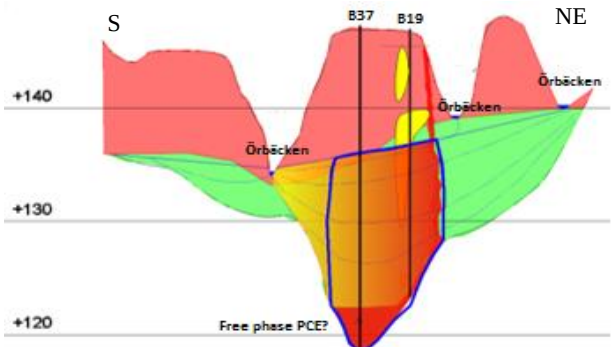

Figure 2.6. Schematic side view of the pollutant spreading from the secondary source. The estimated contaminated area is marked by the blue line. The distance from B19 downstream to Örbäcken is about 100 meters. (SWECO, 2013)

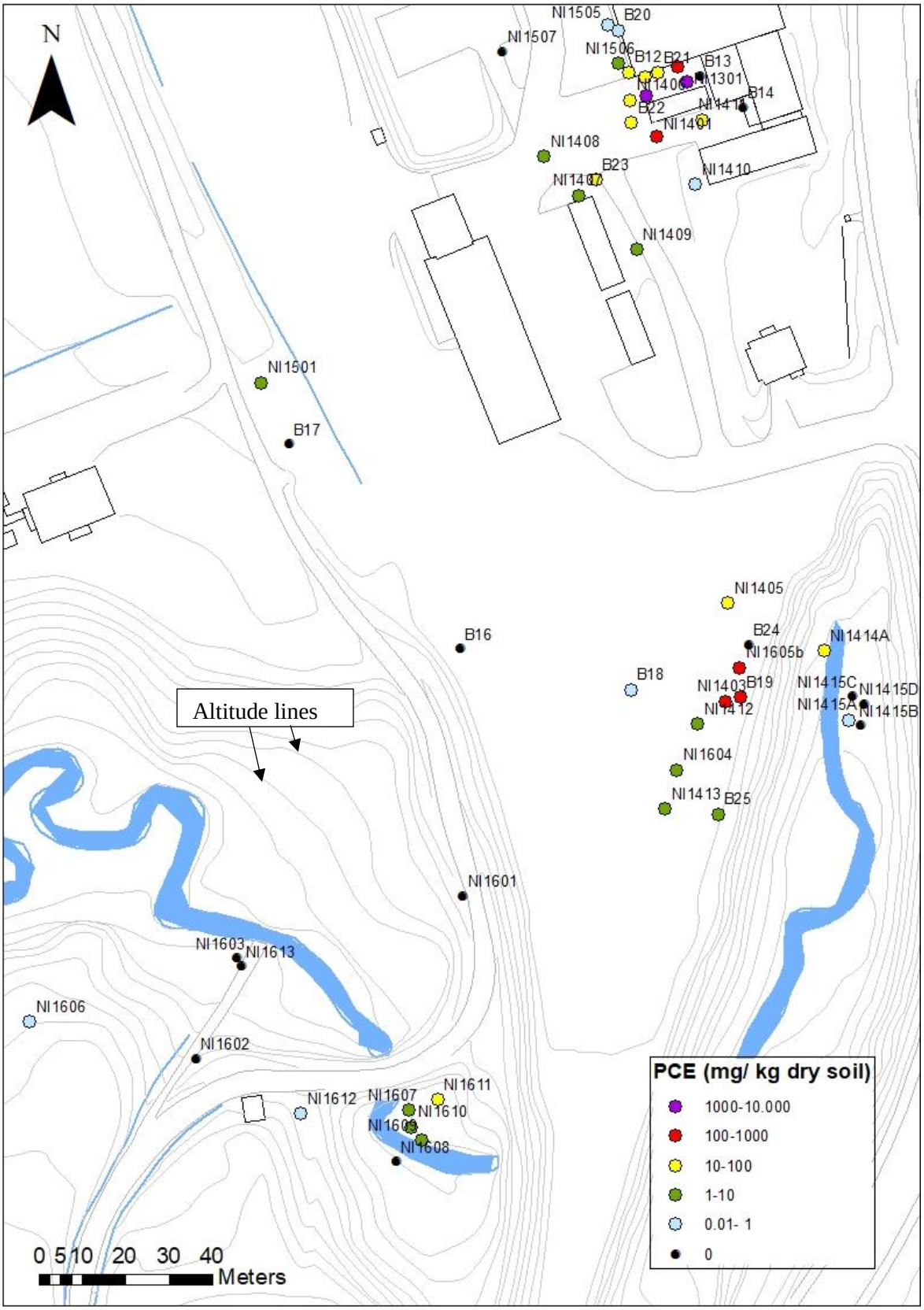

Figure 2.7. Maximum measured soil concentrations of PCE at Hagforstvätten. Map based on (Nilsson, 2017, unpublished data)

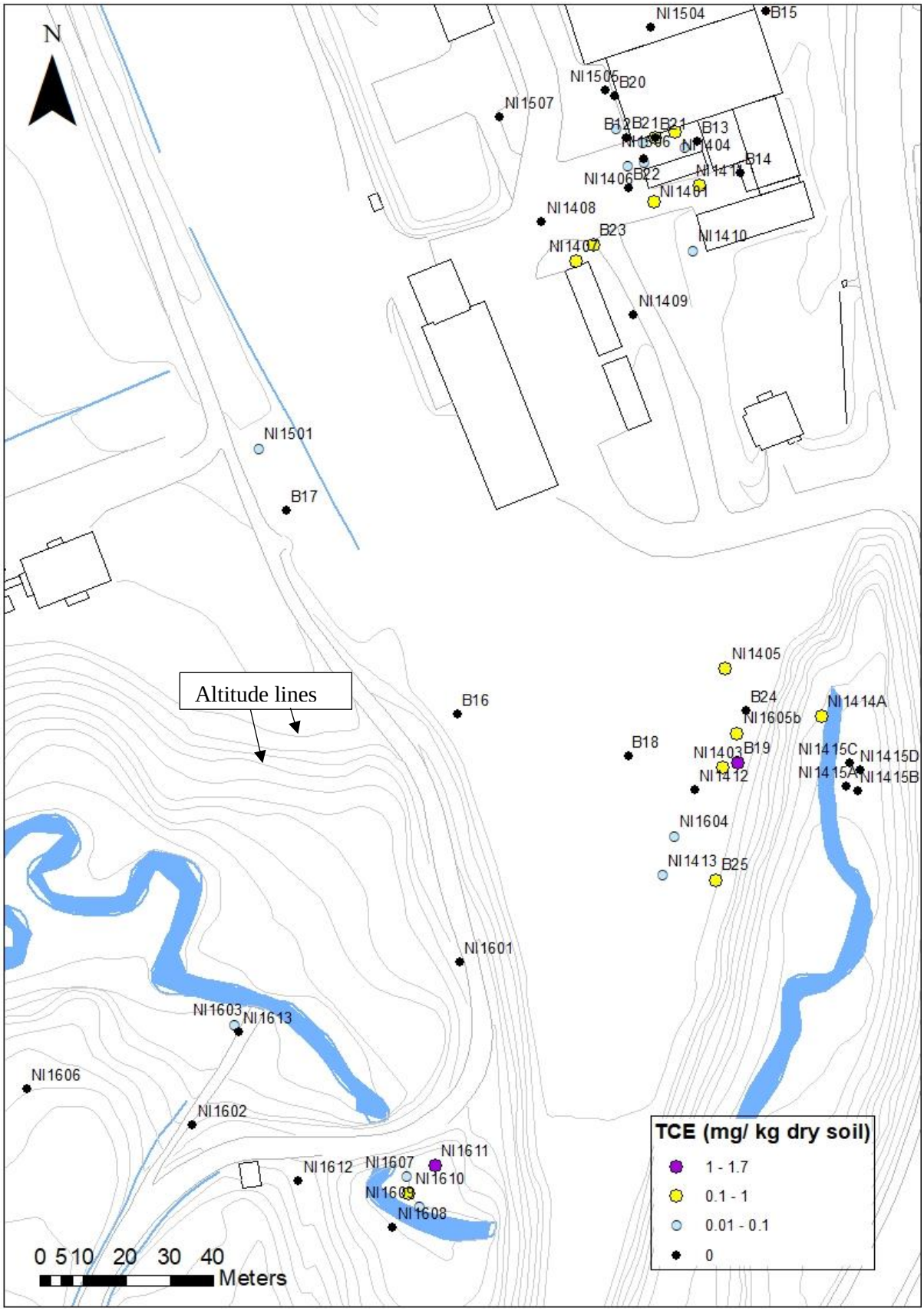

Figure 2.8. Maximum measured soil concentrations of TCE at Hagforstvätten. Map based on (Nilsson, 2017, unpublished data)

The pollution situation is slightly different at the secondary source than at the laundry site. The largest difference is that according to previous investigations by Sweco (2013) there are generally less low permeable sediments at the secondary source and hence only a minor part is adsorbed in fine-grained material above groundwater level. However, the suspected deep hollow in the bedrock might act as a storage of free phase PCE. The PCE cannot readily be transported away with the groundwater because of the bedrock topography, which means a high concentration of PCE at the bedrock surface.

Previous chemical sampling show degradation products and very high concentrations of PCE in the bottom sediments of well B19 (1.2 mg TCE/kg dry soil and 990 mg PCE/kg dry soil) (Nilsson, 2017, unpublished data). The threshold values for residential areas are 0.2 mg TCE/kg dry soil and 0.4 mg PCE/kg dry soil (Pettersson, et al., 2009). Downstream of B19 on the plateau there are indications of PCE in both groundwater and soil sampling. Where the groundwater plume from B19 discharges into Örbäcken PCE is measured to 50 mg/kg dry soil. At the same place the highest levels of the degradation product TCE is measured (1.6 mg/kg dry soil). On the west side of the plateau the chemical samplings are sparse, and the few samplings show no or low levels of PCE and degradation products except at the expected groundwater discharge as mentioned above (figure 2.7 and figure 2.8).

2.5.3 Ongoing degradation processes

The plumes from the main source and secondary source mostly consist of PCE. Levels of the degradation product trichloroethene (TCE) are very low in the soil as seen in figure 2.8 (Nilsson, 2017, unpublished data) and in the groundwater as seen in Appendix B (SWECO, 2013)(Åkesson, 2017, unpublished data). There has been no detection of the final degradation products vinyle chloride and ethane. This indicates that the groundwater is mostly aerobe where the microbial degradation rate of PCE is very slow. However, as mentioned above some degradation is occurring naturally where the groundwater from B19 discharges to Örbäcken. Additionally, degradation is also occurring naturally further downstream of Örbäcken where a thick layer of peat acts as degradation zone of PCE before the groundwater flows into Hagälven (SWECO, 2013).

2.6 Buried pipes and electrical cables

As shown in figure 2.9 there are water pipes and electrical cables buried in the subsurface of the studied site in Hagfors (the figure is more easily seen in Appendix C). These man-made objects might interfere with the survey instruments and cause unwanted anomalies in the results when investigating geological structures and spatial distribution of PCE. However, buried pipes and cables are often placed at shallow depths which make them less likely to disturb the measurements.

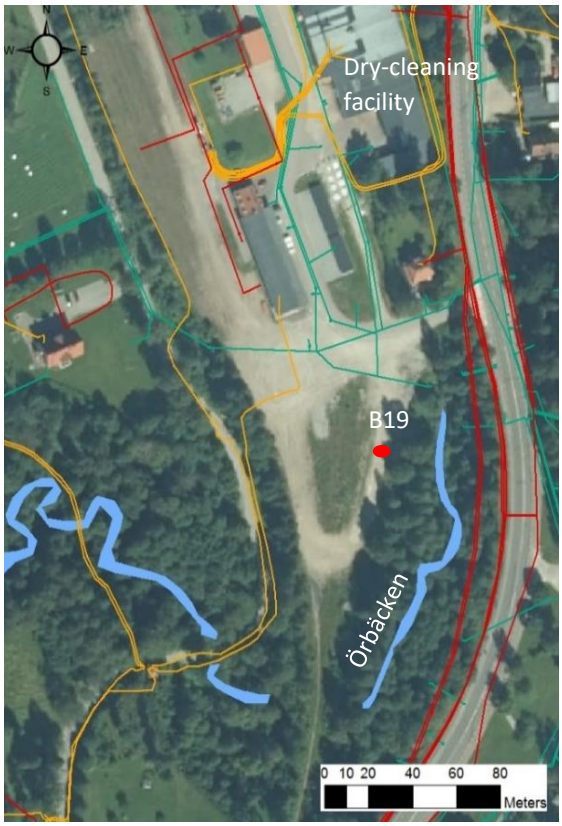

Figure 2.9. Buried water pipes (green lines), electrical cables (yellow) and electrical grounding cables (red) at the studied site. Map based on information from Geomatikk, ELTEL Networks Infranet AB and Hagforskommun 2017-03-01.

3. Theory chlorinated hydrocarbons

3.1 Physical and chemical properties

Tetrachloroethene (PCE) is classified as a chlorinated aliphatic hydrocarbon (CAH). The compound is highly chlorinated with four Cl-atoms (Englöv, et al., 2017). PCE is therefore very volatile, has a higher density than water and is very hydrophobic. PCE belongs to the group Dense Non-Aqueous Phase Liquids (DNAPLs). The main application of PCE started in the early 1900s as degreasing solvent for industry and dry-cleaning purposes, but PCE is forbidden to use in Sweden since 1995 (Englöv, et al., 2007)

DNAPLs exist in four phases in soil and groundwater: free, dissolved, adsorbed and vapour phase (SWECO, 2013). The free form of DNAPLs means that the compound is separated from the water phase, which occurs when the concentration is much higher than the maximum dissolved concentration in the water. The free phase can exist either as larger aggregates or in a residual form as droplets and strings.

The chemical properties of CAH changes with number of hydrogen atoms substituted with chlorine atoms which affects the equilibrium between the phases (Englöv, et al., 2007). The volatility increases with less Cl-atoms, and PCEs daughter product vinyl chloride (VC) with only one Cl-atom is practically a gas. On the other hand, the hydrophobicity increases with more substituted Cl-atoms. This means that PCE is more easily absorbed by the soil compared to VC. The adsorbed proportion of CAH increases with organic matter in the soil and the hydrophobicity of the compounds.

3.2 Degradation process of PCE

Chlorinated hydrocarbons are persistent and degrades very slowly in nature. The most common natural degradation process of highly chlorinated hydrocarbons in soil and groundwater is by reductive dechlorination (Englöv, et al., 2007). The biological process is performed by a special type of bacteria in a reductive environment (i.e. low oxygen levels). PCE has the following degradation steps in reductive dechlorination: PCE (tetrachloroethene) → TCE (trichloroethene) → cDCE (cis-1,2- dichloroethene) → VC (vinyl chloride) → ethane (figure 3.1) (SWECO, 2013). In each step, bacteria release a Cl-atom that is replaced by a H-atom. For less chlorinated compounds (cDCE and VC) the dechlorination takes place in both oxic and anoxic environments (Englöv, et al., 2007).

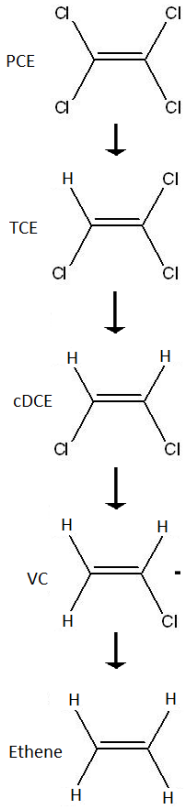

Figure 3.1. The degradation steps in reductive dechlorination of PCE.

Reductive dechlorination could either occur naturally or be stimulated by producing oxygen free zones and adding a certain type of bacteria. Organic-rich soils have a high consumption of oxygen and are therefore suitable natural environments for reductive dechlorination (SWECO, 2013).

The degradation effect is usually higher in zones with dissolved and adsorbed PCE instead of inside zones of free PCE. This is

because it is easier to create reductive zones and distribute the bacteria within PCE that is adsorbed or dissolved. It is also easier to have reductive dechlorination in high permeable soils compare to low permeable soils (SWECO, 2013).

3.3 Toxicity

PCE and its degradation products are very toxic for humans and ecosystems (Pettersson, et al., 2009). CAH from contaminated sites could be spread to humans through intake of contaminated soil and plants, inhalation of dust and volatile compounds, skin contact and drinking water. After intake or inhalation, CAH is stored and accumulates in the body's fat tissues where the compound could damage the central nervous system, bronchus, liver and kidney. Additionally, the degradation products VC and cis-DCE is carcinogenic, while PCE is suspected to be carcinogenic (Englöv, et al., 2007).

The ecotoxicity of PCE is high since already at low concentrations PCE has negative effects on soil species and aquatic life. Investigations of ecotoxicity of CAH on soil and aquatic species have showed that PCE is the most ecotoxic among all CAH (RIVM, 2001). A chronic exposure of 1000 µg/L PCE adversely effected 50 % of the aquatic species. Lowering the chronic PCE-concentration to 3.5 µg/L reduced the species that are adversely effected to 5 %. When it comes to species in the soil a chronical toxicity of 16 mg/kg adversely effected 50 % of the population. A chronical concentration of 0.054 mg/kg have a severe effect on 5 % on the soil species (RIVM, 2001).

3.4 Spreading behaviour

DNAPLs have a complex spreading behaviour in soil and groundwater seen in figure 3.2 (Englöv, et al., 2007). Free phase DNAPL is due to its high density transported vertically by gravity until low permeable layers are reached where the pollutant accumulates (dark red in figure 3.2). Zones of free phase DNAPL that have been created because of the geology (e.g. hollow in bedrock, low permeable layer) act as sources of pollutants. When the capillary forces in the soil are higher than the gravitational forces, free phase PCE forms a residual phase in form of drops and strings in the pore water (dark red dots in the figure). When groundwater passes the zone of free phase a plume with dissolved pollutants is created (orange in the figure). The distribution of the plume is affected by the groundwater flow pattern, dispersion, sorption and degradation effects. The pollutant spreads quickly with the groundwater if the sediments have a high hydraulic conductivity, for example the pollutant spreads faster in gravel sediment and slower in sand and silt layers. Chlorinated hydrocarbons are persistent and have a low sorption capacity which increases the spreading rate of the pollutants. The high

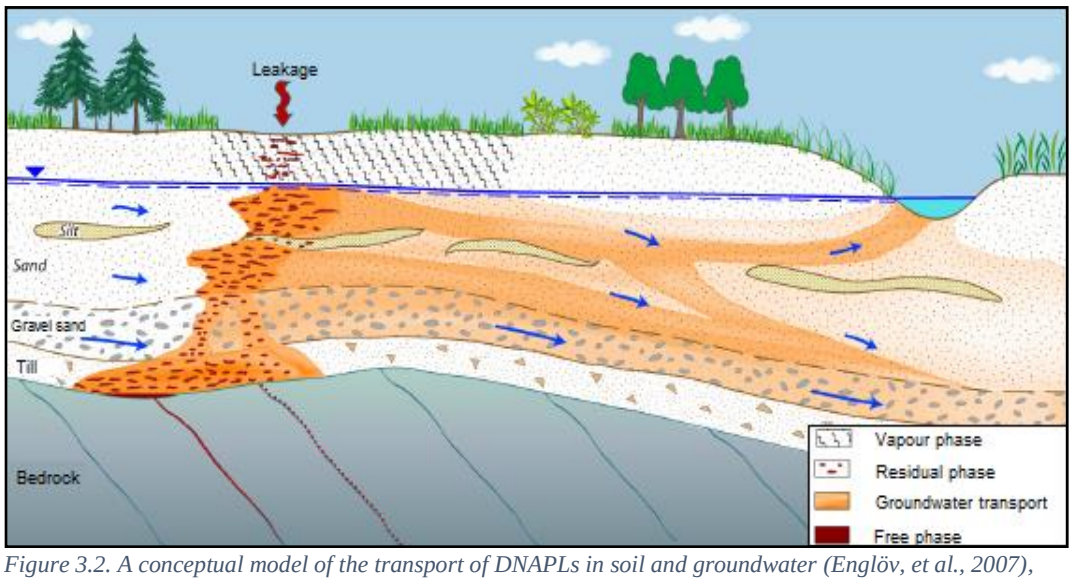

Figure 3.2. A conceptual model of the transport of DNAPLs in soil and groundwater (Englöv, et al., 2007), translated into English.

volatility of chlorinated hydrocarbons leads to a large removal of the pollutant in vapour phase (top black lines in the figure).

3.5 Threshold values

Threshold values indicate the acceptable level of risks for a negative effect on human health, animals and plants, and natural resources such as groundwater, surface water and soil. Threshold values are guidelines in risk analysis where the purpose is to determine the remediation methods and other measures needed to be taken to focus the remediation activities (Pettersson, et al., 2009).

General threshold values for chlorinated hydrocarbons in contaminated soil have been developed by SEPA (Table 3.1) (Pettersson, et al., 2009). There are three different threshold values depending on what needs to be protected: human health, soil or groundwater and surface water. Actions should be taken so that at least the minimum of these three threshold values is reached. The first health risk based threshold values protects people in direct and indirect contact with the pollutant orally, by inhalation or skin contact. The second threshold value protects a functioning soil ecosystem (flora, fauna and microorganism) and is based on the toxicity level of a certain compound for different ground living organisms. The third threshold value protects pollutant spreading to groundwater and surface waters, which is the situation in Hagfors. The groundwater and surface water are valuable to protect to have a safe supply of drinking water and irrigation water, and a non-toxic aquatic environment. In case of volatile pollutants, such as chlorinated compounds, there is a risk that toxic gases are spread into buildings overlying polluted soil or groundwater (Pettersson, et al., 2009).

The general threshold values for contaminated soil (table 3.1) does not include threshold values for vinyl chloride in the soil even though vinyle chloride is the most toxic and carcinogenic degradation product of PCE, since VC practically only exists as gas (Englöv, et al., 2007). The general threshold values are based on the scenario where the contamination source is only above the groundwater table and the leakage is through medium permeable soils. The threshold values are divided into sensitive ground areas (KM= Känslig Mark) and less sensitive ground area (MKM=Mindre Känslig Mark). KM includes residential areas where people can live permanently their whole life time. MKM is typically industry and office areas where people spend a limited time of their life. (Pettersson, et al., 2009)

Table 3.1. General threshold values for contaminated soil (mg/kg dry soil). (Pettersson, et al., 2009)

Pollutant (mg/kg dry soil)	KM	MKM
PCE	0.4	1.2
TCE	0.2	0.6

Because of the pollutant transport in the groundwater there is a risk of ecotoxic effect on the stream Örbäcken and health problems for people inhaling the volatile pollutant. Sweco (2013) have therefore developed site-specific threshold values for groundwater concentrations of PCE and its degradation products in order to protect the affectable ecosystems. When remediating the site, the actions taken should be based on these thresholds value presented in table 3.2. As a comparison, the site-specific values are higher than general threshold values for PCE and TCE in drinking water source (10 µg/L) (Livsmedelsverket, 2015). These general threshold values are not applied to the site since the groundwater is not a potential drinking water resource. The highest measured groundwater concentrations of PCE is well above 1000 µg/L (see figure 2.5).

Table 3.2.Hagfors threshold values for groundwater at 10 meter depth (µg/L) (SWECO, 2013)

Pollutant (µg/L)	KM	MKM
PCE	50	50
TCE	35	50
cDCE	70	70
VC	25	125

4. Theory geophysical methods

Geophysical methods aim to make quantitative observations of physical properties of the Earth's subsurface. Example of properties utilized are electrical conductivity, chargeability or magnetic field strengths that all varies with geological material and structures. Geophysical methods have many different fields of applications. The most traditional ones include exploration surveys in the search for natural resources or engineering surveys for characterising the subsurface before constructions of infrastructures.

However, the application of geophysical methods within the environmental sector has started to increase (Reynolds, 2011). One main reason is that geophysical methods are able to characterise contaminated sites prior the usage of more expensive direct observations such as drilling and digging (Reynolds, 2011). Since they cover large areas relatively fast, they could also be a complement to more traditional methods by finding areas of interest where drillings later could be performed to confirm the result. Hence, by using geophysical methods both time and money can be saved. Since geophysical methods have the advantage of being executed above ground they do not disturb the subsurface or spread the pollutants even more which is an advantage when dealing with contaminated soils (Reynolds, 2011).

It is possible to classify geophysical methods according to if they measure man-induced fields or natural occurring fields. Resistivity and IP measurements, DUALEM and GPR all utilize temporary fields created by man and are therefore classified as active methods. The magnetic gradiometer uses the natural occurring magnetic field of the Earth and is hence categorized as a passive method.

4.1 Electrical resistivity tomography (ERT) and induced polarization (IP)

Geophysical methods where the current flowing in the ground is injected using electrodes is referred to as direct current (DC) even though the polarity might be reversed during short time intervals (Milsom & Eriksen, 2011). When performing subsurface surveys measuring the resistivity and induced polarisation (IP) the electrodes are spread along a cable and secured into the ground. A specific setup of electrodes and measuring sequence is called an electrode array type. When the current is switched on the potential is measured between two alternating electrodes and the resistivity of the subsurface is thereafter calculated. Often, resistivity and chargeability are measured simultaneously. The general approach when measuring IP is to switch off the current and then observe how the potential slowly decreases between two electrodes due to induced electrical polarization in the soil (Milsom and Eriksen, 2011). However, new techniques enable time-saving surveys where IP-measurements are taken without turning of the current (Olsson, et al., 2015).

4.1.1 Electrical resistivity tomography (ERT)

During resistivity measurements, an artificial current is induced into the ground through two current electrodes and the potential is measured between two alternating electrodes, called potential electrodes. Since electrical currents obey Ohm´s law, it is then possible to determine the resistance and hence also the resistivity. The difference between these two terms is that resistance is a non-material property affected by the shape of the object while the resistivity is a material property. By determining the resistance (R), the apparent resistivity of the subsurface (ρ_a) is calculated by using a geometric factor (k) which depends on the chosen electrode array. The relationship is described by the basic array equation (Milsom & Eriksen, 2011):

$$\rho_a = 2\pi k * R$$

Factors affecting the resistivity

There are two main mechanisms causing currents to flow in the subsurface; electronic conduction and electrolytic conduction. Electronic conduction is when a current is created by the flow of free electrons and the phenomenon appears mainly if conductive minerals are present (for example metal sulphides). In electrolytic conduction, the current occurs by the movement of ions present in the pore water. Since the presence of conductive minerals usually is limited, electrolytic conduction by ions is usually the most common mechanisms in the subsurface. Therefore, the resistive properties of the subsurface are highly influenced by the ion concentration in the pore fluid, the type of ions present and the mobility of ions (Reynolds, 2011). These factors might be altered by the release of liquid pollutants such as DNAPLs.

The resistivity of unconsolidated materials and rocks varies within a wide range. However, gravel is usually expected to be more resistive than sand, which in turn is more resistive than clay and silt. Fine-grained particles such as clay and silt have the ability to perform ion exchange and might therefore reduce the resistivity (Burger, et al., 2006). Usually, clay rich soils have a resistivity lower than 100 Ωm (Dahlin, et. al., 2001) while dry gravel and sand might have much higher (sometimes as high as 10 000 Ωm) (Palacky, 1987).

If free-phase PCE is present in the ground, it will increase the measured resistivity since it acts as an electrical insulator. However, this increase in resistivity could be depressed if the electrolytic properties of the pore fluid increases due to the release of chloride ions during the degradation of PCE or mineral weathering. (Johansson, et al., 2015)

4.1.2 Time- domain induced polarization (IP)

When performing surveys with induced polarization the chargeability of the subsurface is determined. Chargeability is measured in millivolts per volt and it describes how well the material stores difference in charge. The set-up with two current electrodes and two potential electrodes used for resistivity measurements is also applied to IP-measurements. However, in time-domain IP-measurements it is of interest to measure how the electrical potential between the two potential electrodes changes with time when the current is abruptly turned off or changes polarity.

The main mechanisms causing induced polarization in metal-free soils is *membrane polarization*. This phenomenon occurs due to restriction of ion movements in the pore fluid when an external electrical potential is applied. A grain surrounded by water will possess a negative surface charge which attracts positively charged ions in the pore fluid, creating an electrical double layer (EDL). When an external current is applied, ions will migrate towards the opposite charged pole. However, the movement might be prevented by ion-selective zones. These obstacles are for example created at pore throats where EDL narrows the passages or around clay particles with attraction for positive ions. Ions will start to accumulate at these ion-selective zones and a potential difference is built up (see figure 4.1). If no external current is applied, then the

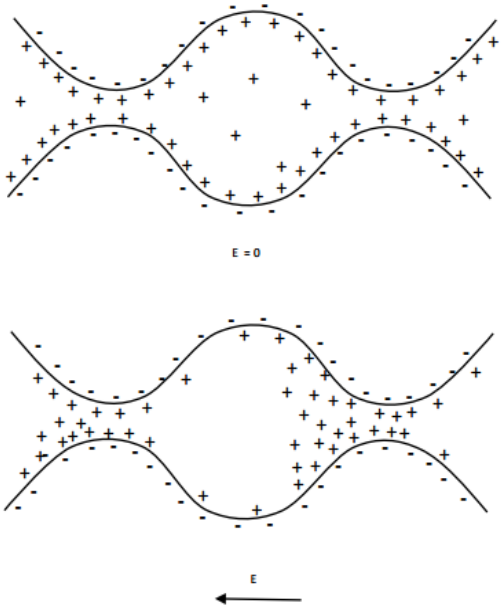

Figure 4.1. The mechanisms behind membrane polarization. When no external voltage is applied, the ions migrate freely by diffusion between interconnected pores. An electrical double layer is created at the grain-water interface. Narrower pore throats will act as ion-selective zones when an external voltage is applied, hence a potential difference is built up. When the external potential is turned off, ions will diffuse back to equilibrium state. (Johansson, et al., 2015).

ions will diffuse back into the pore fluid again. This migration of ions back to equilibrium state is the explanation for why the measured potential does not drop to zero instantly when the current is switched off or changes polarity (figure 4.2). (Johansson, et al., 2015)

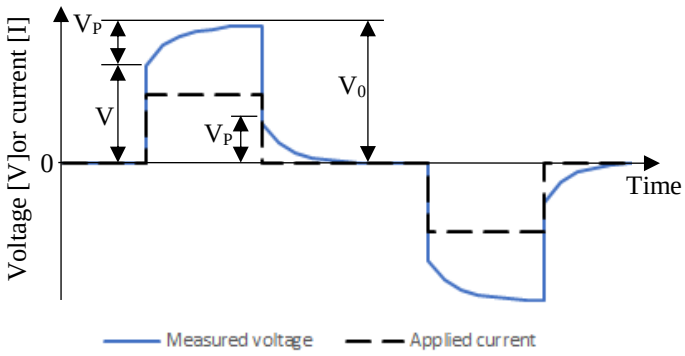

Figure 4.2. Injection of a pulse current and expected behavior for the observed potential measured between the two potential electrodes. V indicates the applied voltage, V_0 denotes the total observed voltage and Vp is the overvoltage created by polarization effects in the subsurface.

When the external current applied to the subsurface is switched off after a short injection time the expected behaviour of the measured potential is shown in figure 4.2. The applied voltage is denoted V and it increases/decreases instantaneously when the current is turned on or off. However, the polarization effects created in the subsurface due to membrane polarization causes an overvoltage V_P that delays the response. The total measured voltage V_0 equals the applied voltage and the overvoltage. When V_P is divided with V_0 the chargeability (millivolts per volt) is achieved. (Reynolds, 2011)

The apparent chargeability (milliseconds) is achieved by measuring the overvoltage decay and integrate with respect of time to determine the area underneath the over voltage decay curve in figure 4.2. The area is then normalized and divided with the observed voltage (Vo). (Reynolds, 2011).

The apparent chargeability is measured in the beginning of an injected pulse when the ground is charging up which is called the delay time. Ideally the delay time should be long enough for the ground to become fully charged. The resistivity is measured during the remaining time of the pulse called the acquisition time. (ABEM Instrument AB, 2016)

Traditionally during resistivity and IP measurements, the current has been applied with 50 % operation time and 50 % off-time (i.e. 50% duty cycle) (figure 4.3). The resistivity has been measured during the on-time and the IP measurements have been taken when the current is abruptly switched off (the off-time). However, a new technique developed by Lund University and Aarhus University operates with a 100% duty time for the current and measures how the potential decreases/increases with time when the polarity of the current changes (figure 4.3). The obvious effect of using a 100 % duty

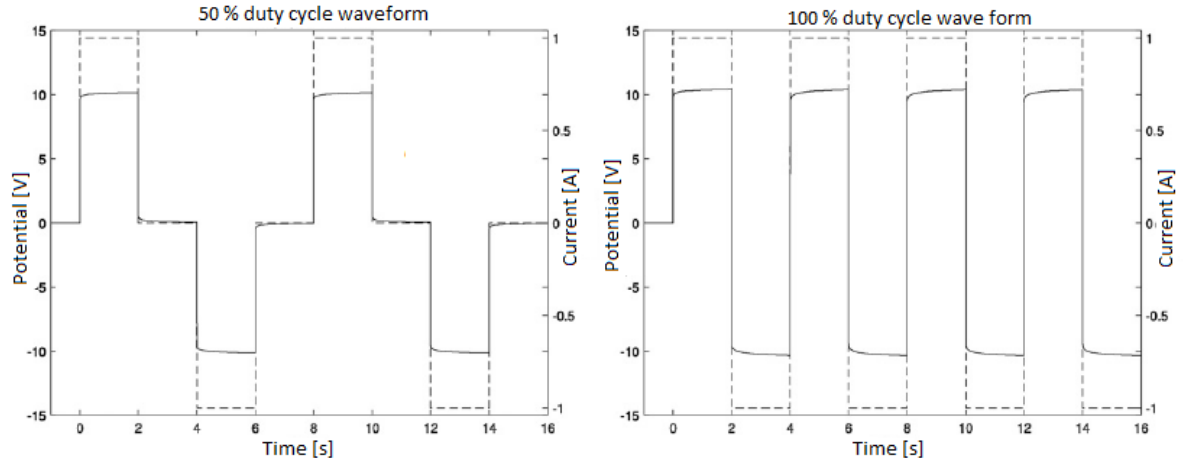

Figure 4.3. Waveform of injected current (dashed line) and measured potential (solid line) for a 50 % waveform duty cycle (left-side) and 100 % duty cycle (right-side). The 100 % waveform collects 8 measurements (stacks) while the 50 % duty cycle collects 4 measurements during the same period of time. (Olsson, et al., 2015)

cycle instead of a 50 % duty cycle is that the field data collection is up to 50 % faster. According to field experiments performed by Olsson P-I et al. (2015), the IP-responses from the two methods are corresponding well. The experiment showed that when the IP is measured during the on-time the magnitude of the overvoltage decay is almost doubled which increases the signal-to-noise ratio and improves the data quality.

Factors affecting the IP-response

Factors affecting the geometry and environment of pore spaces have important roles for the IP-response. Ionic concentration, grain size, grain shape and pore throat diameter will all affect the polarization of the soil (Reynolds, 2011). The presence of clays or grains of electronically conducting minerals (i.e. sulphides) might increase the IP-response (Milsom & Eriksen, 2011).

Studies where IP-measurements have been applied to soils contaminated with DNAPLs have earlier concluded a variety of results. For example, some have interpreted low IP-responses as the presence of DNAPLs while others have observed the opposite. A possible explanation for the different results is that DNAPLs can be present in the soil as different geometrical configurations. (Johansson, et al., 2015)

Johansson et al (2015) distinguish between two major types of configurations: free phase and residual phase. At a free phase, the DNAPL concentration is very high and the pore water is displaced by the chemical. Since DNAPLs (including PCE) are electrical insulators the IP-response is absent at these situations. If DNAPL exists as residual phase where the chemical is present as isolated droplets trapped in the pores (configuration A and B in figure 4.4), an IP-effect could be expected. If degradation occurs, for example in the outskirts of a DNAPL source, a higher IP-response could be expected. This is due to the release of chloride ions and that the residual droplets narrow the ion-selective pore throats increasing the membrane polarization effect. (Johansson, et al., 2015)

Figure 4.4 illustrates four different geometrical configurations where residual DNAPLs are present in the otherwise water-saturated zone. The IP-response varies for the different configurations from absent IP-response (model C and D) to increased IP-response (model A and B). (Johansson, et al., 2015).

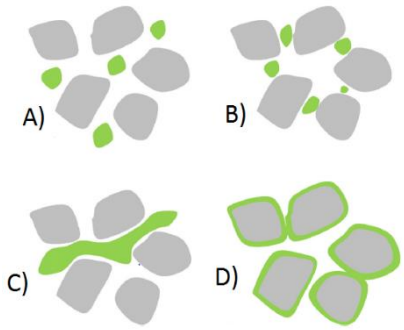

Figure 4.4. Different configurations of residual DNAPLs present in the otherwise water-saturated zone. Green represent the DNAPL and grey the soil grain. A) Residual droplets in pores. B) Residual droplets in the pore throats. C) Residual droplets connected in pores and pore throats. D) Residual DNAPL covering surface of grains. (Johansson, et al., 2015)

4.2 Data processing for resistivity and IP

The achieved raw data from resistivity and IP measurements shows apparent resistivity or apparent chargeability against pseudo depth, in a so called pseudosection (figure 4.5). The pseudosection is only a very approximate picture of the reality since the pseudo depth is an arbitraty depth calculated by assuming a homogenous subsurface (which is most often

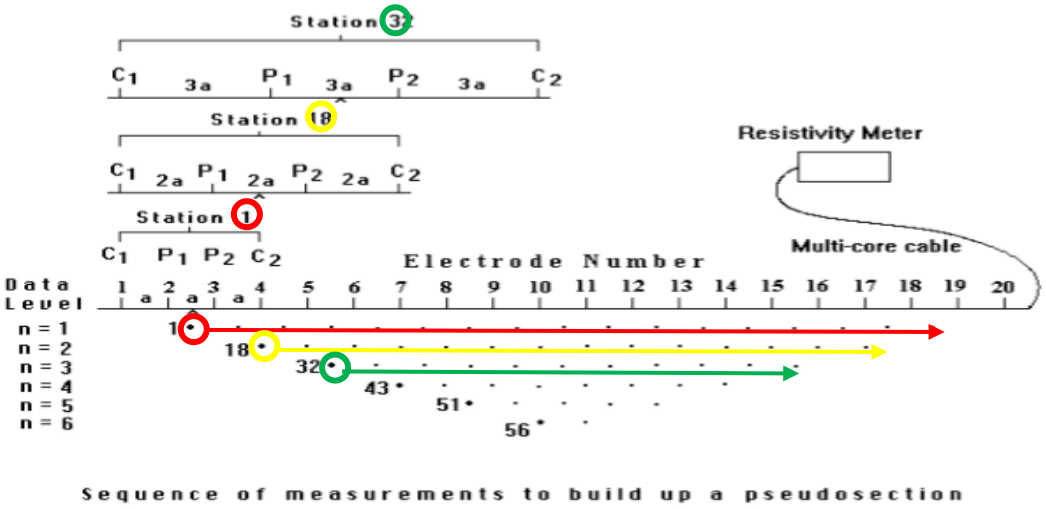

Figure 4.5. Illustration of a resistivity and IP survey forming a pseudosection. C denotes current electrode and P denotes potential electrode. The pseudo depth increases when the distance between current electrodes increases. When the electrodes are shifted along the cable the width of the survey increases giving rise to a cone-shaped pseudosection. Modified version of (Loke, 2016).

not the case in reality). The pseudo depth also depends on the used electrode array, hence different electrode arrays that map the same geology could result in very different pseudosection. For a specific survey the resistivity or IP measurement have the same pseudo depth when the distance between the current electrodes are the same, and when the distance is increased the pseudo depth also increases (figure 4.5). When the potential and current electrodes are shifted along the cable, the width of the survey increases. This movement of potential and current electrodes creates the cone-shaped pseudosection seen in figure 4.5. A computer in the resistivitymeter automatizes the measuring sequence that is pre-determined by the operator. (Loke, 2016)

How deep a resistivity or IP survey reaches depends on the chosen electrode array, the distance between the current electrodes and the conductivity of the geological materials. For example, a shallow high resistive layer will prevent current from being injected deeper down in the soil which decreases the depth of the survey.

In order to achieve a 2D-section showing a satisfactory estimate of the resistivity and chargeability in the subsurface, the pseudosection needs to be inverted using finite element and least-squares inverse methods. This is usually performed using a specially developed software (for example Res2Dinv).

When adapting a model to the pseudosection with apparent resistivity and chargeability it is called inverse modelling. This is an iterative process and it continues until it reaches the pre-determined maximum number of iterations or an end criterion that indicates a good fit to the data. It is also possible to generate apparent resistivities and chargeabilities from a model, which is called forward modelling. However, apparent resistivity has non-uniqueness solutions meaning that a broad range of models can be produce from the same pseudosection. Hence a model better representing reality can be achieved if legitimate assumptions about the geological situation are included in the inversion, so called a-priori information. (Milsom & Eriksen, 2011).

Smoothness-constrained or robust inversion is initial information about the geological situation and should be incorporated in the inversion to limit the number of possible models. Smoothness-constrained inversion produces resistivity and chargeability models that have smooth variation in the modelled values. It could be used for modelling a chemical plume where the resistivity values change gradually. The other common inversion method is robust inversion that model resistivity as homogenous bodies with sharp interfaces, which could be used for modelling some types of geological structures with sharp boundaries. (Loke, 2016)

4.3 Electromagnetic methods (DUALEM, ground penetrating radar and magnetic gradiometer)

Electromagnetic (EM) surveys detect changes in electrical and magnetic properties in the subsurface caused by i.e. different geologies or metal objects. There are two basic laws of physics that most electromagnetic surveys are based on (Burger, et al., 2006):

- Ampere´s law: an electric current produces a corresponding magnetic field
- Faraday´s law: a varying magnetic field will induce an electrical field, hence also a flowing current in conducting bodies

An electromagnetic field can be thought of as waves consisting of two components: one for electric intensity and one for the magnetic force. The two components are oriented perpendicular to each other where one oscillates in the horizontal xy-plane and one in the vertical xz-plane according to figure 4.6 (Reynolds, 2011).

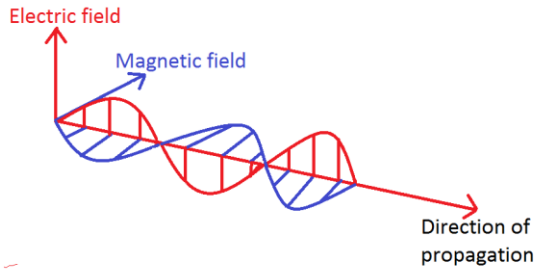

Figure 4.6 An electromagnetic field consist of two orthogonal components: one for electric field strength (red) and one for the magnetic field strength (blue).

The DUALEM method use current-carrying coils for transmitting and receiving electromagnetic fields. The field created by the device is named *primary field* while the receiving field caused by induction in the subsurface is called *secondary field*. The DUALEM compares the primary and secondary field to analyse the subsurface. The DUALEM works in the frequency-domain.

Ground penetrating radar (GPR) also uses electromagnetic waves, however it does not apply the usage of secondary induced fields. Theory for how DUALEM and GPR works are described in more detail in section 4.2.1 and 4.2.2.

When electromagnetic fields propagate down into the subsurface they will lose energy since they induce currents to flow. Eventually the signals become too weak for the receiver to detect. This effect is called attenuation. How deep electromagnetic survey reaches is hence affected by how well the soil attenuates the fields, which depends on the conductivity and chosen frequency. Layers with low conductivity or low frequencies will increase the penetration depth. (Milsom & Eriksen, 2011)

4.3.1 DUALEM

DUALEM surveys result in horizontal surface maps showing the electric conductivity of bodies in the subsurface. The ground resistivity is calculated as the reciprocal mean conductivity. The equipment exists in different sizes depending on which coil setup that is used. Figure 4.7 shows the DUALEM-421S used in the background survey in Hagfors.

Figure 4.7. DUALEM-421S mounted on a sled dragged behind a motorized vehicle.

The transmitter in a DUALEM consist of a current-carrying coil that produces a primary magnetic field according to Ampere´s law. The resulting magnetic field will be in-phase with the electrical field, meaning that they will increase and decrease at the same time according to the top figure in figure 4.8 (Burger, et al., 2006). The magnetic field is sinusoidal altered by changing the current in the transmitter coil and according to Faraday´s law this varying magnetic field will induce voltages in conducting bodies embedded in the subsurface. The induced voltage behaves as a sinus wave that is out of phase compared to the primary magnetic field (seen in figure 4.8) since it lags a quarter of a cycle (90° or π/2 rad) (Reynolds, 2011). The time it takes to generate a secondary induce current in the buried body depends on its conductivity. For good conductors, the time lag between induced voltage and resulting induced current will be high (Reynolds, 2011). The secondary induced currents in the subsurface are often referred to as eddy currents. These eddy currents will in turn create a secondary magnetic field that differs from the primary field in both amplitude and phase according to figure 4.8 (Burger, et al., 2006). The secondary field is detected by a receiver coil. By superimposing the primary magnetic field to the secondary magnetic field a resultant field is achieved. By studying the resulting magnetic field conclusions are made regarding the conductivity and magnetic susceptibility of the subsurface (Reynolds, 2011).

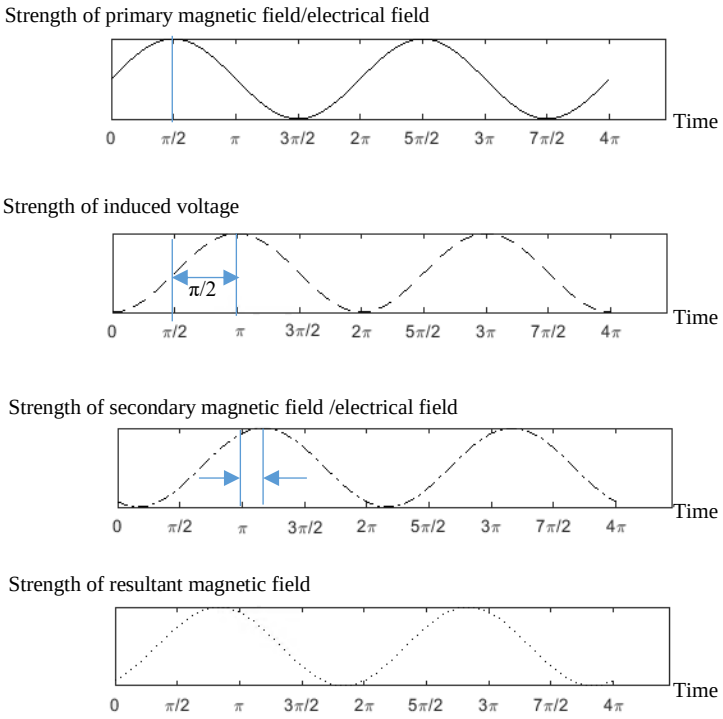

Figure 4.8. Illustration of how the primary magnetic field transmitted by the DUALEM transforms into the secondary magnetic field detected by the DUALEM. Resulting magnetic field is created by superimposing the primary field to the secondary field. The secondary field will be out of phase compare to the primary magnetic field since the induced voltage in the conducting body will lag a quarter of a cycle compare to the primary magnetic field and the time it takes to generate the secondary magnetic field depends on the conductivity of the body.

The penetration depth of a DUALEM survey is dependent on the distance between the transmitter and receiver coil as well as the applied frequency. A greater distance generates a higher survey depth, however only to a certain level. The depth is also affected by the attenuation effect described above. (Milsom & Eriksen, 2011)

The DUALEM equipment exists with different numbers of receiving coils. The receiving coils are separated at different distances from the transmitter and placed into pairs with one horizontal and one vertical coil. This arrangement enables simultaneous sampling of data at different depths. (Dualem, no date).

4.3.2 Ground penetrating radar (GPR)

Surveys performed with GPR results in vertical depth profiles of the subsurface. The profiles are generated by measuring the arrival time of electromagnetic waves that have been reflected at interfaces between different geological units and objects in the subsurface. The reflections are caused by differences in magnetic permeability, conductivity or relative electrical permittivity (Milsom & Eriksen, 2011). Magnetic permeability describes how easily a material becomes magnetized while electrical permittivity describes how well a material stores and releases electromagnetic energy as electrical charges (Styles, 2012). Objects able to detect are for example groundwater table, bedrock and layers of sorted unconsolidated materials.

A GPR system's main components are a transmitting antenna, a receiving antenna and a timing unit (figure 4.9). The antennas transform electrical signals to and from electromagnetic waves. The radio waves that are reflected back by the subsurface due to differences in materials magnetic and dielectric properties are received by the antenna. The amplitude of the reflected waves and time from transmission is measured by the timing unit and is the output of the GPR-system. (Annan, 2009)

Figure 4.9. Electromagnetic survey of the subsurface with a GPR in Hagfors. The antenna transmitting and receiving the electromagnetic wave is moved along the surface. The control unit is carried by the operator.

4.3.3 Magnetic gradiometer

With magnetic surveys, it is possible to investigate the subsurface by detecting differences in magnetic susceptibility (Reynolds, 2011). Applications for magnetic surveys could for example be to locate magnetisable objects in the ground (buried water pipes or electrical wires) or differentiate between geological units with different magnetic susceptibilities.

Depending on the electron structure, different minerals and rocks possess different susceptibilities and will therefore react differently in an applied external magnetic field (Reynolds, 2011). Table 4.1 presents rock types present in the surroundings of Hagfors according to SGU (2017) their expected susceptibilities according to Reynolds (2011). Diamagnetic materials are magnetised in such a way that they counteract the external magnetic field, resulting in weak negative susceptibilities. An example of this is quartz. Magnetite is however a mineral that easily becomes magnetized (Milsom & Eriksen, 2011). Rocks such as gabbro and basalt that contain magnetite often show high susceptibilities. Granite generally possess a low susceptibility, however if the rock contains magnetic minerals the susceptibility increases as shown in table 4.1.

Table 4.1. Rock types present in the surroundings of Hagfors according to SGU (2017) and their expected susceptibilities according to Reynolds (2011)

Rock type	Magnetic susceptibility (SI × 10^6)
Granite	10 - 65
Granite with magnetic minerals	20 – 50 000
Gabbro	800 – 76 000

It is also possible to detect and locate buried metal objects with magnetic surveys. Man-made objects in steel and iron such as pipelines causes anomalies due to high susceptibilities (Milsom & Eriksen, 2011). By studying the result conclusions regarding shape and the depth of the target can be estimated (Styles, 2012). The magnetic response of pipelines is characterised by linear anomalies. Pipes that are aligned in east-west direction behaves as dipoles that produces a positive and negative anomaly along the pipe. Pipes oriented in north-south direction produces only a negative or positive anomaly (Reynolds, 2011). Wells or drilling boreholes with metal casing with deep vertical extension behaves as monopoles, which means that they are detected as positive anomalies only (Styles, 2012).

The Earth itself also possess a magnetic field that is affected by solar winds. Variations in solar intensity can cause short-time variations in the observed magnetic field. It is therefore necessary to account for these external variations if the aim is to detect anomalies in magnetic fields due to differences in the subsurface. With a gradiometer, this is solved by having two magnetometers stationed above each other with a fixed vertical distance (usually 50-100 cm apart from each other) (see figure 4.10) (Milsom & Eriksen, 2011).

Changes due to the varying external field are eliminated by analysing the difference between the two observed field strengths. The result shows anomalies of the magnetic field strength that are only caused by local changes in the subsurface. Gradiometers are often suitable for investigating the shallow subsurface (Styles, 2012).

Figure 4.10. Magnetic survey with a gradiometer in Hagfors. The two vertically aligned magnetometers are seen in front of the operator.

5. Procedure of fieldwork

Data was acquired with two field campaigns during spring 2017. A background survey was performed in the end of March and due to frozen ground, the ERT and IP survey had to be postponed until mid-April.

5.1 Background survey

The aim for the first field campaign was to investigate the hydrogeology and potential disturbances for the upcoming ERT and IP measurements. The equipment used were GPR, magnetic gradiometer and DUALEM. The DUALEM survey and processing of the data was performed by the HydroGeophysics Group at Aarhus University. Specifications for the equipment used in the background survey are listed below:

- Geometrics' G-858G MagMapper, operated as a magnetic gradiometer
- Malå GX radar with a 160 kHz antenna
- DUALEM-421S with distances of 4,2 and 1 meters between transmitter and dual receivers

The first field campaign focused on the plateau and the adjacent creek west of the studied site. Data was acquired using GPR and magnetic gradiometer along parallel lines with a spacing of 1-2 meter. Figure 5.1 shows the location of the lines sampled with the GPR and the magnetic survey.

Since neither the GPR or the magnetic gradiometer had any internal GPS, a manual TOPCON GR-3 GNSS receiver was used to determine start and end points for each line. The Swedish national reference system SWEREF99 TM and the Swedish national height system RH2000 where used. These coordinates where later linearly interpolated using MATLAB (version 9.1) to illustrate the pathway of the survey. Due to large snow packs, some of the lines had to be interrupted as seen in figure 5.2 at the next page.

The area of the data collected by DUALEM is shown in figure 5.1. The instrument was

Figure 5.1. Map of measurements for Dualem. The survey was performed by Aarhus University. (Jesper Bjergsted, 2017, unpublished data)

pulled on the ground by a motor vehicle. The instrument had an internal GPS.

5.1.1 Data processing

The data from the magnetic gradiometer was processed and illustrated using the software MagMap (version 5.04). The difference between the two magnetometers where plotted in a coloured 2D-surface map in order to illustrate the variations in magnetic field caused by the subsurface.

The data collected with the GPR was processed using the software Reflex-Win (version 4.5.1). The processing of raw data followed the procedure according to the following sequence:

- Energy decay
- Time moving
- Bandpassfiltering
- Hyperbolic velocity analysis
- Kirchoff's migration
- Envelope

The processed GPR-sections were plotted in 3D in Voxler Version 3.3.1843 using the start and endpoints from the GNSS receiver.

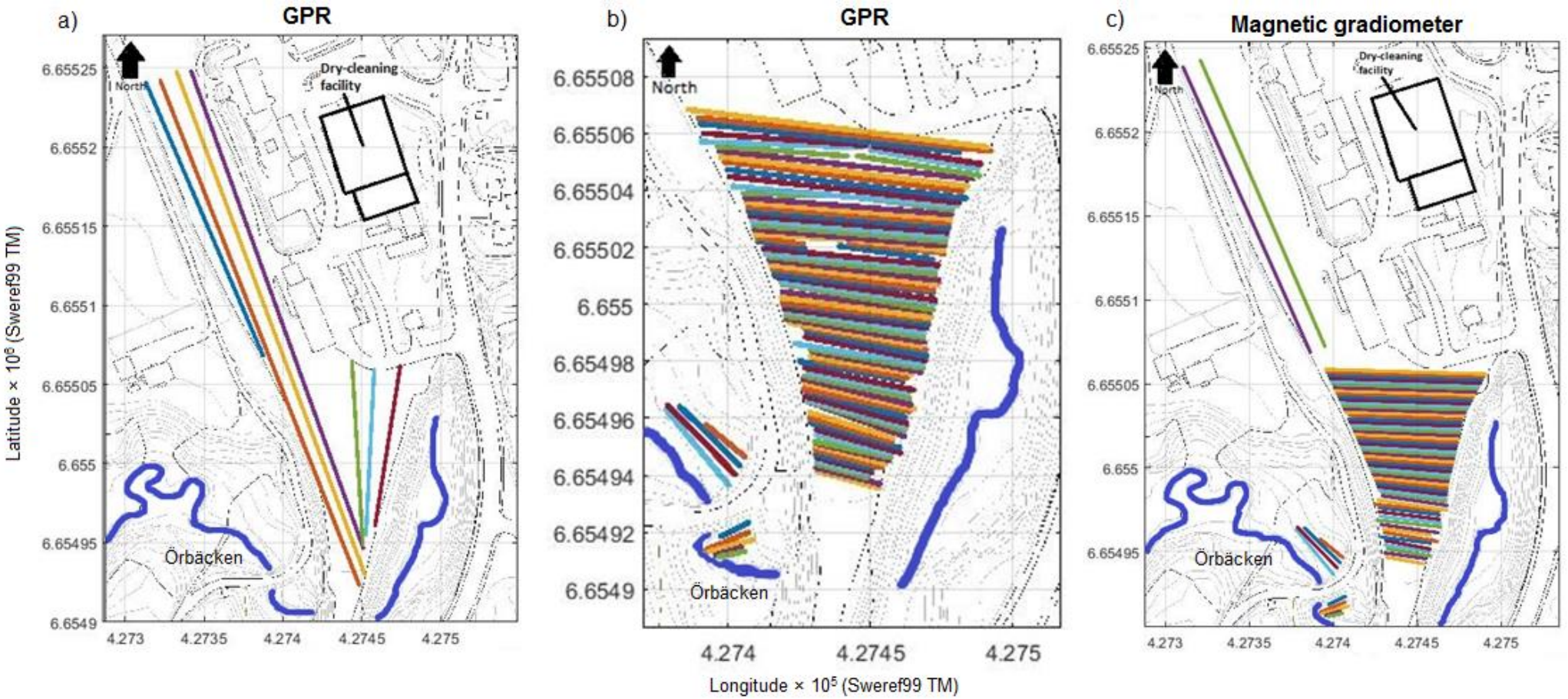

Figure 5.2. The locations of the lines sampled with GPR and magnetic gradiometer during the field campaign in the end of March 2017. a) Sampling of GPR with 7 parallel lines in south-north direction on the flat area b) Sampling of GPR with 87 parallel lines in east-west direction on the flat area and with 9 lines in the west creek close to Örbäcken. c) Sampling with the magnetic gradiometer with 66 parallel lines in east-west direction and 2 parallel lines in south-north direction on the flat area. The location of the lines in the creek are the same as for the GP survey.

The maximum depth of the DUALEM survey was 8 meters below ground surface. The collected data was processed and inverted with Aarhus Workbench and Aarhus inversion by the HydroGeophysics Group at Aarhus University.

5.2 ERT and IP survey

The resistivity and chargeability were measured along profiles as seen in figure 5.3 to cover the secondary source at B19, its plume and the plume from the main source underneath the dry-cleaning facility. In total seven lines were measured to detect zones of free phase PCE, silt and clay bodies and degradation zones of PCE shown by previous investigations by NIRAS and Sweco.

Profiles 1-4 stretch in east-west direction and are starting in the low-lying creek on the east side of the plateau, cross the higher altitude plateau and are ending in the low-lying creek on the west side of the plateau. The profiles were located to cover areas of interest and to take advantage of the topography of the site. By crossing the plateau, higher data resolution was achieved in deeper parts of the soil close to the bedrock. The length of profile 1 was about 80 meters, while profile 2,3 and 4 were about 160 meters. Profile 5 was measured in south to north direction down in the creek parallel to Örbäcken and have a length of 120 meters. Line 6 and 7 were placed on the top of the plateau and each profile had a length of about 200 meters. The different profiles had different electrode distances (1 – 2.5 m). Details for each profile is seen in appendix D (e.g. electrode spacing and total profile length).

A separated cable layout was used with one current transmitting cable and one cable measuring the potential in order to reduce electromagnetic coupling effects in the potential cable and thus improving the data quality (Dahlin & Leroux, 2012). The two parallel cables were shifted to each other and the take-outs on each cable were connected to every second electrode by so called jumpers. Where two cables where linked together, one electrode was overlapped i.e. used both by the last outtake at the ending cable and the first on the continuing cable. The profiles had different electrode spacing and total number of electrodes. The minimum electrode spacing was 1 meter and the maximum 2.5 meter. The total number of electrodes on one profile varied from 82 to 162 electrodes (Appendix D for details).

The investigated area had a lot of hard and dry surfaces such as packed gravel and some asphalt on the plateau, resulting in a high electrode contact resistance. Therefore, drilling of small holes and wetting around the electrodes with starch based gel (Revert Optimum from Johnson Screens®) was needed to reduce the contact resistance. The electrode contact resistance was kept below 20 kOhm for all profiles. The electrodes were made of stainless steel. The GPS-positions of the electrodes were acquired with a TOPCON GR-3 GNSS receiver. The used coordinate systems were the Swedish national reference system (SWEREF99 TM) and the Swedish national height system (RH2000).

The resistivity and IP-measurements were performed with the ABEM instrument Terrameter LS 2. An additional switching unit of type ES10-64 was used since the electrode numbers in the profiles exceeded the maximum number of electrodes that could be measured by the Terrameter. The Terrameter recorded the full waveform of the data to be able to extract the IP-signal. The data acquisition time was reduced by using a 100 % duty cycle. The total pulse length (the on-time) was determined to 2 sec which consisted of 0.8 sec of delay-time and 1.2 s of acquisition time.

During measurements, two different electrode arrays (with different electrode setups and measuring sequences) where used to be able to compare the resistivity and IP-results. The electrode arrays determine the positions of the current electrode pair and the potential electrode pair. The chosen arrays were pole-dipole and multi-gradient. In pole-dipole arrays the depth of penetration is increased since the distance between the current electrodes are large: one current electrode is positioned along the profile of evenly

distributed electrodes, and one is located far away from the profile (Milsom & Eriksen, 2011). The remote electrode was stationed so that the minimum distance between the remote electrode and the profiles where 400 meters. a multi-gradient array, both current electrodes are positioned on the profile with the pair of potential electrodes in between. The multigradient array gives higher resolution at shallower depths.

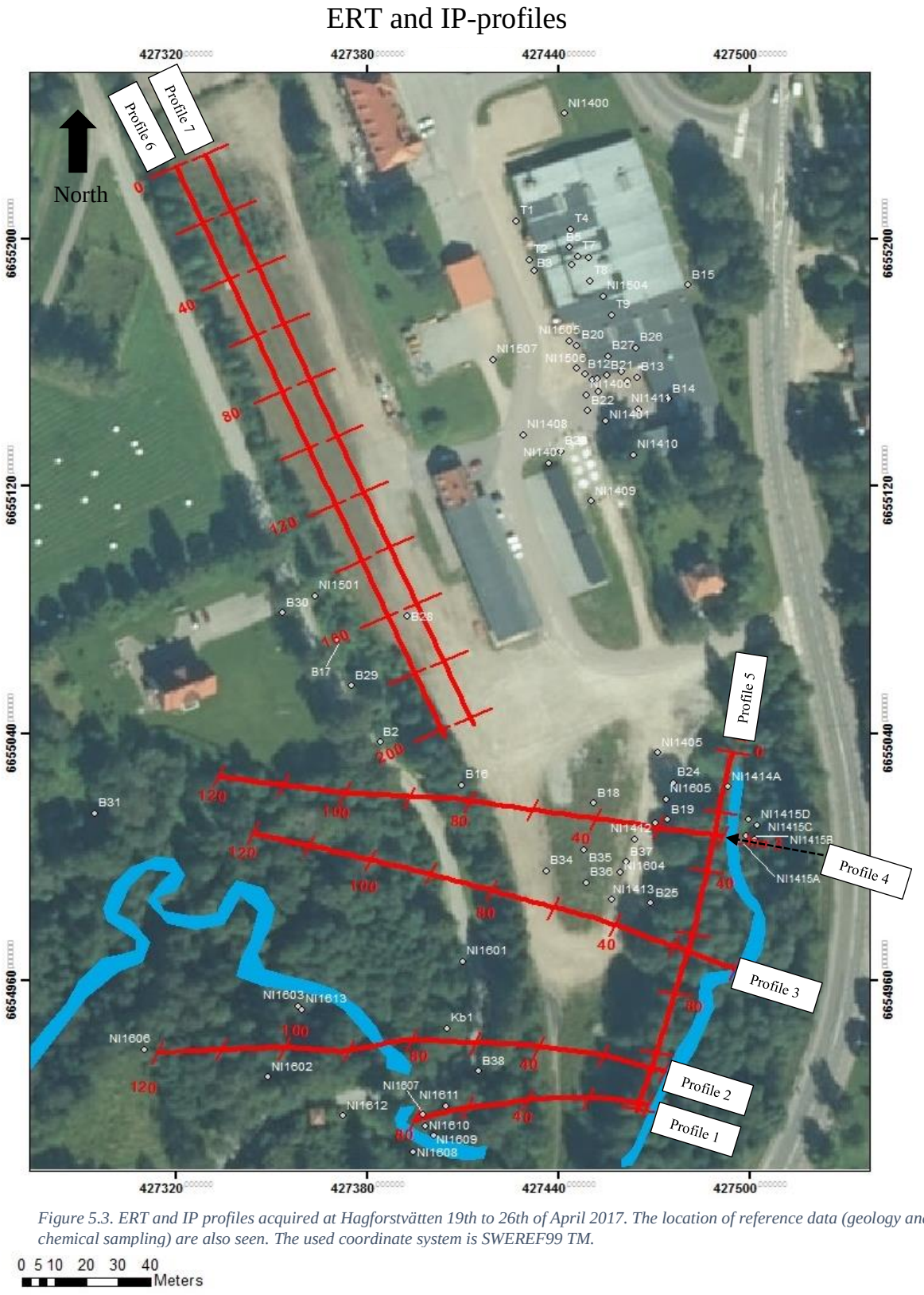

Figure 5.3. ERT and IP profiles acquired at Hagforstvätten 19th to 26th of April 2017. The location of reference data (geology and chemical sampling) are also seen. The used coordinate system is SWEREF99 TM.

5.2.1 Data processing of ERT and IP

The measured resistivity and chargeability were downloaded from the instrument with ABEM Terrameter LS Toolbox version 2.0.1.2. Coordinates and topography for the electrode positions measured with GNSS receiver during the fieldwork were added to the resistivity and chargeability data. Since all positions could not be measured with GNSS receiver (due to bad satellite signal) some electrode positions were interpolated in Matlab. The IP-signal was extracted from full waveform at 100 % duty cycle.

In the pre-processing of the pole-dipole data negative resistivity values were discovered in all ERT-profiles and later removed. Multi-gradient did not have any negative resistivity data. Negative chargeability data was seen for both electrode arrays, however they were not removed for inversion. Negative IP-data could occur under natural circumstances, and it is often a misunderstanding that they should be removed (Loke, 2016).

The measured data were acquired as pseudo sections. As mentioned in section 4.3 *Data processing for resistivity and IP,* pseudo sections are only an approximate picture of the subsurface since the measured data points are plotted on arbitrary depths. Inversion uses an algorithm that calculates the apparent resistivity from the measured resistivity, and creates a 2D-model of the resistivity or chargeability in the subsurface. This is an iterative process that tries to find the smallest difference between the calculated and measured data and hence find the model with the best fit to the measured data. The inversion software used was Res2dinv 32-bits version 3.71.118. All of the ERT-profiles had bad data points that could be due to for example bad electrode contact or measuring errors. These points were removed before inversion in order not to affect the results. The inversion method used was robust modelling (the so called L1-norm) which produces sharp interfaces between low and high resistivity zones. It was used because the collected ERT data had strong heterogeneities with high contrast in resistivity values. The number of iterations were set to 10, and the model that was chosen were the model with the smallest mean residual. Residual is a measure of the mean absolute difference between actual and modelled values. Hence, it is an indication of the reliability of the inverted model. Usually 10 iterations are enough to find the best fitted model to the actual data.

Generally, the quality of the multi-gradient data was good for all profiles, while the pole-dipole data was unsatisfactory for some profiles. The pole-dipole data was unsatisfactory because of its high data residuals, which means that the difference between actual and modelled resistivity or chargeability is high. The residuals for profile 3, 4, 6 and 7 measuring resistivity with pole-dipole were 20.1, 13, 11.6 and 15 % respectively. The residuals for the resistivity and IP measured with multigradient. The residuals for the multigradient measuring resistivity and IP varied from 0.8 % to 7%.

The inverted 2D-profiles of resistivity and chargeability were illustrated in Erigraph (version 2.20.00). The profiles were then added to a 3D-subsurface model in GeoScene3D.

5.3 Creating a 3D-model in GeoScene3D

The software GeoScene3D (version 10.0.13.531) was used to create a 3D model visualising topography, bedrock surface, geological and chemical reference data and ERT and IP results.

The topography where added as a digital elevation model (DEM) created from LIDAR data in 2*2m raster format (Lantmäteriet, 2009). The DEM was then draped with an orthophoto covering the studied site (Lantmäteriet, 2015).The bedrock surface was interpolated using inverse distance weighting (IDW) based on data achieved through (Nilsson, 2017, unpublished data).

Information from previous drillings performed by NIRAS contributed with information regarding soil type were added as vertical wells (Nilsson, 2017, unpublished data).

Data from NIRAS with measured concentrations of PCE and its degradation products at the site where added as xyz points with different colours illustrating the degree of pollution of the samples (Nilsson, 2017, unpublished data). No 3D interpolation of the plumes was performed since the data was too sparse.

The inverted ERT and IP profiles where exported to xyz format using Res2Dinv (32-bits version 3.71.118) and then added to the 3D-model.

5.4 Reference data

The geological and chemical reference data from NIRAS and S.Åkesson at Lund University were used in combination with the inverted ERT and IP-profiles. The geological and chemical reference data were used to confirm the correlation between geology and resistivity and IP. The reference data has also been used to facilitate the interpretation of which IP and resistivity responses that are caused by geology and which that are caused by pollutants.

6. Results & interpretation

In this chapter, the results from the background survey are presented followed by results from the resistivity and IP measurements. The results are continuously interpreted as they are presented.

6.1 Background survey

This section describes the results and interpretation of the magnetic gradiometer, DUALEM and GPR.

6.1.1 Magnetic gradiometer

Figure 6.1-6.3 show surface maps of the measured magnetic field caused by magnetic materials in the subsurface. The plotted parameter is the magnetic anomaly, i.e. the plot shows the difference between the two magnetometers to eliminate natural occurring variations in the external magnetic field.

Observe that the scales and colour intervals of the maps are different.

The areas covered in figure 6.1-6.3 are seen in figure 5.2c, section 5.1 *Background survey*. Figure 6.1 shows the magnetic field on the plateau, while figure 6.2 and 6.3 covers the creek on the west side of the plateau.

Generally, the magnetic response is very varied with many small local anomalies which has been interpreted as if the site is highly influenced by human activities. For example, the strongest anomalies (darkest red/blue) could be explained by metallic objects remaining in the subsurface from the former railway. Other man-made magnetisable objects like pipes, power-lines and wells with metal casings that have high magnetic susceptibilities could also cause strong anomalies. One power-line located in the northern part in east-west direction was seen (marked as A in figure 6.1).

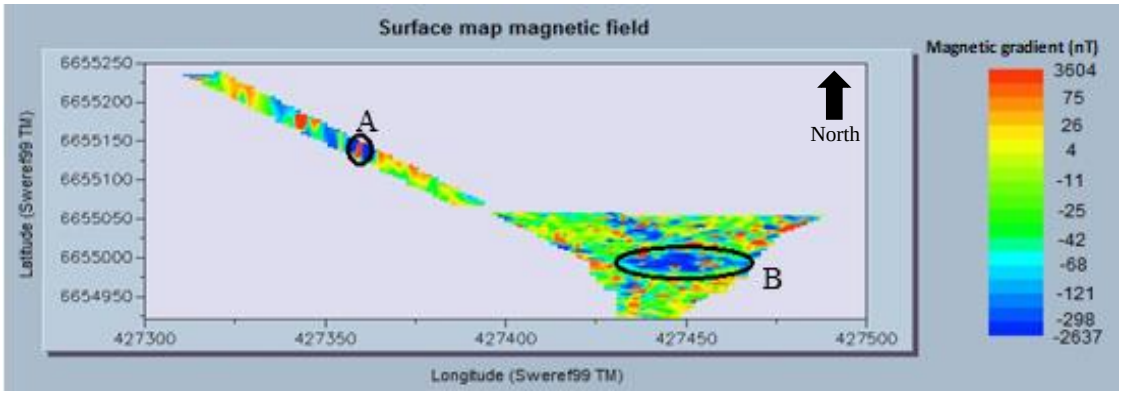

Figure 6.1 Magnetic field strength on the plateau. Negative magnetic anomalies (blue) and positive magnetic anomalies (red) are detected. The positive anomaly in the north west is caused by a power line. The center of the plateau has an interesting negative anomaly.

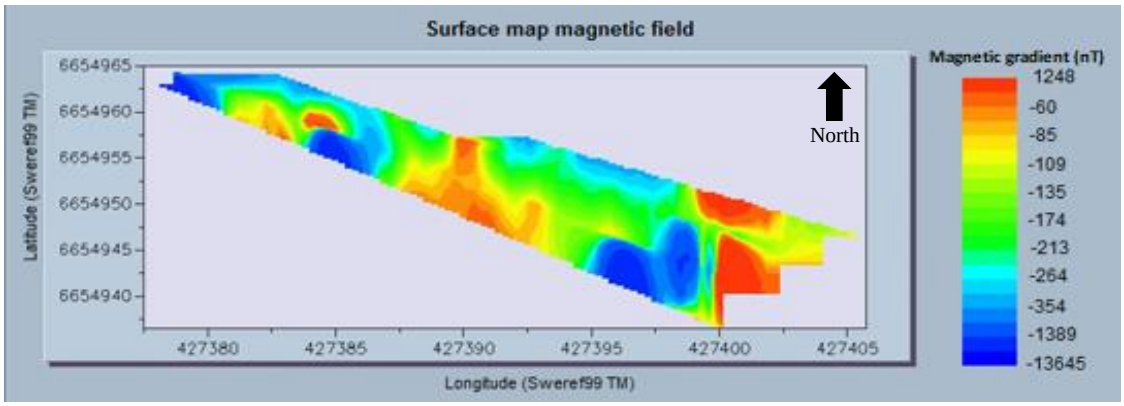

Figure 6.2 Magnetic field strength on the west creek north of the small gravel road. The lines are in south-east to north-west direction with Örbäcken on the left side. Negative magnetic anomalies (blue) and positive magnetic anomalies (red) are detected.

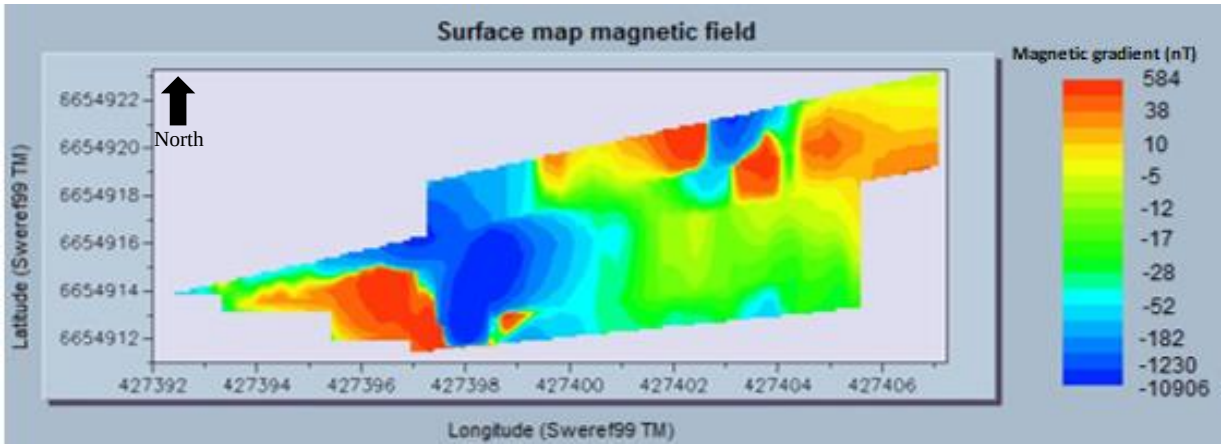

Figure 6.3 Magnetic field strength on the west creek north of the small gravel road. The lines are in south-east to north-west direction with Örbäcken on the left side. Negative magnetic anomalies (blue) and positive magnetic anomalies (red) are detected.

Pipes further south on the plateau are not seen, probably due to other magnetic materials in the soil that supress the pipe anomalies or because of nonmagnetic pipe materials.

The moderately strong anomalies plotted as weaker colours could be due to different minerals and materials in the filling material. However, a wide negative magnetic anomaly that weakens the external magnetic field was observed southwest of the secondary source (marked as B in figure 6.1).

6.1.2 DUALEM

General trends from the resistivity data collected by the DUALEM were observed but detailed interpretation was avoided since the data quality was poor. This is partly due to the increased ground resistivity caused by frozen ground during the time of measurement. The increased resistivity leads to low signal-to-noise ratio. Additionally, a high noise level was observed in the area due to man-made conductive structures that disturbed the ground resistivity measurements. (Bjergsted Pedersen, 2017, unpublished data).

The DUALEM survey covered a depth of around 8 meter below surface. However, at some areas the depth of investigation was less. The results showed that the first 0-4 meters are more high resistive (200-5000 ohmm) while 4 to 8 meters have lower resistivity (10-200 ohmm) (figure 6.4). Higher resistivities might be caused by coarser grain sizes or frozen ground. From this the filling material is

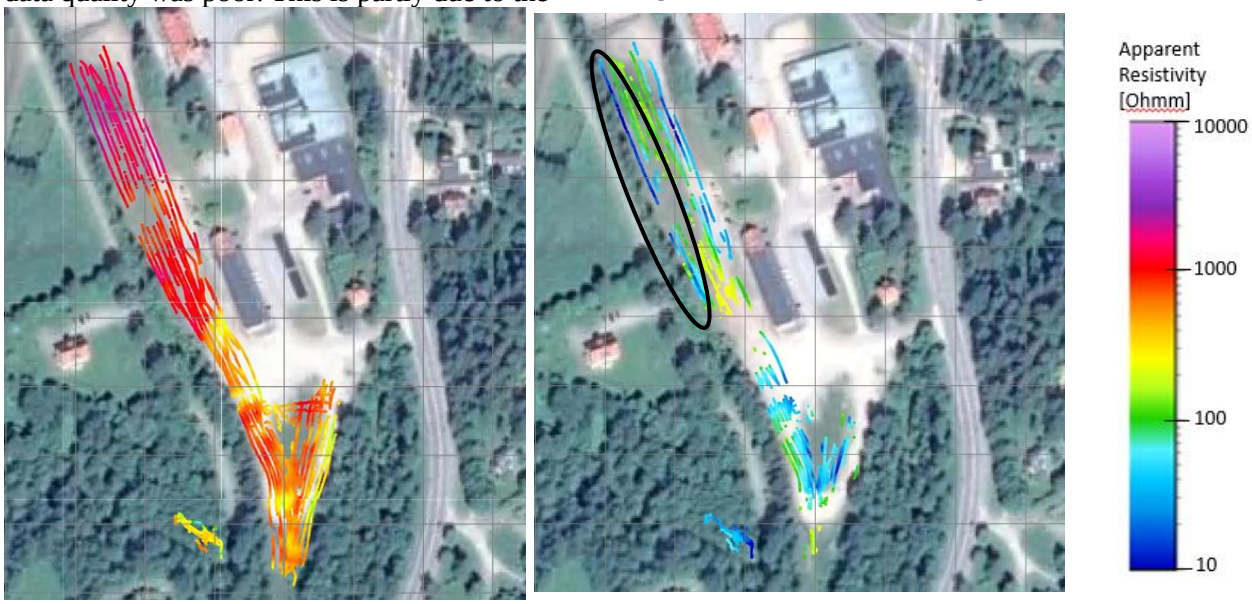

Figure 6.4 A) Mean resistivity for 1-2 meters depth B) Mean resistivity for 7-8 meters depth. The marked low resistivity zone coincide with the location of a power line (Bjergsted Pedersen, 2017, unpublished data)

estimated to reach 2 - 4 meters below the ground surface. The lower resistivities at depths greater than 2 - 4 meters indicate a layer of more fine grained material of sand, silt and clay.

Some low resistive zones on deeper levels could also be explained by conductive man-made structures. For example, there are low resistive patterns on the edges of the northern survey area, which coincide with power cables (marked with black lines in figure 6.4)

Another trend seen in the resistivity maps are that the resistivity is higher in the northern part and lower in the southern part of the plateau for all depths. This makes it likely that the soil material is coarser in the north compared to the south.

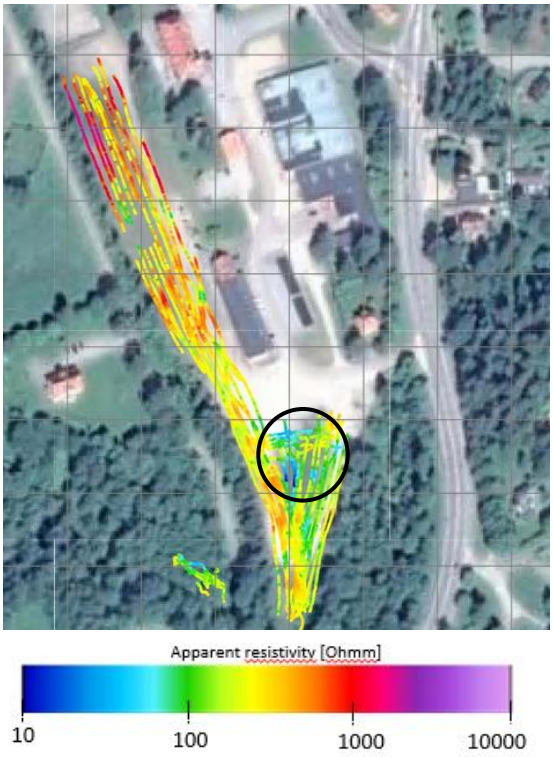

Figure 6.5. A low resistivity zone is detected on the middle of the plateau (marked in black) which coincides with a strong magnetic field from the magnetic survey. (Bjergsted Pedersen, 2017, unpublished data)

It is also seen that the depth of penetration is lower in the southern part which indicates more fine grained soil that attenuates the signal. In figure 6.5 there is a low resistive area south on the plateau which coincide with a strong magnetic field seen in the gradiometer data (area B with black borders in figure 6.1.

Thus, this low resistivity zone is probably caused by magnetic materials rather than grain sizes since a difference only in grain size does not change the magnetic field. See Appendix E for further resistivity data.

6.1.3 Ground penetrating radar (GPR)

On the south-north oriented GPR-profiles a reflective surface about 6-7 meters below surface have been detected on the whole plateau. The reflected surface is however not continuous, but is repeatedly seen at the same depth. The reflective surface is best seen in the GPR-profile running along ERT-profile 6 (Appendix H).

One possible cause of the reflective surface could be the groundwater table that was measured 6-10 meters below surface on the plateau in April 2017. On the other hand, the source of the reflection could be the interface between coarser and finer material.

A Voxler model of the GPR-sections on the plateau is seen in figure 6.6. Here a cross-section going south to north has been made in order to high-light the low amplitude 3D-body seen in the northern part the plateau (marked in black circle). The 3D-body extends approximately 30 meters south to north and 30 meters in east-west direction. The cross-section is taken where the body is largest. The low amplitude body indicates that the electromagnetic waves are attenuated faster compared to the surrounding, which could be due to presence of a larger silt and clay body. The area is situated too far north of ERT-profile 4, hence it could not be included in the interpretation of the ERT and IP survey.

Except for the reflective layer discussed above, the processing of the GPR-data has not led to any significant discoveries that could facilitate the interpretation of ERT and IP. Remains from the railway or more reflective layers have not been detected, which is in accordance with previous suspicions of that the site is very heterogenous.

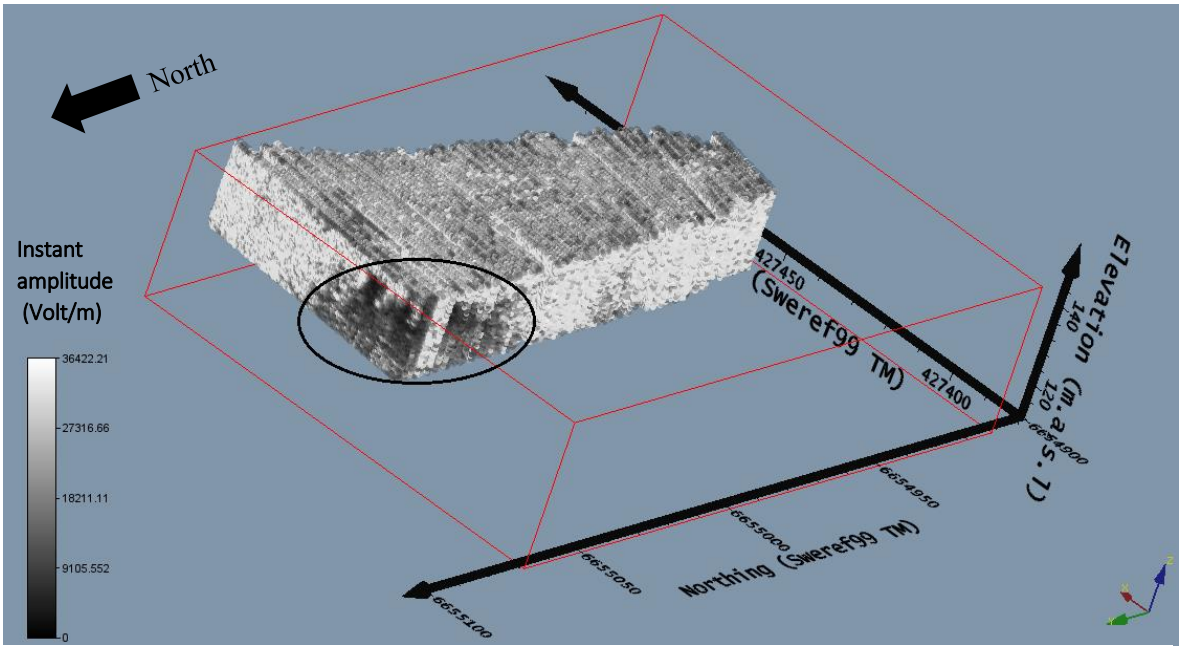

Figure 6.6. 3D-model of the GPR-sections on the plateau. The 3D scatter plot shows a cross-section that high-lights a low amplitude body in the northern part of the plateau.

6.2 ERT, IP-profiles and reference data

This section presents the results from the ERT and IP survey together with geological and chemical reference data. An interpretation of the geology and pollutant situation is presented in two different subsections, each followed by a selected pair of ERT and IP profiles with corresponding geological and chemical reference data. However, all interpreted profiles (1-7) are presented in large format in Appendix F and all geological and chemical reference data are presented in Appendix G.

An overview of the results from the profiles measuring resistivity and IP using multi-gradient array are seen in figure 6.7 and 6.8.

Before interpreting the inverted profiles with resistivity and chargeability, the quality of the data should be mentioned. After inversion, the pole-dipole data for profile 3,4, 6 and 7 had high residuals (11.6 – 20.7 %). The mean residual describes how well the modelled data fits the measured values. A high residual means that the inversion becomes less trustworthy. However, the pole-dipole data for profile 3, 4, 6 and 7 correlate well with models achieved with multi-gradient array. Because of this and since the data measured with pole-dipole array reveals information from deeper depths, the profiles with high residuals are still presented. However, models with high residuals should be interpreted with caution. The IP-data collected with pole-dipole array for profile 1 have been excluded from the results due to large artefacts created by the inversion. Pole-dipole data were never collected for profile 2.

While analysing the inverted results it is also important to keep in mind that the resolution is highest at the surface and decreases with depth since the measurements becomes sparser further down. This is probably why the inversion tends to vertically extend the structures in the deeper parts of the model. Sometimes, structures appearing in the shallower parts of the model extend below the expected bedrock surface (for example seen in profile 4, Appendix E). Therefore, the boundary between bedrock and soil is not seen in most profiles. Also, some profiles show very strong local square-shaped anomalies with high contrasts in resistivity or chargeability (seen in pole-dipole array for profile 4, Appendix E). These objects are likely to be artefacts due to the inversion procedure.

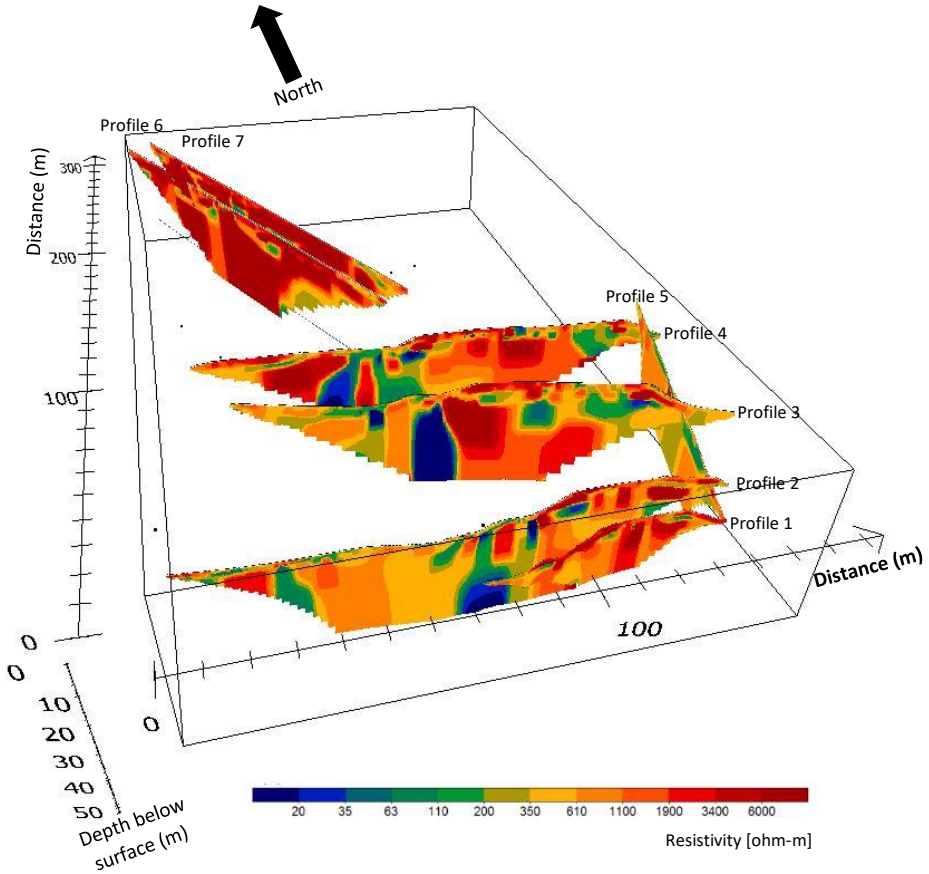

Figure 6.7. Resulting profiles measuring resistivity with multi-gradient array. Profile 1-4 are crossing the plateau in west-east direction and are located south of the main source. Profile 5 is located along Örbäcken down in the east creak while profile 6 and 7 are located in the northern part of the studied area (see figure 5.3).

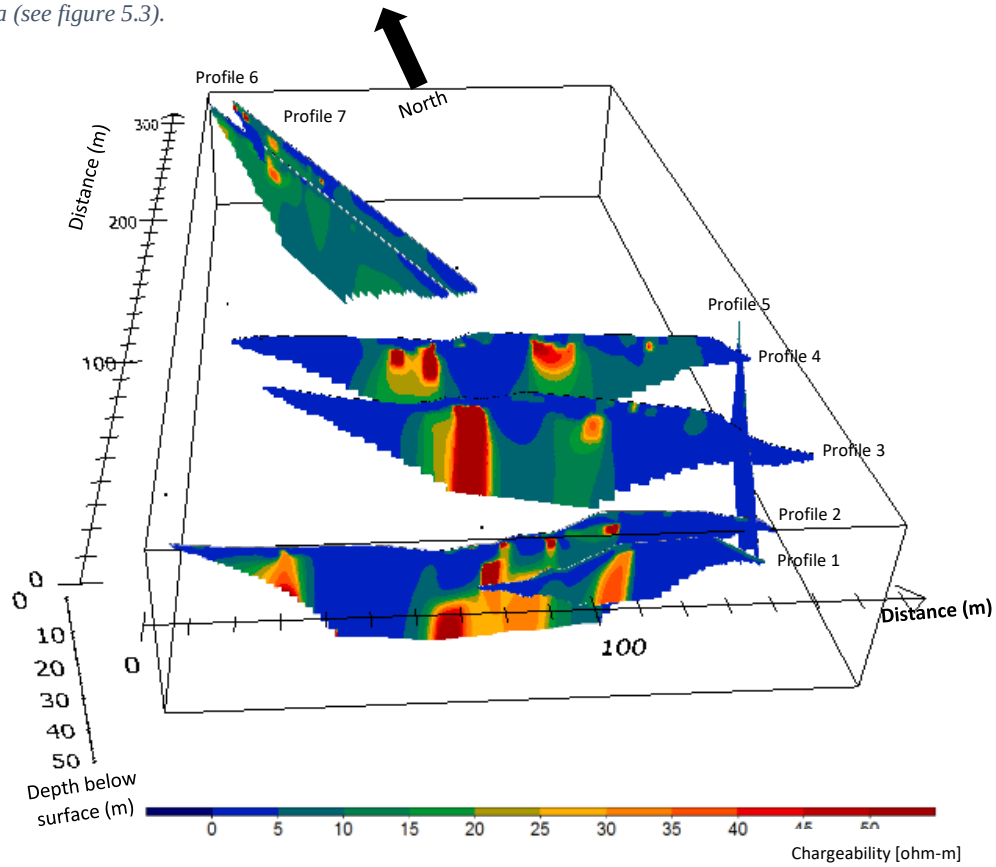

Figure 6.8. Resulting profiles measuring induced polarization (IP) with multi-gradient array. Profile 1-4 are crossing the plateau in west-east direction and are located south of the main source. Profile 5 is located along Örbäcken down in the east creak while profile 6 and 7 are located in the northern part of the studied area (see figure 5.3).

The inverted profiles have been studied together with geological drilling samples and chemical reference data from the site provided by NIRAS and S.Åkesson. The reference data were used together with the ERT and IP-profiles to interpret the geology and spreading of PCE. Some selected drillings and chemical samples are presented together with the ERT and IP results. Before presenting the data from the geological drillings, the geology was simplified and classified according to dominating grain size or material in the sample.

The number of wells in the proximity of the profiles is unsatisfactory to be able to interpret with high certainty which anomalies that are caused by geology, man-made structures or pollutant. Since the site is very heterogenous the interpretation of geology in areas with sparse reference data is uncertain.

6.2.1 Interpretation of geology

All profiles on the plateau (1-7, excluding profile 5) show that the resistivity varies on a broad range with very local zones of low and high resistivity (figure 6.7). This supports the idea that the site has a very heterogenous geology with glaciofluvial deposits, silt and clay bodies in a mixture. It is difficult to see continuous layers and trends, and therefore the site probably also has a high degree of man-made influence from the former railway track that was situated at the site. The local variations in apparent resistivity and chargeability are largest close to the ground surface where the disturbance by humans most likely occurred.

Profile 1-4 (southern part of the plateau)

The most northern and southern profile (profile 4 and 1) crossing the plateau are used to visualise general trends observed in the geology south of B19. Resistivity and IP results from profile 4 and 1 are presented in figure 6.9 and 6.11 further below. However, similar trends were seen in profiles in between (profile 2 and 3).

All four profiles crossing the plateau showed a high resistive layer in the top soil which probably correspond to a coarse filling material 0 - 5 meters below the surface (profile 1, figure 6.9). Beneath there is a low resistivity layer interpreted as a natural layer of the finer grain sizes sand, silt and clay. Indications of coarser filling material that is interrupted by small low resistivity anomalies corresponding to finer filling material is detected in profile 4 (figure 6.11). The profiles on the plateau shows a general trend with high resistivities at the surface followed by a section with lower resistivities that overlies higher resistivites closer to the bedrock (figure 6.9 and 6.11). Drillings in the proximity of profile 4 have partly been able to correlate this trend with coarser filling material at the top followed by a silt and clay rich layer and coarser bottom material (figure 6.12). However, as mentioned before it was not possible to confirm the geology in many parts of the profiles due to lack of reference data.

All the profiles 1 - 4 went down in the east and west creek and showed lower resistivities closer to Örbäcken (figure 6.7). At the river bank, finer material has probably been able to settle during flooding's creating a sandy top soil rich in silt, clay and organic matter. This trend is for example seen at the west side of profile 1 where finer materials also have been detected in drillings (figure 6.9 and 6.10).

Profile 1 – 4 crossing the plateau showed a high abundance of small embedded clay and silt bodies that are not covered in the pointwise drillings. These have been interpreted from very low resistivities (0-110 ohmm) situated mostly 0 - 10 meters below the surface. According to ground level measurements executed April 2017 this is above ground water table (Jansson, 2017, unpublished data). In accordance with previous investigations (SWECO, 2013), a more fine-grained soil was distinguished close to B19 (profile 4, figure 6.11).

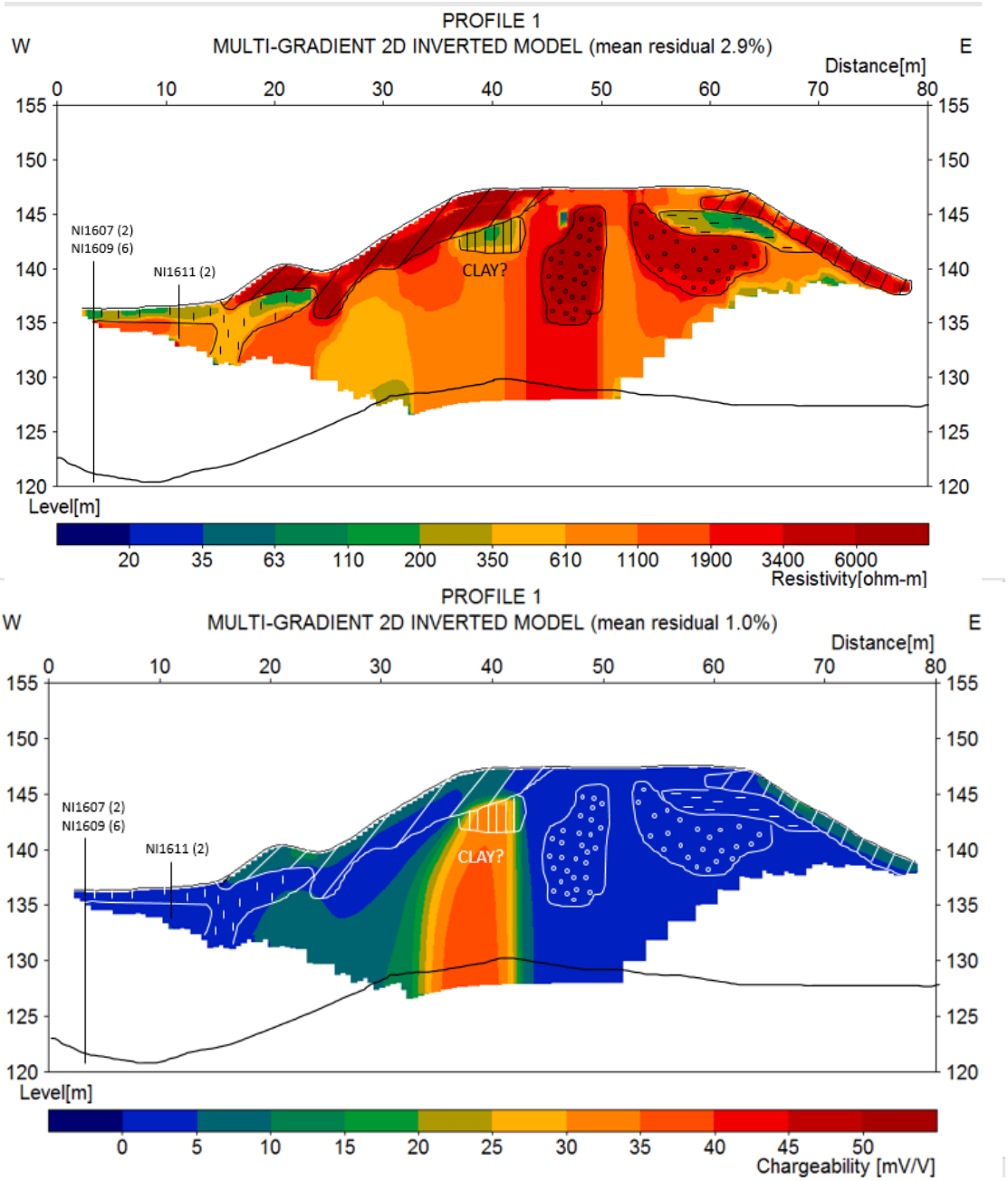

PROFILE 1

Interpretation:

- Coarse filling material
- Sand and gravel
- Clay, silt and sand
- Fine grained soil and organic matter
- Clay and silt

Figure. 6.9. Resistivity and IP result for profile 1 (furthest south on the plateau). Interpolated bedrock surface shown as continuous black line and interpreted geology marked according to system on right hand side. Position for geological and chemical reference data marked as vertical black lines. Name of sample presented above together with offset to profile (meters) within brackets.

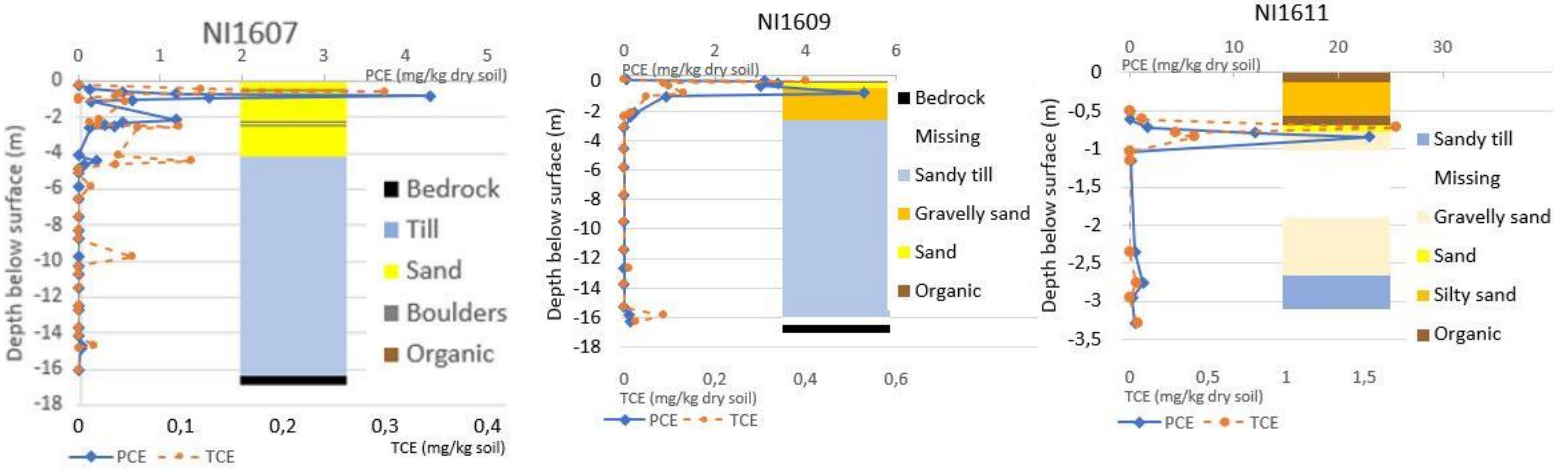

Figure. 6.10. Geological and chemical reference data in the proximity (offset < 10 meters) of profile 1. Illustrations are based on previous drillings and samplings at the contaminated site (Nilsson, 2017, unpublished data).

PROFILE 4

(Continuing next page)

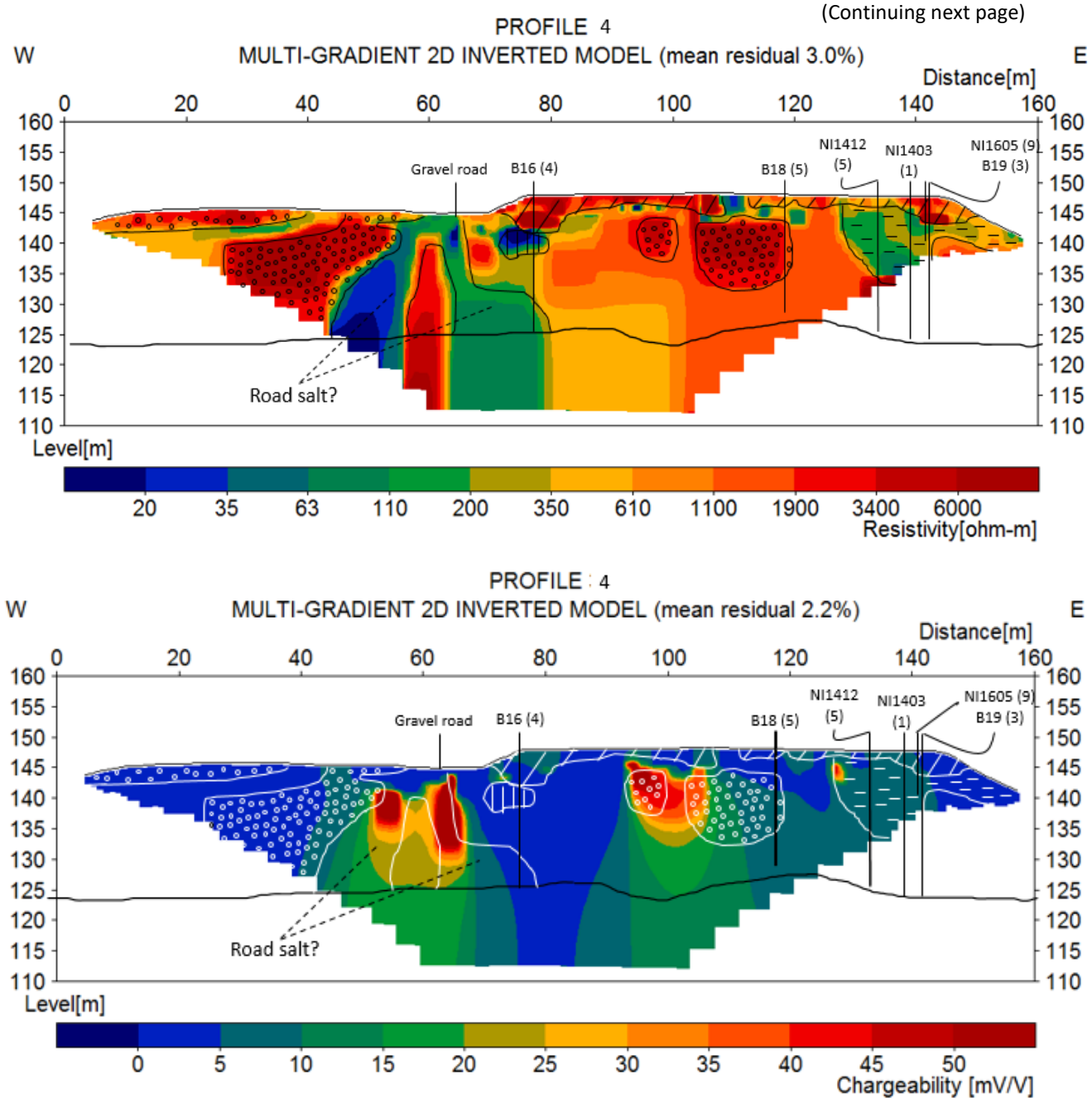

Figure 6.11. Resistivity and IP result for profile 4, multi-gradient array (intersecting well B19). Interpolated bedrock surface shown as continuous black line and interpreted geology marked according to system at the bottom. Position for geological and chemical reference data marked as vertical black lines. Name of sample presented above together with offset to profile (meters) within brackets.

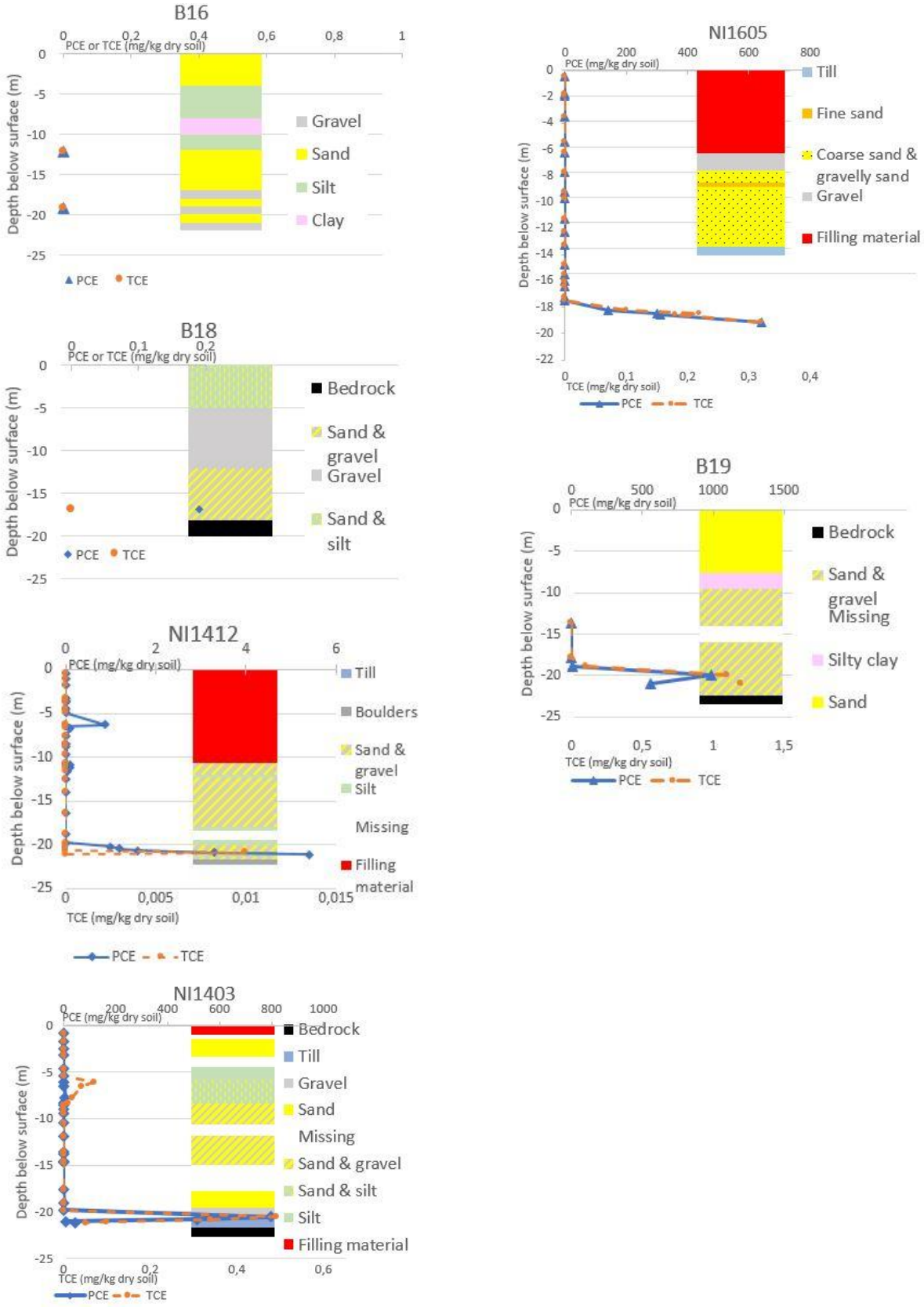

Figure 6.12. Geological and chemical reference data in the proximity (offset < 10 meters) of profile 3. Illustrations are based on previous drillings and samplings at the contaminated site (Nilsson, 2017, unpublished data).

All four profiles going over the plateau (1-4) showed a low resistivity body at a depth of 5-10 meters in the western portion of the plateau. These anomalies are interpreted as a continuous layer of clay and silt rich sand going south to north. It is seen in both the most southern and northern profile (profile 1 and 4).

Only by looking at the resistivity measurements it is difficult to identify soils with clay. The IP response differs among the low resistivity areas interpreted as more clay and silt rich bodies. The reason for this could be due to the fact that the relationship between chargeability and clay content is non-linear. Chargeability peaks at a clay contents of 3- 8 % (Slater & Lesmes, 2002), thus some clay lenses might not show an IP-effect.

On the west side of profiles 2 - 4 there are resistivity and IP animalities that traverses in south-north direction on all profiles (figure 6.7 and 6.8). The location of the low resistivity and high chargeability anomalies are underneath a small gravel road that crosses the study area. It has been confirmed from Hagfors municipality that de-icing salts have been applied during winter 2016/2017. Since salt increases the groundwater conductivity it could hence explain the decreased resistivities and IP-effect (Dahlin & Leroux, 2006). An alternative explanation is that the road is built on finer material.

Profile 5 (east creek)

The only section where the bedrock is clearly visible is in the pole-dipole data for profile 5 that runs along Örbäcken in the east creek (figure 6.13). The bedrock has been interpreted as two high resistivity zones with a low resistivity zone in between. This could indicate presence of a fracture or depression in the bedrock. Previous drillings have detected a bedrock depression east on the plateau south of B19 (SWECO, 2013) which is in the proximity of the suspected fracture/depression seen in profile 5. Above the bedrock, the soil is dominated by finer grain sizes and organic matter.

Profile 6 and 7 (northern part of plateau)

The former railway station was situated at the northern part of the survey area where profile 6 and 7 are located. Previous drillings have indicated a more homogenous geology in this area compared to the southern part. According to drillings the homogenous subsurface consists of sand and gravel. In the ERT profiles 6 and 7 (Appendix F) the coarse soil has been interpreted as a high resistivity zone from the surface to the interpolated bedrock. As seen in figure 6.7 the resistivity is higher in the northern part of the plateau compared to the southern part.

Local zones with low resistivities and increased chargeability were observed in both profile 6 and 7 at a depth of 5 - 10 meters (Appendix F). Since these anomalies are situated above the expected groundwater level they are not considered as caused by pollutants. A transition between higher and lower resistivites at a depth of 5 meters was also detected by the DUALEM (Appendix E). Additionally, the GPR-lines measuring parallel to profile 6 and 7 detected a reflecting layer at a depth of approximately 5 meters (Appendix H). The coinciding results from the ERT, DUALEM and GPR have been interpreted as if there is a silt and clay rich layer appearing in the northern part of the study area at a depth of approximately 5 meters. This layer has most probably been missed by the sparse drillings in the northern part.

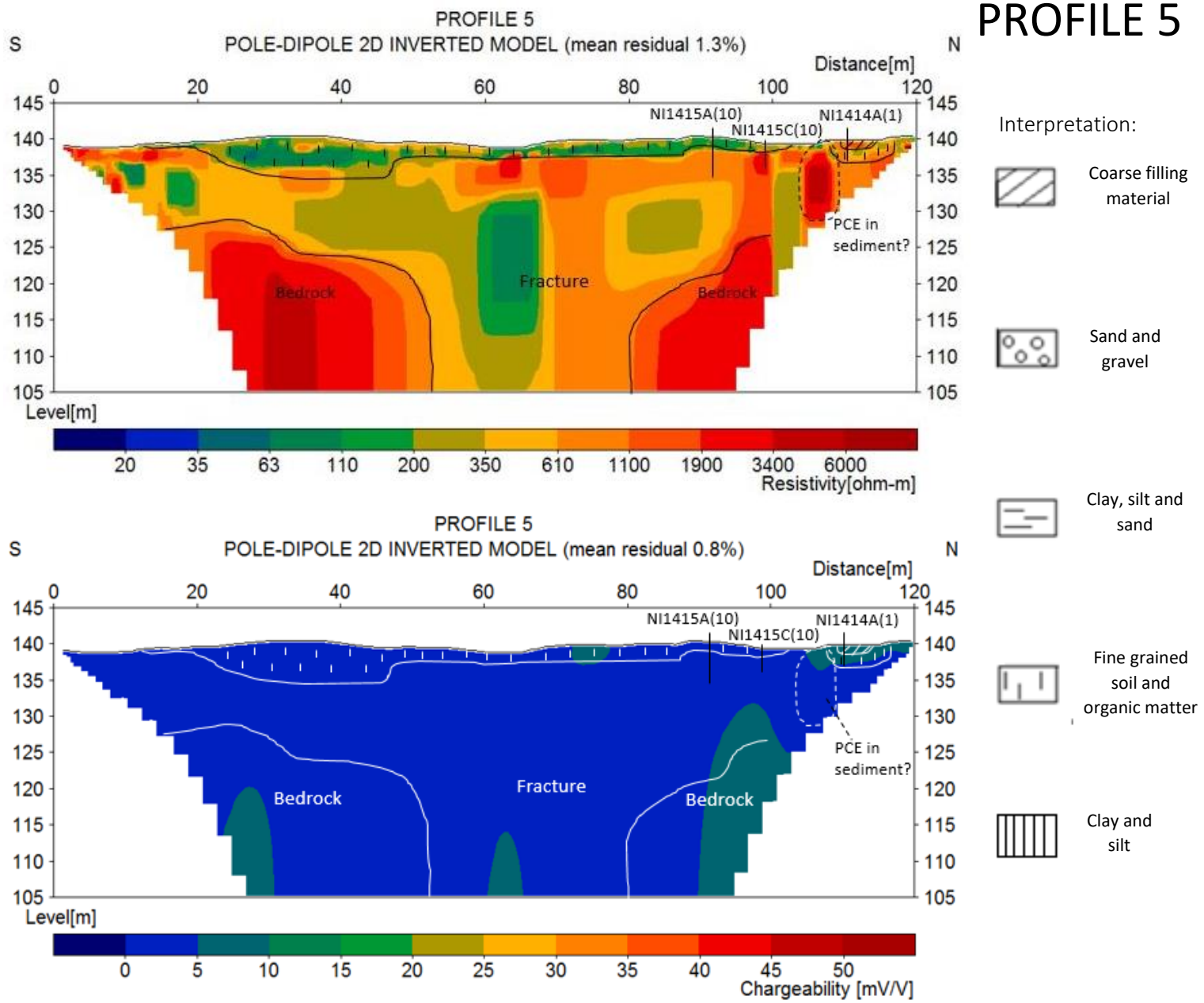

Figure 6.13. Resistivity and IP result for profile 5 in east creek. Interpreted geology marked according to system at right hand side. Position for geological and chemical reference data marked as vertical black lines. Name of sample presented above together with offset to profile (meters) within brackets. Note! Compared to other profiles the bedrock is interpreted from resistivity and not interpolated from bore holes.

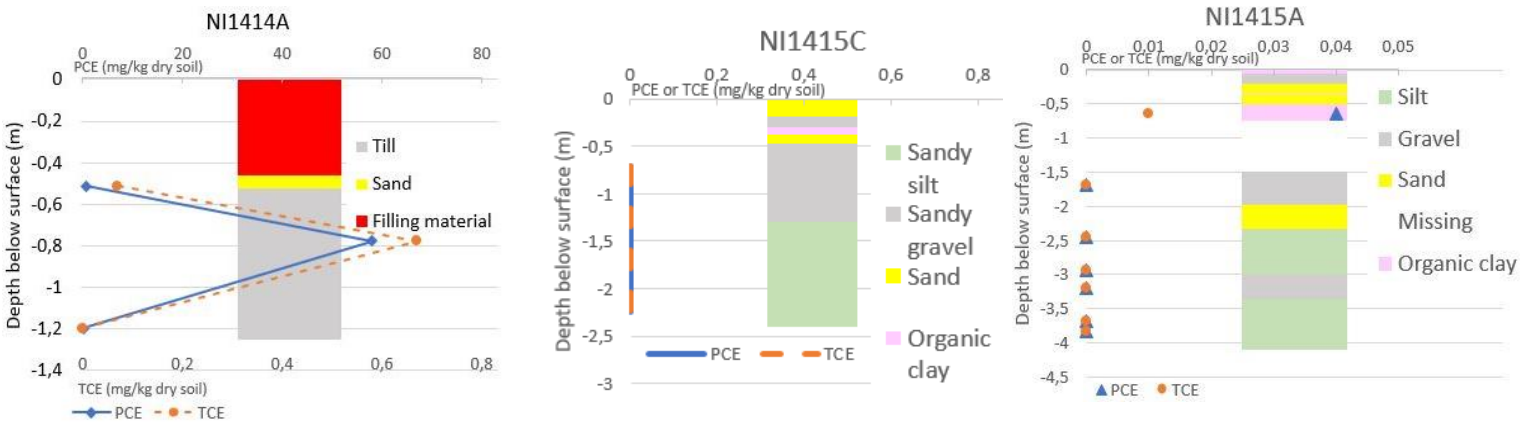

Figure 6.14. Geological and chemical reference data in the proximity (offset < 10 meters) of profile 5. Illustrations are based on previous drillings and samplings at the contaminated site (Nilsson, 2017, unpublished data).

6.2.2 Interpretation of pollutant situation

The work with interpreting anomalies in resistivity and chargeability as caused by pollutants have been done with carefulness since many parts of the studied site are not covered by geological and chemical sampling and the subsurface is characterized by inhomogeneous geology influenced by human activities. In a more homogenous subsurface it might have been easier to distinguish an unexpected anomaly not explained by geology.

While resistivity reflected differences in geological changes such as grain size, the chargeability did not vary with the same extent between different geological layers or structures. The IP result was however used more when interpreting the spreading of pollutant.

Free phase PCE usually occurs at the source since it is characterised by high concentrations. According to a study performed by S. Johansson et al. (2015) the expectations were to have high resistivities and absent IP response at the source. Residual phase and/ or degradation zone is usually expected in the outskirts of the source or in the groundwater plume where the concentration is suspected to be lower. The IP response for a residual phase was expected to increase while the resistivity was expected to decrease (Johansson, et al., 2015).

However, in reality the IP and resistivity response is complicated by environmental factors such as water saturation or microbial degradation that changes oxygen level and releases ions (Johansson, et al., 2015). The interpretation of IP as caused by pollutants was further complicated since a response for a residual phase or degradation zone might be similar the IP-response of clays and organic matter.

To distinguish the cause of IP-effects, anomalies above the groundwater table (situated 0 - 10 m below ground level) were interpreted as clays or man-made metallic objects. This was due to that DNAPLs are mostly transported at the bedrock by the gravity since they have a higher density than water. Additionally, the magnetic survey showed that the area had a highly varied magnetic field at shallow depths probably caused by man-made metals in the ground or different metallic minerals. These objects are also able to create IP-effects.

Indications of the presence of PCE and degradation products

In profile 4, 6 and 7 indications of the presence of DNAPLs at B19 and in the groundwater plume from the main source have been observed. However, it has not been possible to detect any clear evidence of the presence of PCE in the groundwater plume from B19 by using ERT and IP measurements. The directions of the main and secondary groundwater plume are seen in figure 2.5 in section 2.4 *Hydrogeology*.

At well B19 in the pole-dipole data for profile 4 (figure 6.15) it is seen from geological reference data (figure 6.12 presented above) that the bottom layer consists of gravel and sand. However, a low resistivity anomaly is seen in the deeper parts of well B19 that does not correspond to the geology. The same zone has an increased IP-effect. These results do not correspond to the expected high resistivity and absent IP response for free-phase DNAPLs in a source zone. The results might however be created if the outer part of the source with free-phase DNAPLs exists as a residual phase and/or degradation zone. That degradation is occurring in the source is strengthened by chemical soil and groundwater samplings that show moderate concentrations of the degradation product TCE in B19 (Nilsson, 2017, unpublished data). Enhanced concentrations of dissolved iron, copper and chloride ions have also been detected (Åkesson, 2017, unpublished data). Dissolved iron is an indication of reduced environment (low oxygen levels) that enhances reductive dechlorination of PCE. An outer zone with high concentration of dissolved ions and PCE in residual phase could cause a lowering of resistivity and an increase of chargeability which are seen in profile 4 (figure 6.15). However, it should be mentioned that the data

residuals are high for the pole-dipole array for profile 4 where the secondary source is detected (13.0 % for resistivity and 11.6 % for IP).

The profile also contains squared shaped artefacts from the inversion.

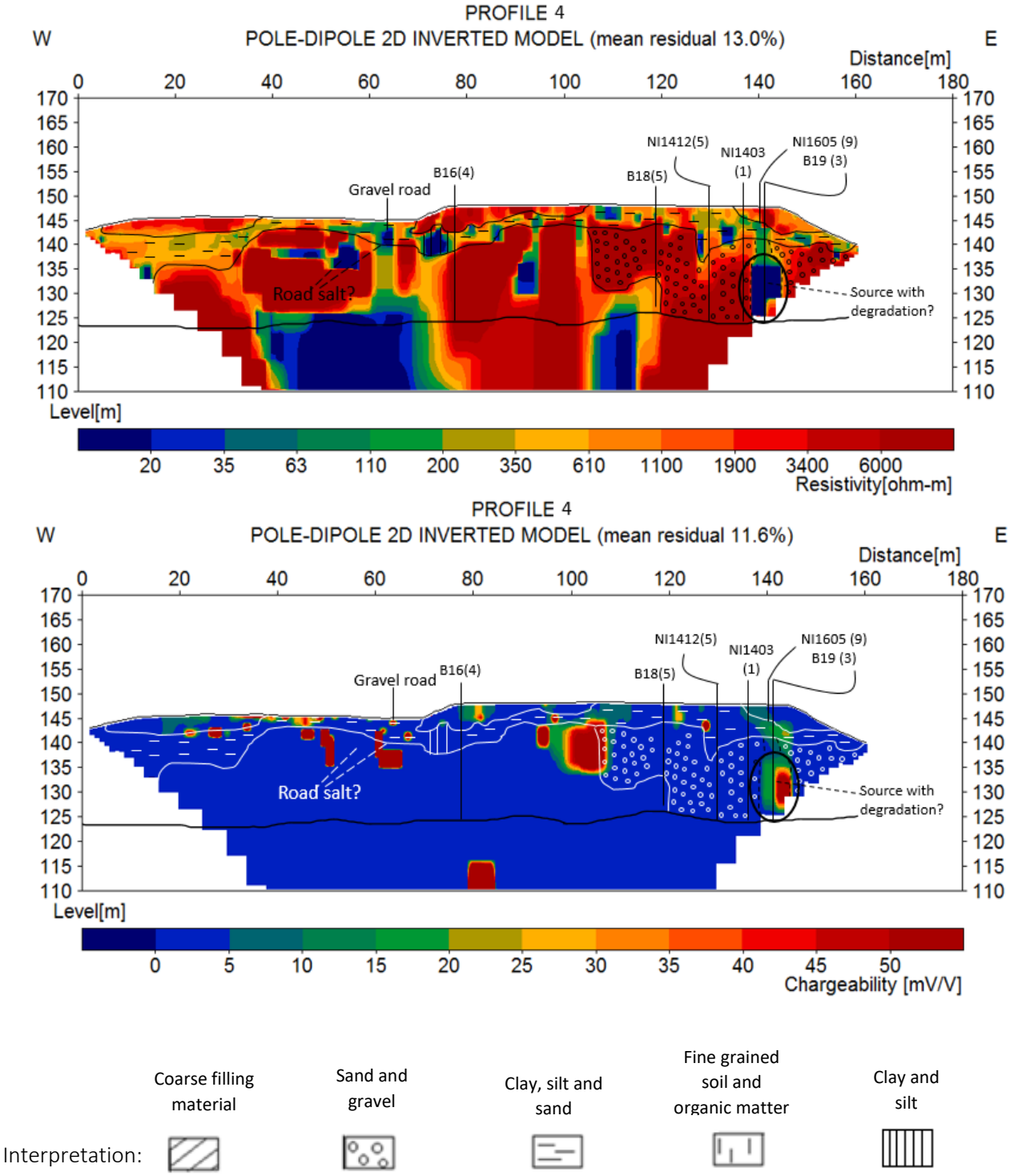

Figure 6.15. Resistivity and IP result for profile 4, pole-dipole array (intersecting well B19). Interpolated bedrock surface shown as continuous black line and interpreted geology marked according to system at the bottom. Position for geological and chemical reference data marked as vertical black lines. Name of sample presented above together with offset to profile (meters) within brackets.

As mentioned in section 6.2.1 *Interpretation of the geology*, low resistive areas at a depth of 5 – 10 meters where discovered in the northern part of the study area. Since they are located above the expected groundwater level, they were considered as caused by silt and sand rather than caused by pollutants. However, a low resistive zone is appearing close to the bedrock in both profile 6 and 7. Figure 6.16 displays the resistivity and IP for profile 7, which is the profile where the anomalies are best seen. However, the mean residual of 15 % is high but the same resistivity and IP features where seen in both arrays for profile 6 and 7 (Appendix F). Since DNAPLs are insoluble in water and have a high density, they are expected to travel in the same direction as the slope of the bedrock. The low resistivity anomaly in profile 6 and 7 is placed at the bedrock and coincides with the location of the suspected groundwater plume from the main source (SWECO, 2013). Hence, the anomaly could be caused by a plume migrating from the main source upstream. The low resistivity and slightly increased chargeability would indicate a residual phase of PCE containing degradation products. This is partly supported by low concentrations of PCE and TCE detected in wells downstream Profile 6 and 7 (wells NI1501 in figure 2.7 and 2.8 in section 2.5 *Pollutant situation* and well B29 in Appendix B*).*

However, it is also possible that the low resistive area close to the bedrock is caused by the silt and clay rich layer that extends further down than 5 – 10 meters as indicated by DUALEM and GPR. In order to find the cause of the low resistive area, it is suggested to perform geological drillings in the area or execute chemical sampling.

In profile 5 that was measured along Örbäcken in the east creek a high resistivity zone stretching down from the top sediments was seen in the northern part (figure 6.13 presented above). This has been interpreted as a possible zone of PCE resting in the sediments of the stream and the reason for this is further discussed in section 7. *Discussion.*

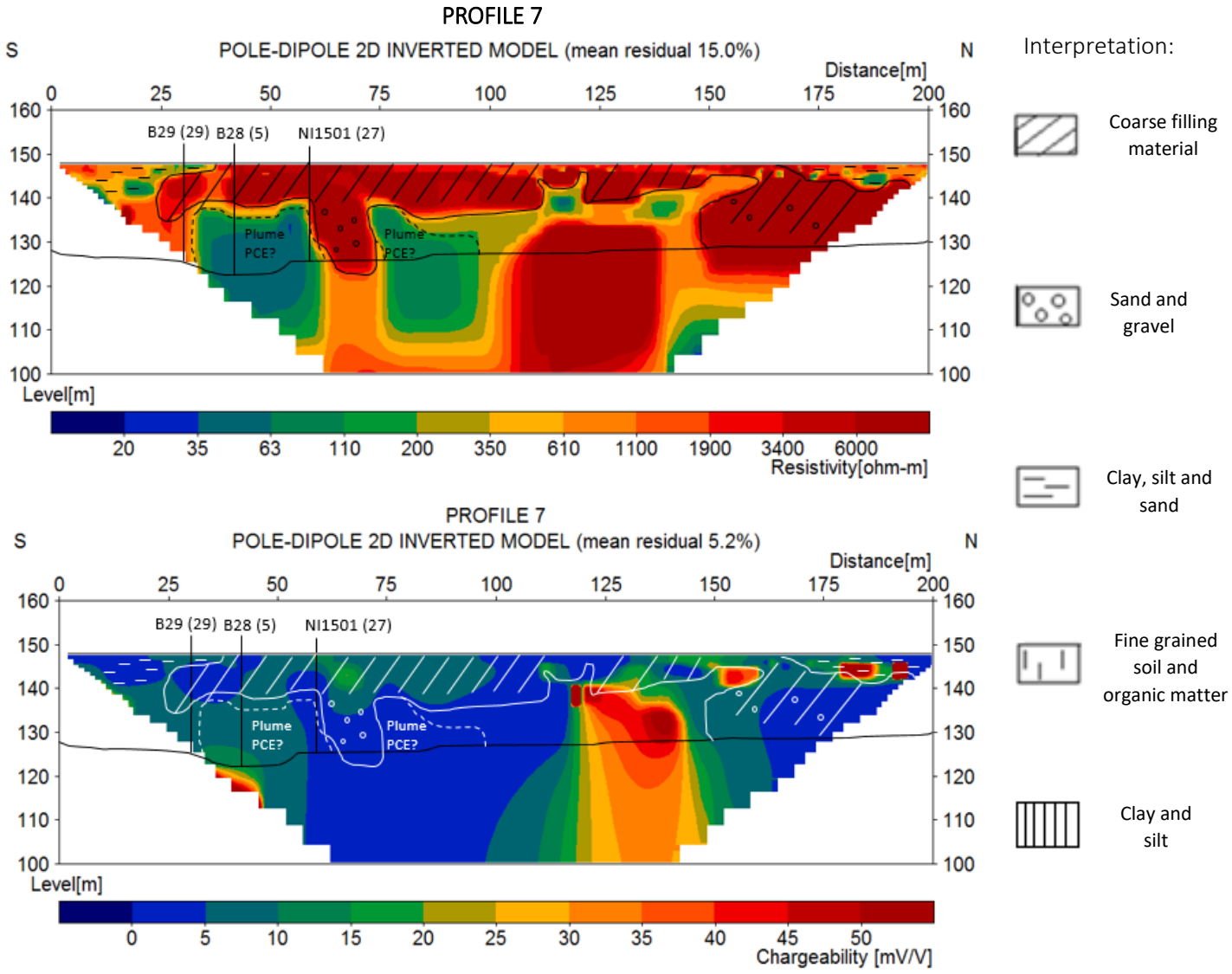

Figure 6.16. Resistivity and IP result for profile 7. Interpolated bedrock surface shown as continuous black line and interpreted geology marked according to system at the right-hand side. Position for geological and chemical reference data marked as vertical black lines. Name of sample presented above together with offset to profile (meters) within brackets.

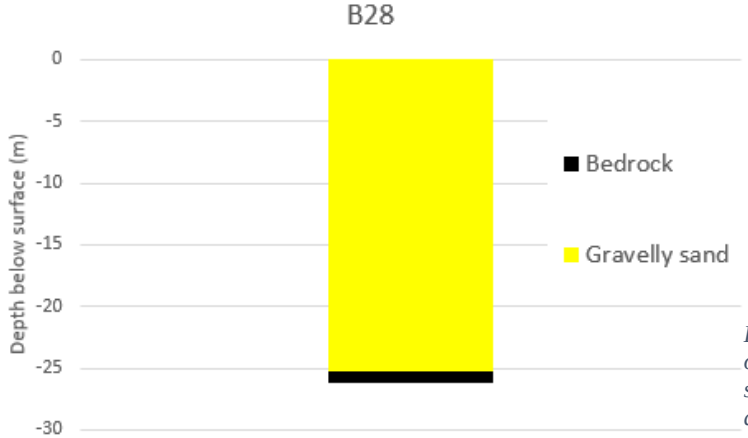

Figure 6.17. Geological data in the proximity (offset < 10 meters) of profile 7. Illustrations are based on previous drillings and samplings at the contaminated site (Nilsson, 2017, unpublished data).

7. Discussion

The main aim with performing ERT and IP was to identify geological features, man-made structures and investigate if it was possible to locate source of contaminant, degradation zones and groundwater plumes of PCE. By using ERT and IP it was possible to locate the secondary source close to the bedrock at well B19 and see indications of that degradation occurs in the outer part of the source zone. Even though the concentration of degradation products is relatively low (about 1.2 mg TCE/kg dry soil) it has been shown from a previous study by Johansson et al. (2015) that concentrations of cis-DCE of 0 - 22 mg/kg dry soil give a response in frequency domain IP. Even if this study used time-domain IP, the anomalies in IP and ERT at the secondary source are similar to the results that Johansson et al. (2015) interpreted as a degradation zone.

In the profiles downstream the main source at the dry-cleaning facility, indications of a PCE plume following the bedrock was observed. However, there are several possible explanations for this low resistive body. The GPR-profile going parallel with ERT-profile 6 shows a layer on 6-7 meters depth that coincide with the position of the low resistive body. The layer could correspond to the groundwater or finer material that reduces the resistivity. The DUALEM survey in the northern part of the plateau shows that there is a transition from higher to lower resistivity around 5-6 meters below surface.

The PCE plume from the secondary source was not possible to detect. Since the yearly load of measured PCE to Örbäcken is very high it was expected to find evidence of pollutants also in the direction of groundwater flow from B19. Either the concentrations are too low to affect the ERT and IP measurements, or the complicated geology makes it hard to identify an anomaly as caused by the PCE plume. Since the groundwater flows are high, it is possible that PCE has been out-washed in the coarse soil during a longer period of time. The high resistive zones seen at the bedrock in the middle of the plateau in profile 3 (Appendix F) could be indications of a plume with free-phase PCE (high resistivity and no chargeability) however the circumstances are too uncertain to draw conclusions.

It was also of interest to investigate if geophysical methods could contribute with a better understanding of the pollutant situation and geology at the site compared to previous traditional surveys with drilling and chemical sampling. Regarding the geology an important insight from the geophysical surveys is that there is more mixing between natural geology, man-made structures and contaminant than expected. For example, the top 10 meters showed objects with sharp boundaries and high contrast to the surrounding indicating man-made influences in the natural geology. Resistivity and IP measurements were also able to interpret the extent of previous detected local clay and silt-rich bodies, supporting a heterogeneous geology. A better mapping of silt and clay rich areas is of high importance since it contribute to a better understanding of potential traps of PCE that could work as sources through back-diffusion. It has been seen that PCE measured from chemical sampling coincides with low resistive bodies (clay and silt-rich) in the top soil at the secondary source and in the east creek. Unfortunately, ERT and IP survey contributed with a limited insight of the bedrock surface. In most profiles, the bedrock could not be detected since the depth of investigation often was shallower than the expected bedrock surface. However, indications of an undiscovered and larger depression or fracture in the bedrock down in the east creek where detected with ERT.

Previous surveys in the area have not paid much attention to the east creek. Here few drillings and chemical samplings have been done. However, if the old water pipe that leached process water from the dry-cleaning facility continued eastwards beyond well B19 and discharged in Örbäcken, PCE might still be resting in the stream sediment. PCE has been detected in the creek and below the suspected spot where the leaking pipe discharged (figure 6.14, well NI1414 A). If

this is the case, this might be the cause of the high resistivity zone seen in profile 5 (figure 6.13). As mentioned above, the results indicated that a larger depression or fracture exists in the creek. If PCE has been released into the creek by the water pipe it has probably followed the bedrock and been trapped in the depression/fracture. This could act as a long-term source of PCE release, contributing to the high measured concentrations in Örbäcken further downstream.

Regarding the pollutant situation, some conclusions from previous investigations are supported by ERT and IP. However, the geophysical methods contributed with sparse new information of the pollutant spreading. This was mostly due to difficulties and uncertainties when it comes to interpreting the result as caused by pollutants or geology.

With the current knowledge with applying ERT and IP on sites polluted with DNAPLs our opinion is that the method is more suitable for contaminated areas where the geology is less varied and anomalies caused by PCE easier could be distinguished. However, even though the interpretation is difficult at inhomogeneous sites such as Hagforstvätten, ERT and IP are good complements to drilling and chemical sampling since they are able to detect areas of interest that otherwise might have been missed with pointwise measurements. We think that the area has potential of applying ERT and IP measurements in the future, especially for monitoring high PCE concentrations at the secondary source.

8. Conclusions

This study was conducted at Hagforstvätten and succeeded to locate the secondary source at B19 as a degradation zone of PCE by using the geophysical methods ERT and IP. This zone was indicated by low resistivities and high chargeabilities. The expected groundwater plume containing DNAPLs from the secondary source was not detected. Either the concentrations are too low to affect the ERT and IP measurements, or the inhomogeneous geology makes it hard to identify an anomaly as caused by the PCE plume. In the groundwater flow direction from the main source a zone of low resistivity and slightly higher IP body along the bedrock have been detected. This could origin from a PCE plume containing degradation products (seen in chemical reference data) or a clay and silt-rich body (detected in the GPR-survey).

Regarding the pollutant situation, it has been possible to confirm some of the conclusions from previous investigations by using ERT and IP. However, in general the geophysical methods contributed with sparse new information of the pollutant spreading. This was mostly due to that the number of wells in the proximity of the profiles was unsatisfactory to be able to interpret with high certainty which anomalies that were caused by geology, man-made structures or pollutant. The geophysical survey including GPR, DUALEM, magnetic gradiometer, ERT and IP concluded that the site has very varied geology and man-made structures. This made the interpretation of resistivity and chargeability in areas with sparse reference data uncertain.

Compared to previously performed traditional methods with drilling and chemical sampling, the ERT and IP measurements could in more detail describe the extent of previously detected local clay and silt-rich bodies. It is of high importance to know the extent and location of these bodies since they can sustain high groundwater concentrations of PCE due to back-diffusion even though the source is remediated. Additionally, the ERT results showed indications of an undiscovered and larger depression or fracture in the bedrock below the creek east of the secondary source. If process water from the dry-cleaning has been discharged into the creek the depression could act as a long-term storage of PCE. The geophysical survey including GPR, DUALEM, magnetic gradiometer, ERT and IP concluded that the plateau is very inhomogeneous with local variations in geology and man-made conductive objects. How much of the area that is actually man-made was not possible to determine.

It is our opinion that it is a challenge to locate pollutants by using ERT and IP at inhomogeneous or less well-known subsurfaces. Even though the interpretation is difficult at inhomogeneous sites, ERT and IP are good complements to drilling and chemical sampling since they increase the understanding of the area and how the pollutants can be spread or stored in the subsurface. Since the methods provide continuous data sampling they can detect areas of interest that otherwise might have been missed with pointwise measurements. We think that the area has potential of applying ERT and IP measurements in the future, especially for monitoring high PCE concentrations at the secondary source.

It is highly important to continue to work towards a better understanding of the hydrogeology and pollutant situation at the site. The highest concentration of PCE that have been measured exceeds the threshold value recommended by SEPAs (mentioned in section 3.5 *Threshold values*) more than hundred times. Even if the high contamination was caused by the past, it is the responsibility of present generations to preserve a healthy and sustainable environment for humans and ecosystems in the future.

9. Recommendations

Our opinion is that Hagforstvätten has potential of applying ERT and IP measurements in the future, especially for monitoring high PCE concentrations at the secondary source. If future investigations with ERT and IP should be performed, there are a few recommendations that should be considered.

The southwest part of the plateau could be complemented with a few more drillings and chemical sampling to investigate the cause of the large high resistive zones appearing in profile 1, 2 and 3 (Appendix F). It is suspicious with a continuously high resistive layer in the flow direction from B19. The same investigations should be applied to the northern part of the plateau where more information is needed to find out if the low resistive area close to the bedrock is caused by silt and clay or pollutants from the main source. A drilling in the east creek to confirm the bedrock depression is also recommended. If an in-situ remediation of the secondary source is to be monitored in the future, an additional profile should be placed going from south to north and crossing B19 in the middle to increase the resolution in the deeper parts of the secondary source where the measured PCE concentration is the highest.

Generally, the background resistivities above and below the groundwater table at the plateau are very high (> 6000 Ohmm) which is unexpected for wetted unconsolidated sediments. This phenomenon is particularly seen in profile 6 and 7 (Appendix F), and it has not been able to explain the cause of it. However, it is important to investigate these results more in order to increase the understanding of the hydrogeology at the site.

10. References

ABEM Instrument AB, 2016. *User Manual Terrameter LS 2.* Sundbyberg: ABEM Instrument AB.

Annan, A., 2009. Electromagnetic principles of Ground Penetrating Radar. In: *Ground Penetrating Radar Theory and Applications.* s.l.:Elsevier, pp. 3-40.

Anon., 2010. *Res2dinv ver 3.59 Rapid 2-D resistivity and IP inversion using least-squares method.* s.l.:Geotomo software.

Bjergsted Pedersen, J., 2017. HydroGeophysicsGroup Aarshus University. 2017-05-08. Unpublished data.

Burger, R., Sheehan, A. & Jones, C., 2006. *Introduction to Applied Geophysics.* New York, London: W.W Norton & Company.

Dahlin, T., Larsson, R., Leroux, V., Svensson, M. & Wisén, R., 2001. *Geofysik i släntstabilitetsutredningar*, Linköping: Statens Geotekniska Institut.

Dahlin, T. & Leroux, V., 2006. Time-lapse resistivity investigations for imaging saltwater transport in glacioflucial deposits. *Environmental Geology*, Volume 49, pp. 347-358.

Dahlin, T. & Leroux, V., 2012. Improvements in time-domain induced polarisation data quality with multi-electrode systems by seperating current and potential electrodes. *Near Surface Geophysics*, Volume 10, pp. 545-565.

Dualem, no date. *DUALEM Products.* [Online]
Available at:
http://www.dualem.com/products.html
[Accessed 2017 03 30].

Englöv, P. et al., 2007. *Klorerade lösningsmedel - identifiering och val av efterbehandlingsmetod.* [Online]
Available at:
http://www.naturvardsverket.se/Documents/publikationer/620-5663-8.pdf?pid=3273
[Accessed 2017 03 02].

Hedenström, A., 2012. Map of the quaternary deposits 12 12D Uddeholm SO, scale 1:100 000. Sveriges Geologiska Undersökning. K 421.

Jansson, R., 2017. Lund University. 2017-06-01. Unpublished data.

Johansson, S., Fiandaca, G. & Dahlin, T., 2015. Influence of non-aqueous phase liquid configuration on induced. *Journal of Applied Geophysics*, pp. 295-309.

Lantmäteriet, 2009. *GSD-Höjddata, grid 2+.* [Online]
Available at: https://zeus.slu.se/get/?drop=
[Accessed 2017 03 31].

Lantmäteriet, 2015. *GSD-Ortofoto, färg med 0,5 m upplösning.* [Online]
Available at: https://zeus.slu.se/get/?drop=
[Accessed 2017 06 25].

Lantmäteriet, 2017. *Ekonomisk karta över Sverige (12 D Uddeholm 1g Hagfors).* [Online]
Available at:
https://etjanster.lantmateriet.se/historiskakartor/s/show.html?showmap=true&archive=RAK&sd_base=rak2&sd_ktun=52414b5f4a3133332d31324431673639&archive=RAK
[Accessed 2017 06 09].

Loke, M. H., 2016. *Tutorial : 2-D and 3-D electrical imaging surveys.*

Lundegård, P., Lindh, A & Gorbatschev, R., 1992. Map of the bedrock geology of Värmland county, scale 1:125 000. Uppsala: SGU. Sveriges Geologiska Undersökning. Ba 45.

Milsom, J. & Eriksen, A., 2011. *Field Geophysics.* John Wiley Sons.

Månsson, C.-H., 2016. *DCIP-undersökning av nedlagd kemtvätt, Hagfors,* Göteborg: Tyréns.

Naturvårdsverket, 2017. *De flesta förorenade områdena är kända.* [Online]
Available at:
http://www.naturvardsverket.se/Sa-mar-miljon/Mark/Fororenade-omraden/
[Accessed 2017 02 21].

Nilsson, F., 2017. NIRAS. 2017-02-27. Unpublished data.

Olsson, P.-I., Dahlin, T., Fiandaca, G. & Auken, E., 2015. Measuring time-domain spectral induced polarization in the on-time: decreasing acquisition time and increasing signal-to-noise ratio. *Journal of Applied Geophysics,* Volume 123, pp. 316-321.

Palacky, G., 1987. *Resistivity characteristics of geologic targets, in Electromagnetic methods in applied geophysics, ed. M.N. Nabighian, Soc. Of Expl. Geoph., Tulsa, s 53 – 130.*

Parker, B., Chapman, S. & Guilbeault, M., 2008. Plume persistence caused by back diffusion from thin clay layers in a sand. *Journal of Contaminant Hydrology,* Volume 102, pp. 86-104.

Pettersson, H., Södergren, S., Back, P-E., Holmqvist, J., Leback, J., Ludvigsson, J., Rolén, S., Törneman, N., Ask, I., Sternbeck, J., 2009. *Riktvärden för förorenad mark - Modellbeskrivning och vägledning.* [Online] Available at: https://www.naturvardsverket.se/Documents/publikationer/978-91-620-5976-7.pdf?pid=3574 [Accessed 2017 03 02].

Reynolds, J., 2011. *An Introduction to Applied and Environmental Geophysics.* Chichester UK: John Wiley & Sons.

RIVM, 2001. *Ecotoxicological Serious Risk Concentrations for Soil, Sediment and (ground)water: Updated proposals for first series of compounds.* [Online] Available at: http://www.rivm.nl/bibliotheek/rapporten/711701020.pdf [Accessed 2017 03 02].

SGU, 2017. *Jordarter 1:25000 – 1:00000.* Acceessed through kartvisaren [Online]. Aviable at: https://apps.sgu.se/kartvisare/kartvisare-jordarter-25-100.html [Accessed 2017-10-01].

Slater, L. D. & Lesmes, D., 2002. Ip interpretation in environmental investigations. *Geophysics,* 67(1), pp. 77-88.

Sparrenbom, C., Åkesson, S., Johansson, S., Hagerberg, D., Dahlin, T., 2016. Investigation of chlorinated solvent pollution with resistivity and induced polarization. *Science of the Total Environment.*

Stads- och kommunhistoriska institutet, 2008. *Hagfors historia.* [Online] Aviable at: http://ortshistoria.se/stad/hagfors/historia [Accessed 2017-10-01]

Styles, P., 2012. *Environmental Geophysics - everything you ever wanted (needed!) to know but were afraid to ask!.* Houten The Nederlands: EAGE.

SWECO, 2013. *Hagforstvätten, huvudstudie,* Karlstad. [Online] Aviable at: http://resource.sgu.se/dokument/samhallsplanering/FO/hagfors/HS-2013-01-25-inkl-bilagor.pdf [Accessed 2016-12-01].

Åkesson, S., 2017. Lund University. 2017-06-10. Unpublished data.

Appendix A – Hydrogeological profiles

The location of the longitudinal hydrogeological profiles for the secondary source at well B19 (section B, see figure 2.4 *in chapter 2.3 Geology*) from (SWECO, 2013). Green lines indicate the width of an esker according to earlier investigations by Sweco. The extent or even the presents of the esker at the site could be questioned since the subsurface deviates from expected glaciofluvial deposits caused by an esker. The orange lines are stormwater pipes from Huvudtvätten to the secondary source.

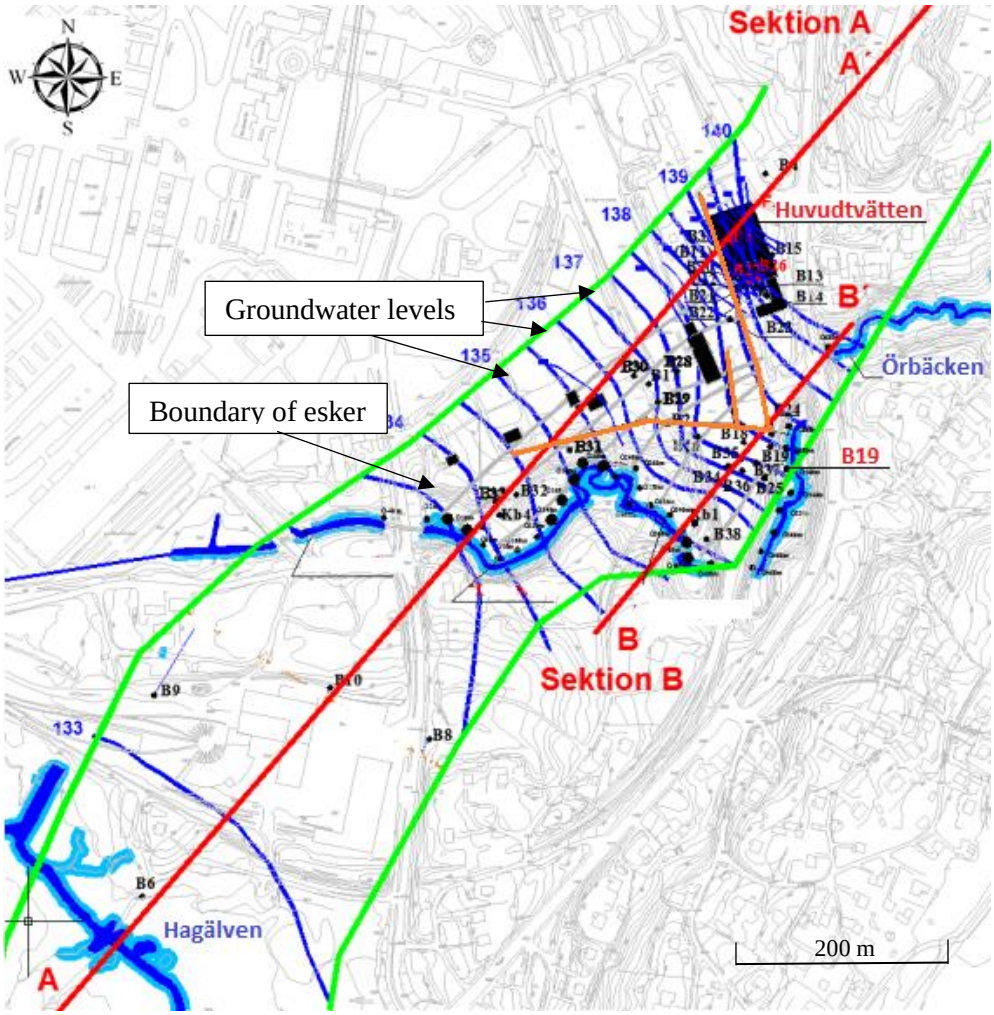

Appendix B - Groundwater sampling of PCE, TCE and ion concentrations

The two figures below show the maximum measured groundwater concentrations of PCE and TCE at the plateau. The dry-cleaning facility is located about 10 meter north of the map. The groundwater sampling was performed by (SWECO, 2013) during 2008-2012 and by (Åkesson, 2017, unpublished data).

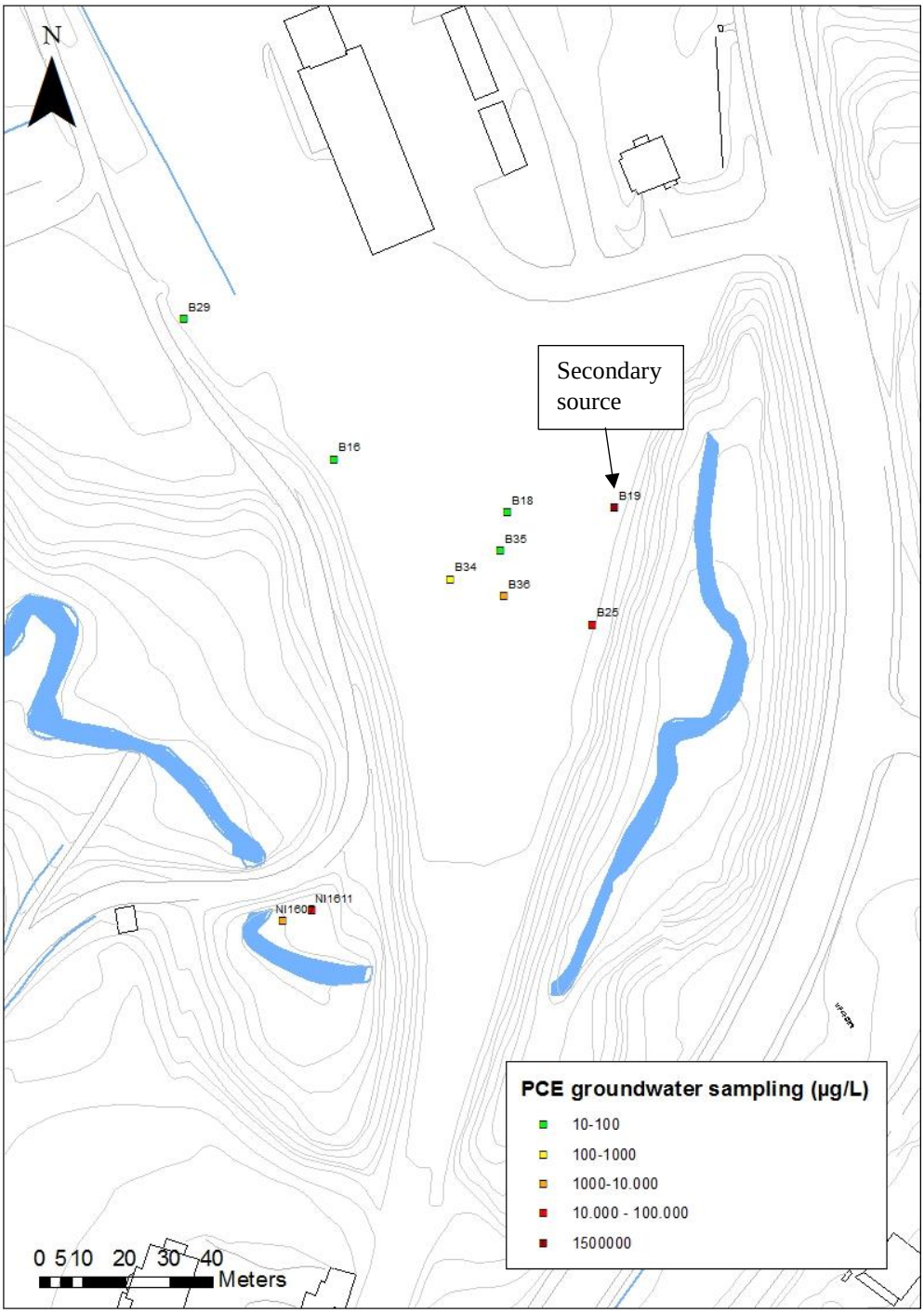

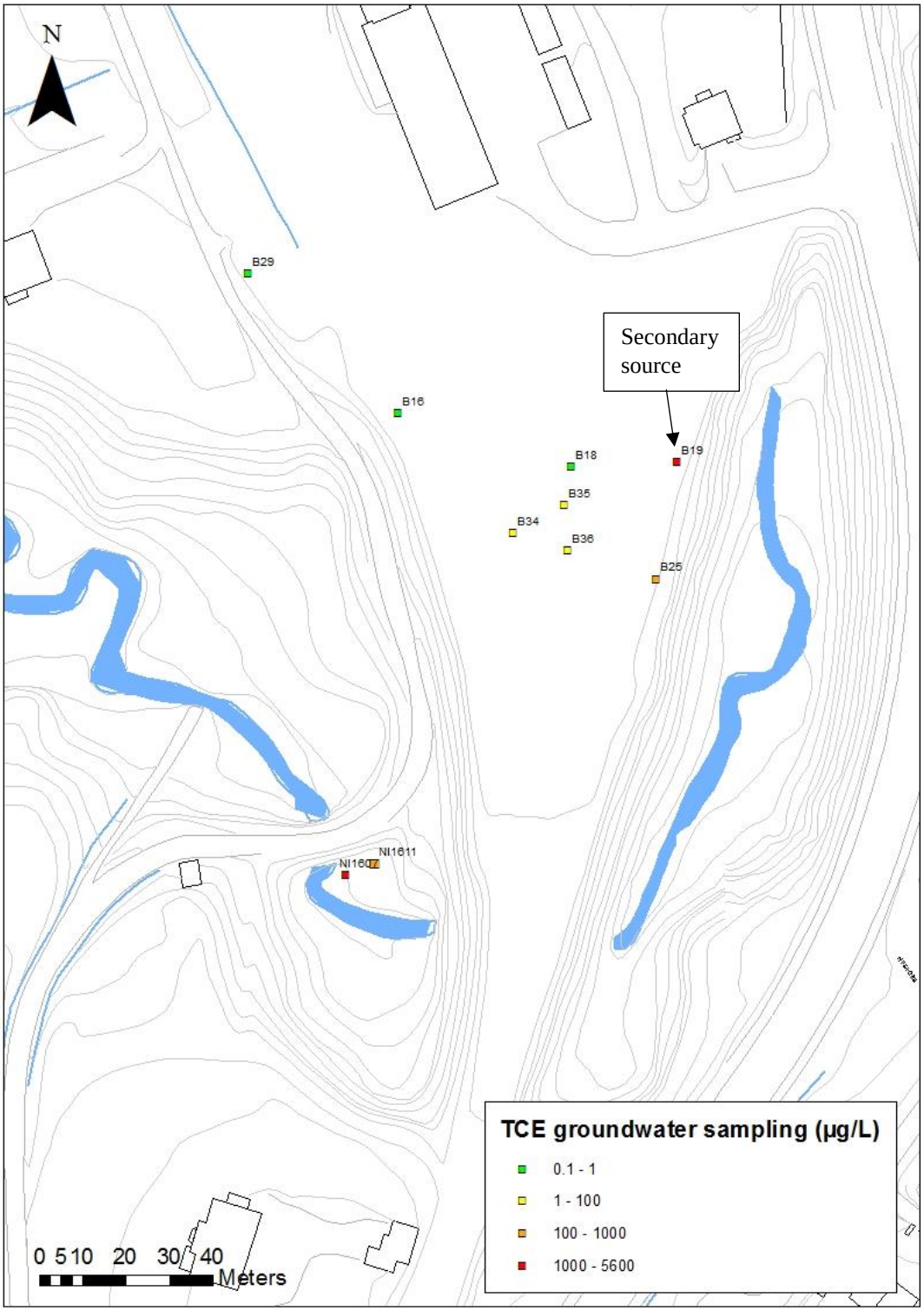
N
B29
Secondary source
B16
B18
B19
B35
B34
B36
B25
NI1611
0 5 10 20 30 40
Meters
TCE groundwater sampling (µg/L)
0.1 - 1
1 - 100
100 - 1000
1000 - 5600

The table below presents groundwater concentrations of PCE, its degradation products and different ions from selected wells that was sampled in April 2017 (Åkesson, 2017, unpublished data).

Well		**NI1607:1**	**NI1607:2**	**NI1607:3**	**NI1611**	**B29**	**B19**
Date		2017-04-25	2017-04-25	2017-04-26	2017-04-19	2017-04-26	2017-04-27
Depth filter	*mbs*	0.61-1.61	3.99-4.99	14.43-15.43	? (Botten)	14.5-15.5	22.07-22.17
Tetrakloreten(PCE)	*µg/L*	10000	29	2100	11000	39	220000
trans-1,2-dikloreten (c-DCE)	*µg/L*	<10	<5.0	<5.0	<10	<0.1	<100
Trikloreten (TCE)	*µg/L*	280	180	1900	220	0,32	1800
Vinylklorid (VC)	*µg/L*	<20	33	<10	<20	<0.2	<200
Klorid, Cl	*mg/L*	15	41	10	12	25	20
Järn, Fe** (syrauppslutet)	*mg/L*	1,6	1,3	5,6	2,3	0,78	86
Järn, Fe** (surgjort)	*mg/L*	0,68	1,2	1,9	0,58	0,29	32
Koppar, Cu (syrauppslutet)	*µg/L*	1,7	<0.5	3,4	3	2	47
Koppar, Cu (surgjort)	*mg/L*	<0.02	<0.02	<0.02	<0.02	<0.02	0,04
EC*	*µS/cm*	338	602	220	296	277	340

*Elktriskkonduktivitet mätt i fält

** Summa järn

Appendix C – Buried pipes and cables

Map on locations of pipes and cables based on information from Geomatikk, ELTEL Networks Infranet AB and Hagforskommun 2017-03-01.

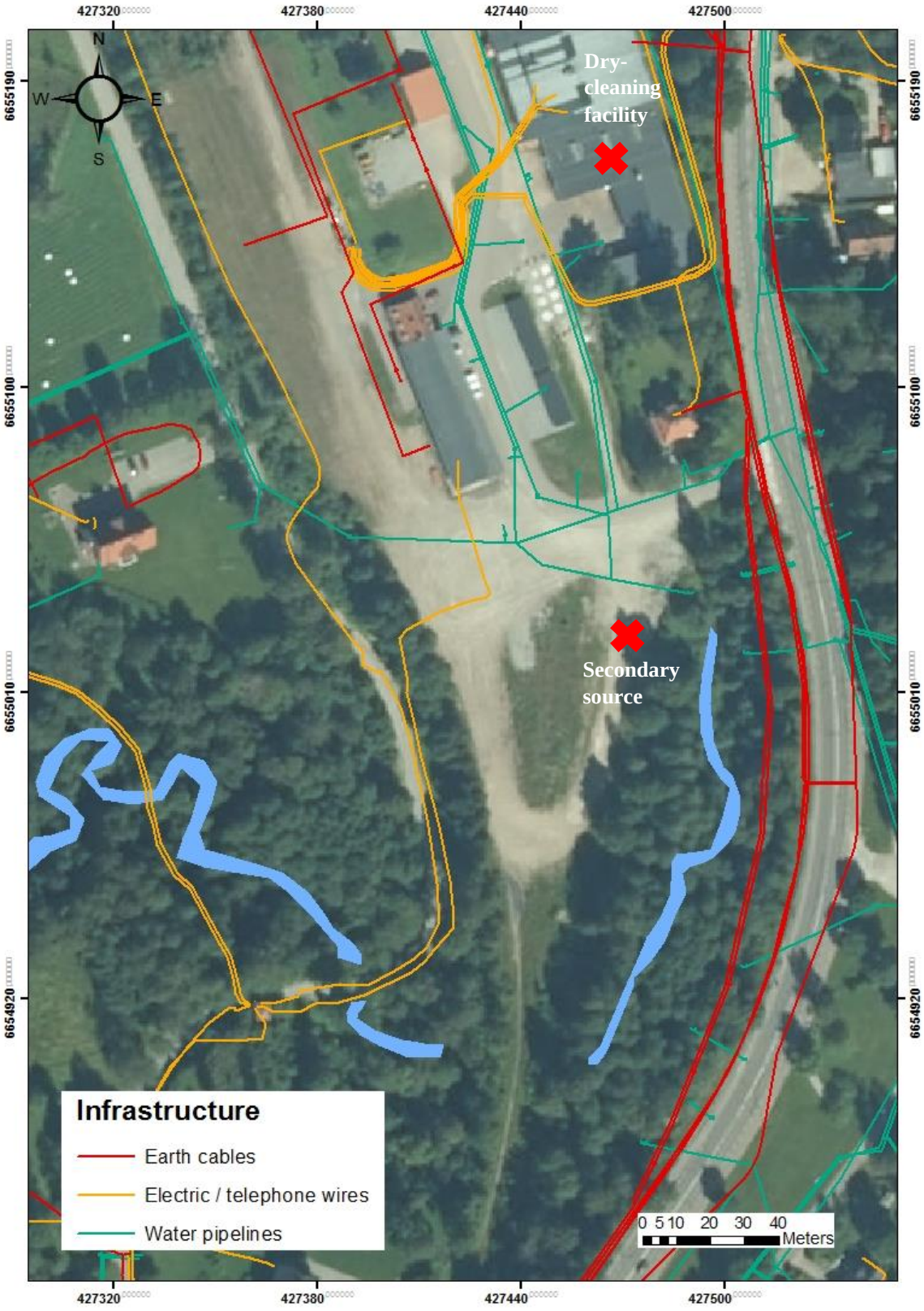

Appendix D – Cable layout

Descriptions of the cable layout and the electrode distance for DCIP-line 1-7 are shown in the table below.

Line	Total number of cables	Cable take-out spacing (m)	Shifting* (m)	Electrode distance (m)	Total number of electrodes	Total profile length (m)
1	2*2	2	1	1	82	81
2	4*2	2	1	1	162	161
3	4*2	2	2	2	82	162
4	4*2	2	2	2	82	162
5	3*2	2	1	1	122	122
6	2*2	5	2.5	2.5	82	202.5
7	2*2	5	2.5	2.5	82	202.5

The cable layout of line 1 is seen below. The cables had 2 meter take-out spacing, and when one of the cables were shifted 1 meter it means that the electrode distance were 1 meter since a separate cable layout is used, i.e. 2 parallel cables. The number of take-outs was 21 for each cable and since cable 1 and 2 overlapped with one take-out the number of electrodes is (21* 2)-1= 41. Since parallel cables are used the total number of electrodes is 2*41=82, which gives a total length of 81 m.

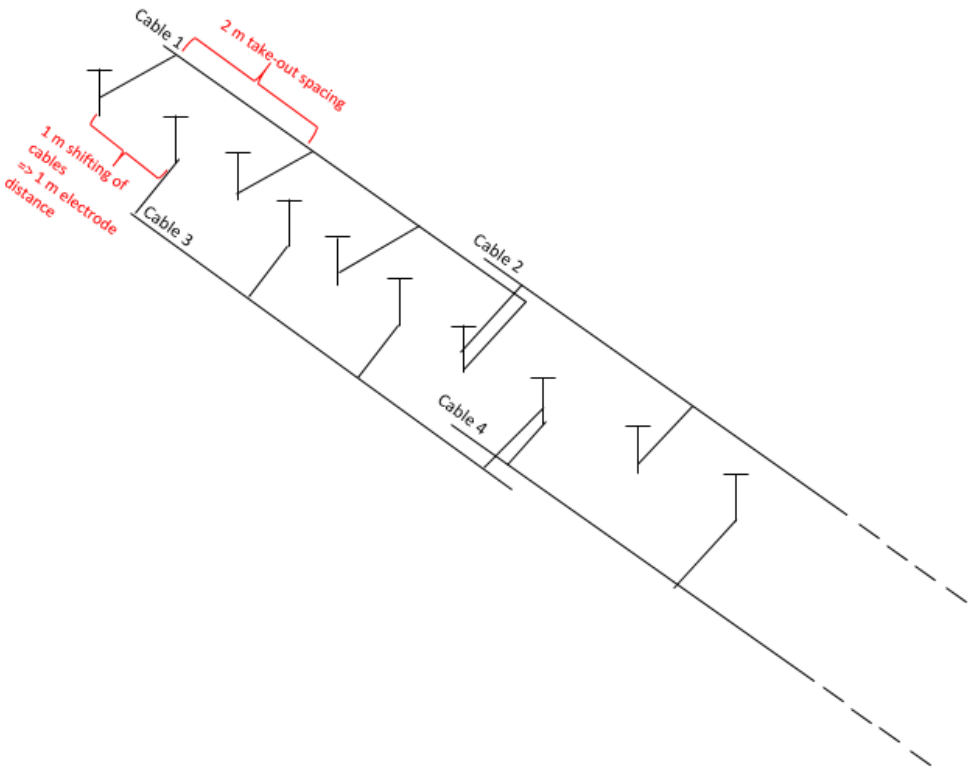

Appendix E - DUALEM

The Dualem survey have been performed in collaboration with the HydroGeophysics group at Aarhus University. All data are collected and later also compiled by them. Horizontals maps of data residuals and mean resistivities for different depths (0-1, 1-2 meter and so on until 7-8 meter) are shown in the figures below (Bjergsted Pedersen, 2017, unpublished data). Furthermore, vertical profiles of the calculated mean resistivities are also presented. The data residuals in the survey area are shown below. The residuals are high due to the resistive ground and the high noise level. The data quality is lower in the north compared to the south.

The mean resistivity for different depths (0 to 8 meter) with 1 meters interval are shown below.

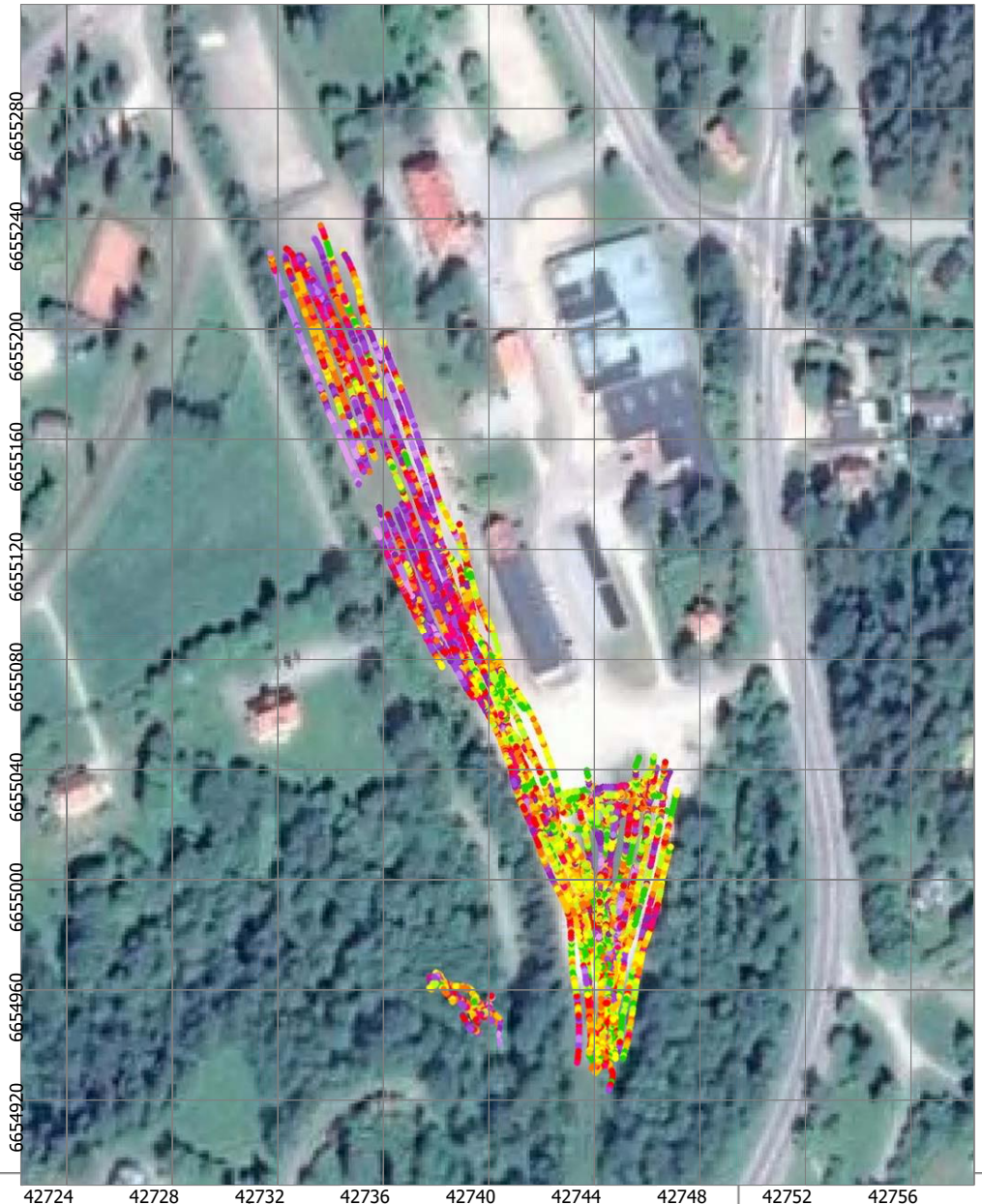

LUND UNIVERSITY
HydroGeophysics Group
AARHUS UNIVERSITY

GCM Hagfors 2017

0 0.2 0.4 0.6 0.8 1 1.2 1.4 1.6 1.8 2 2.2 2.4 2.6 2.8 3 3.2 3.4

Data Residual
Below one corresponds to a fit within one standard deviation

UTM 33N WGS84

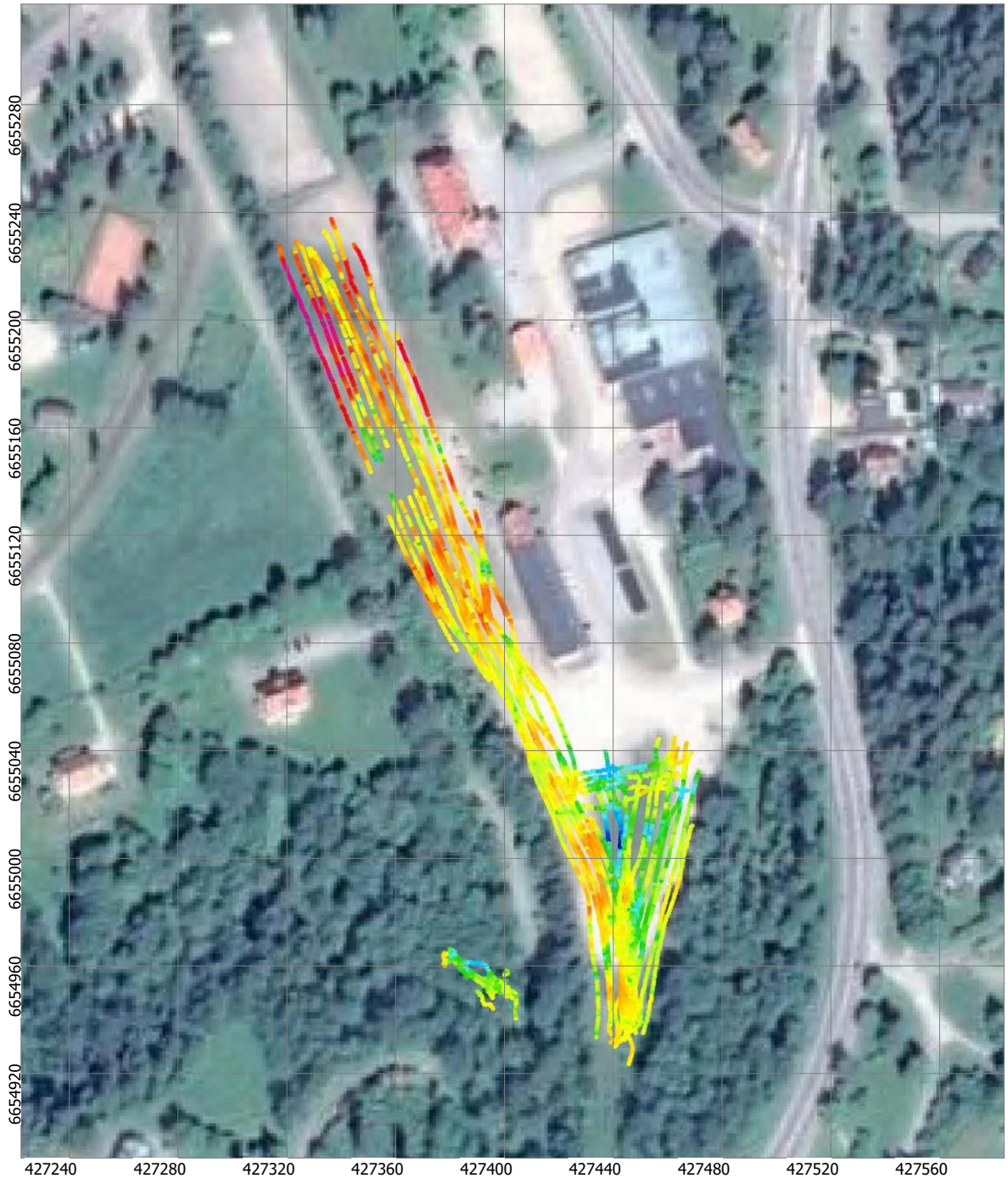

.

LUND UNIVERSITY
HydroGeophysics Group
AARHUS UNIVERSITY

GCM Hagfors 2017

10 100 1,000 10,000
Resistivity [Ohmm]

Mean Resistivity - Depth, 0-1 m (ohmm)
SCI Smooth Model - Point theme

UTM 33N WGS84

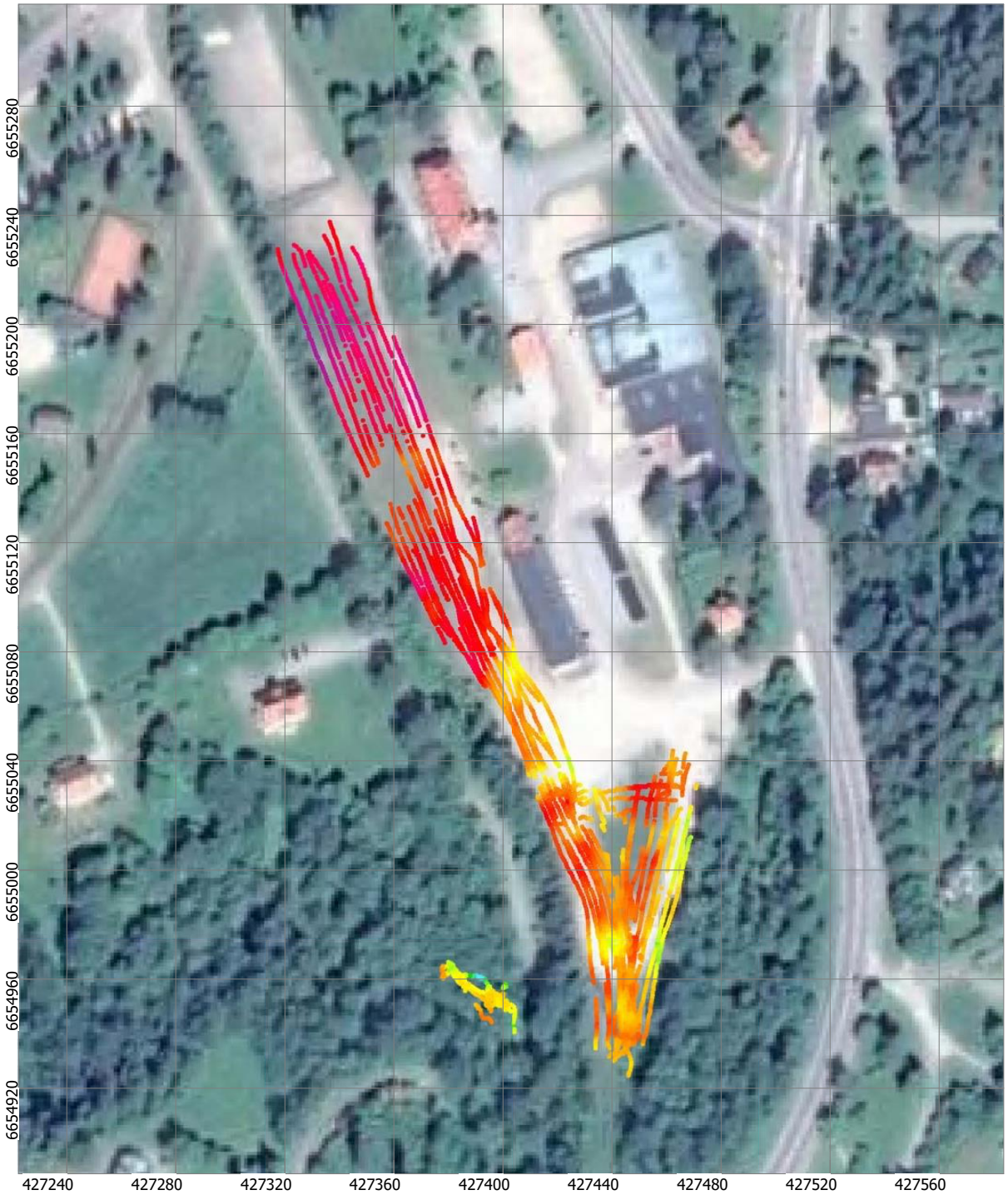

LUND UNIVERSITY
HydroGeophysics Group
AARHUS UNIVERSITY

GCM Hagfors 2017

10 100 1,000 10,000
Resistivity [Ohmm]

Mean Resistivity - Depth, 1-2 m (ohmm)
SCI Smooth Model - Point theme

UTM 33N WGS84
100 m

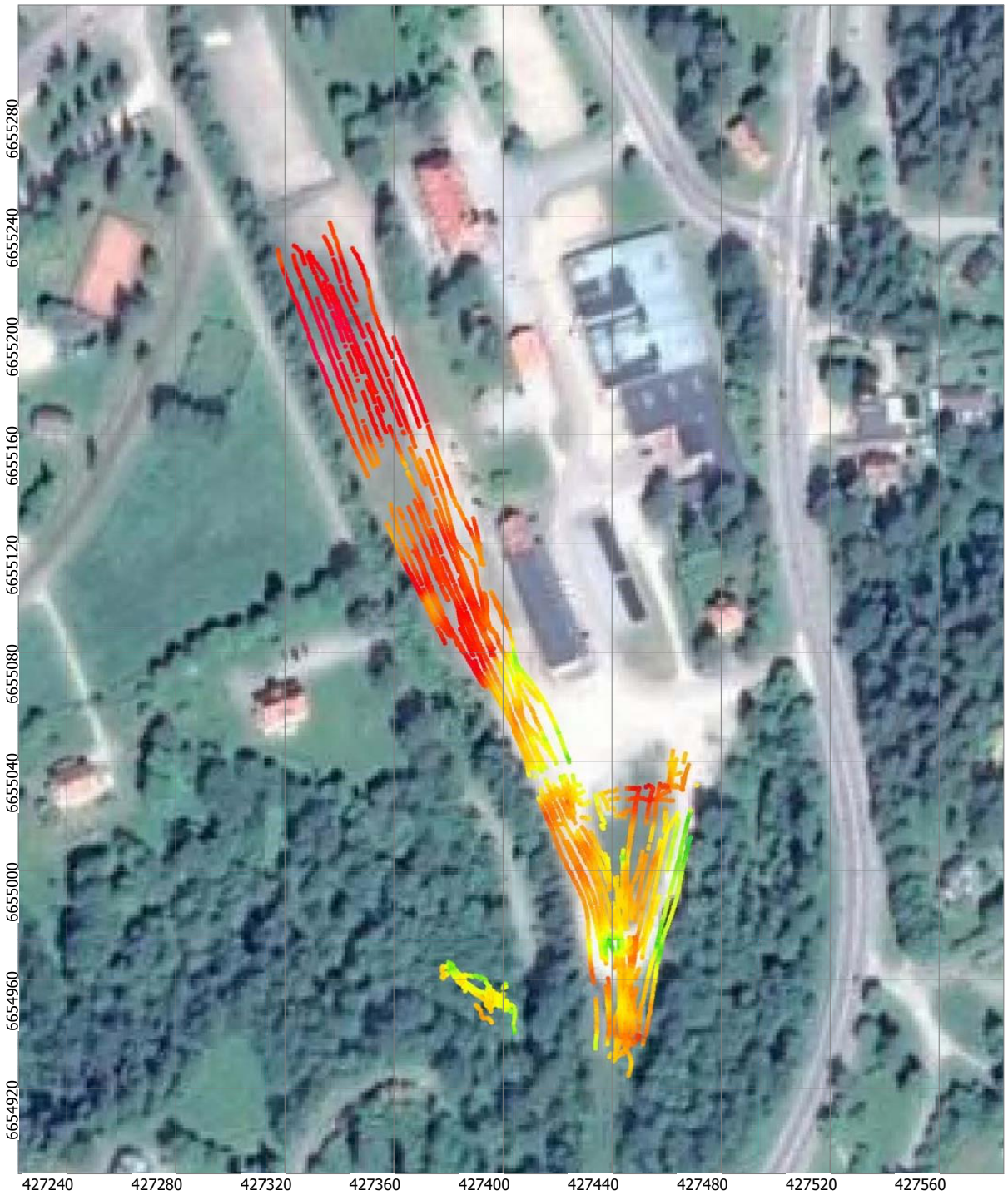

LUND UNIVERSITY
HydroGeophysics Group
AARHUS UNIVERSITY

GCM Hagfors 2017

10 100 1,000 10,000
Resistivity [Ohmm]

Mean Resistivity - Depth, 2-3 m (ohmm)
SCI Smooth Model - Point theme

UTM 33N WGS84
100 m

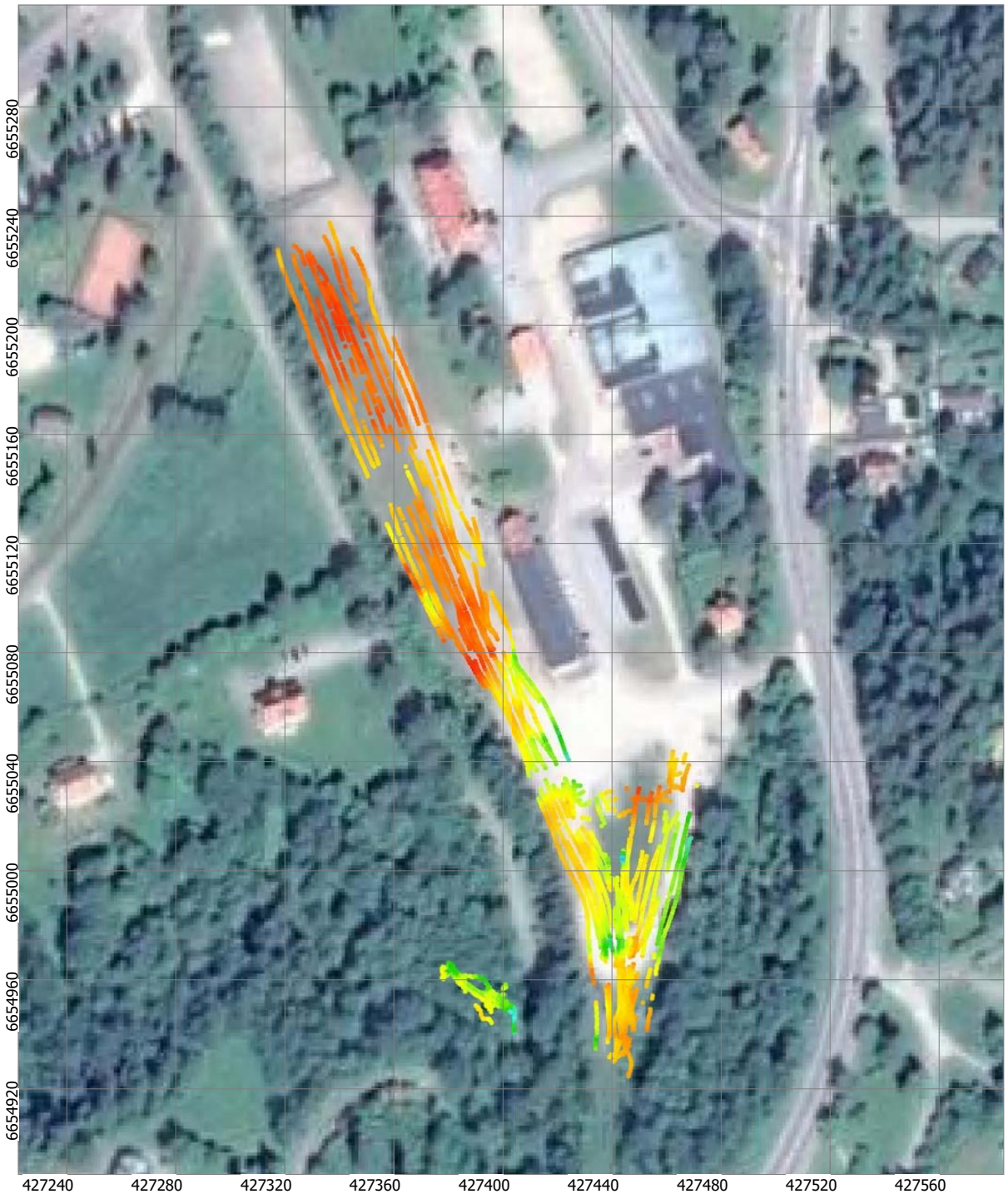

LUND UNIVERSITY
HydroGeophysics Group
AARHUS UNIVERSITY

GCM Hagfors 2017

Mean Resistivity - Depth, 3-4 m (ohmm)
SCI Smooth Model - Point theme

10 100 1,000 10,000
Resistivity [Ohmm]

UTM 33N WGS84
100 m

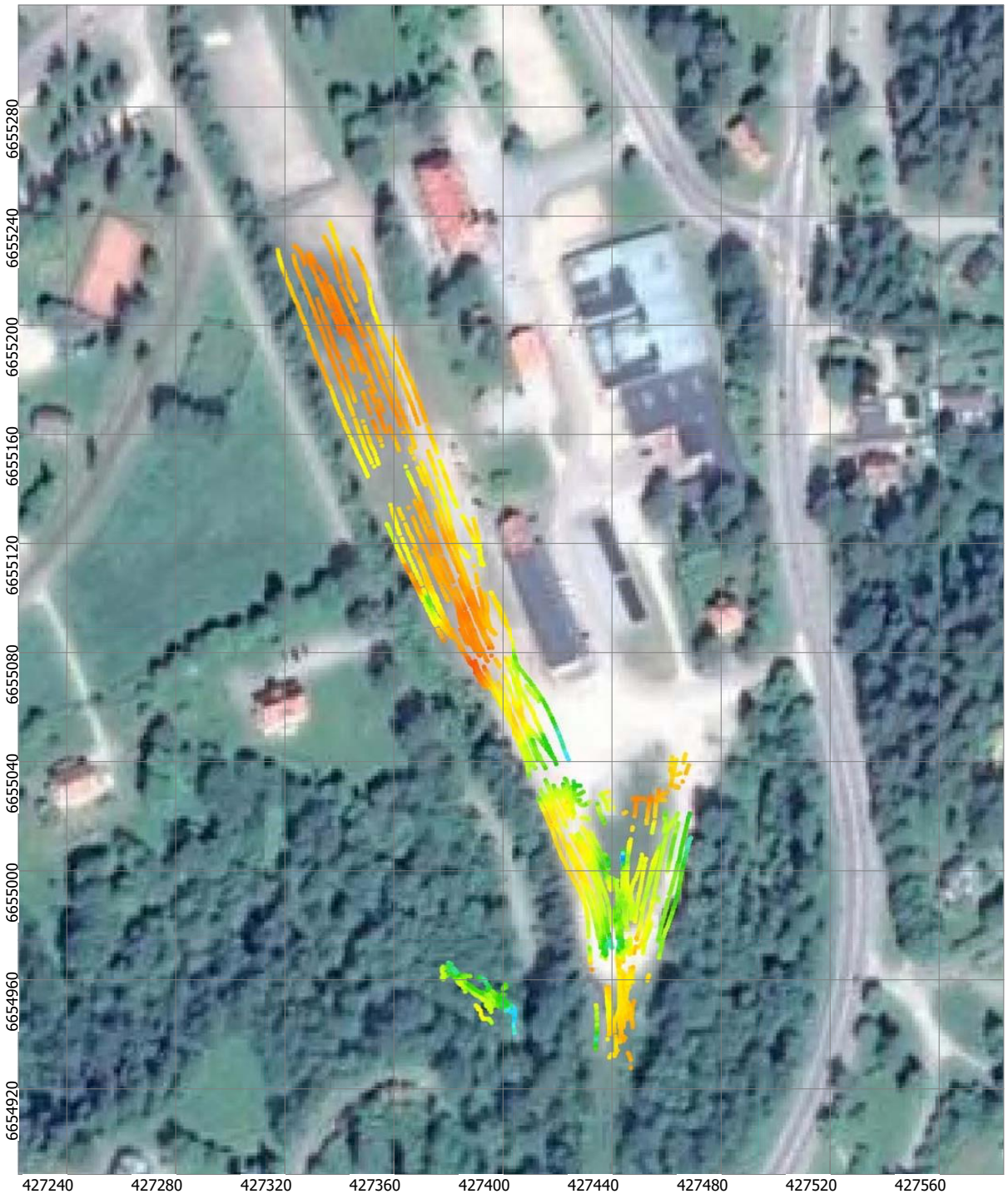

LUND UNIVERSITY
HydroGeophysics Group
AARHUS UNIVERSITY

GCM Hagfors 2017

10 100 1,000 10,000
Resistivity [Ohmm]

Mean Resistivity - Depth, 4-5 m (ohmm)
SCI Smooth Model - Point theme

UTM 33N WGS84
100 m

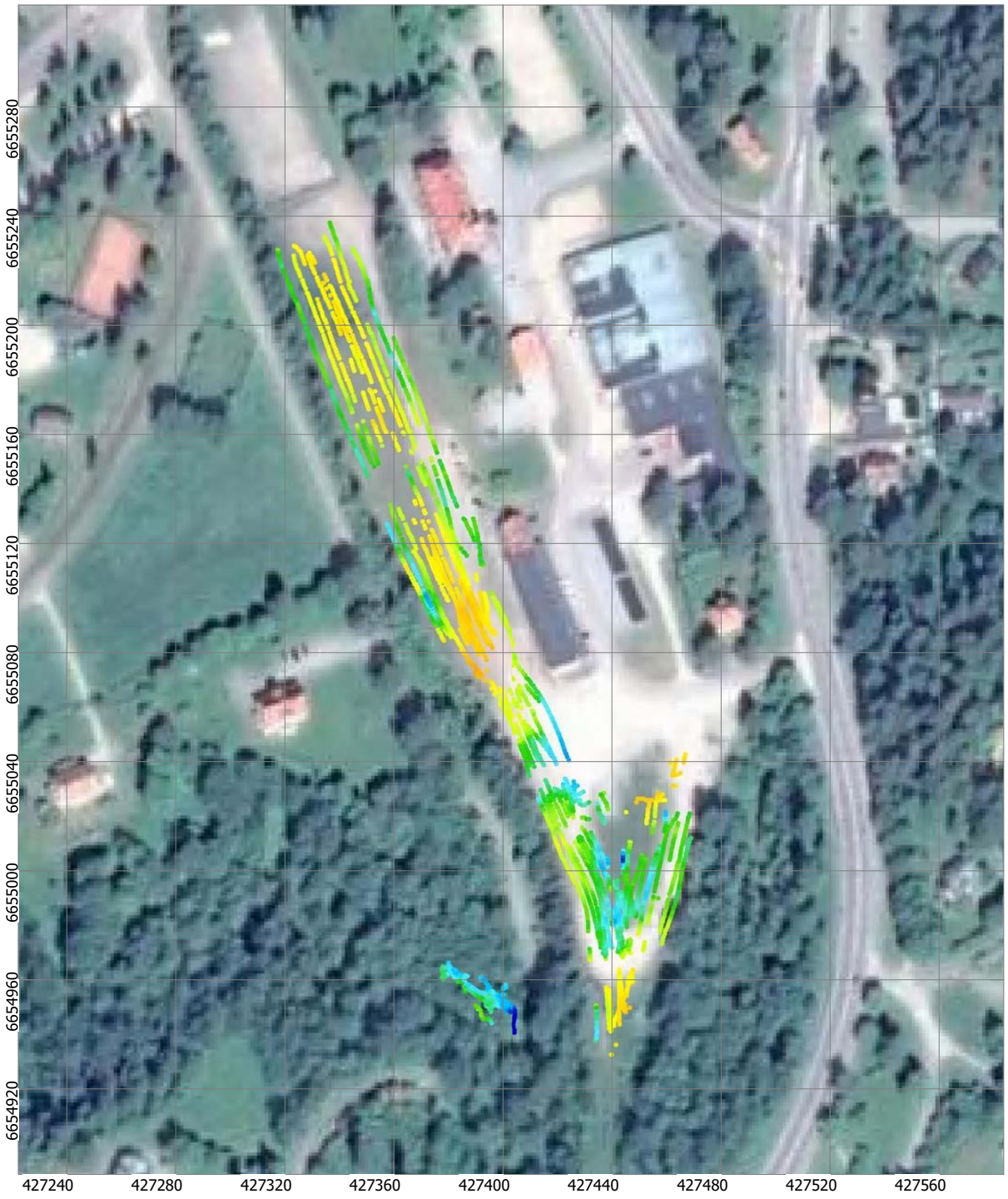

LUND UNIVERSITY
HydroGeophysics Group
AARHUS UNIVERSITY

GCM Hagfors 2017

10 100 1,000 10,000
Resistivity [Ohmm]

Mean Resistivity - Depth, 5-6 m (ohmm)
SCI Smooth Model - Point theme

UTM 33N WGS84
100 m

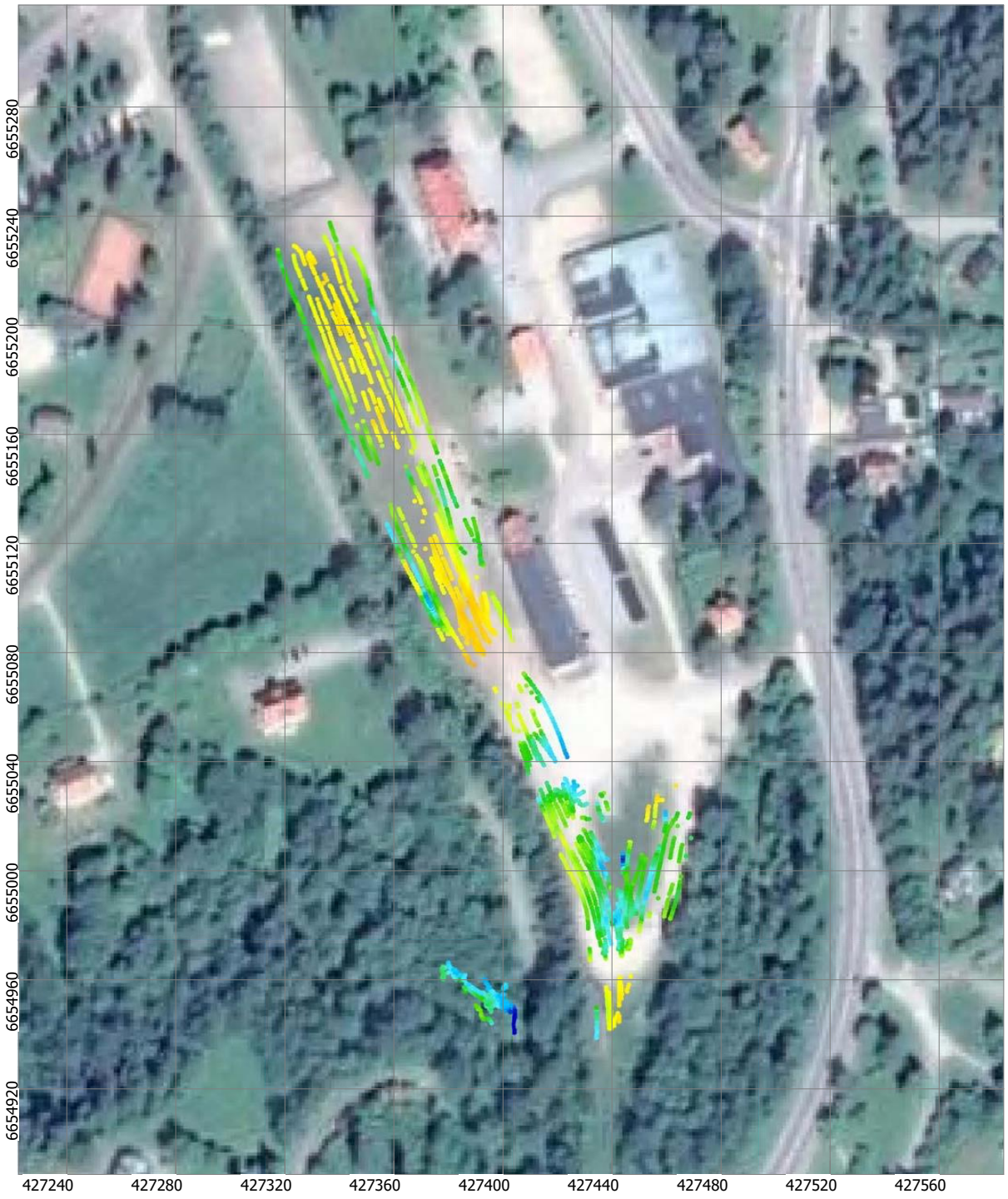

LUND UNIVERSITY
HydroGeophysics Group
AARHUS UNIVERSITY

GCM Hagfors 2017

10 100 1,000 10,000
Resistivity [Ohmm]

Mean Resistivity - Depth, 6-7 m (ohmm)
SCI Smooth Model - Point theme

UTM 33N WGS84
100 m

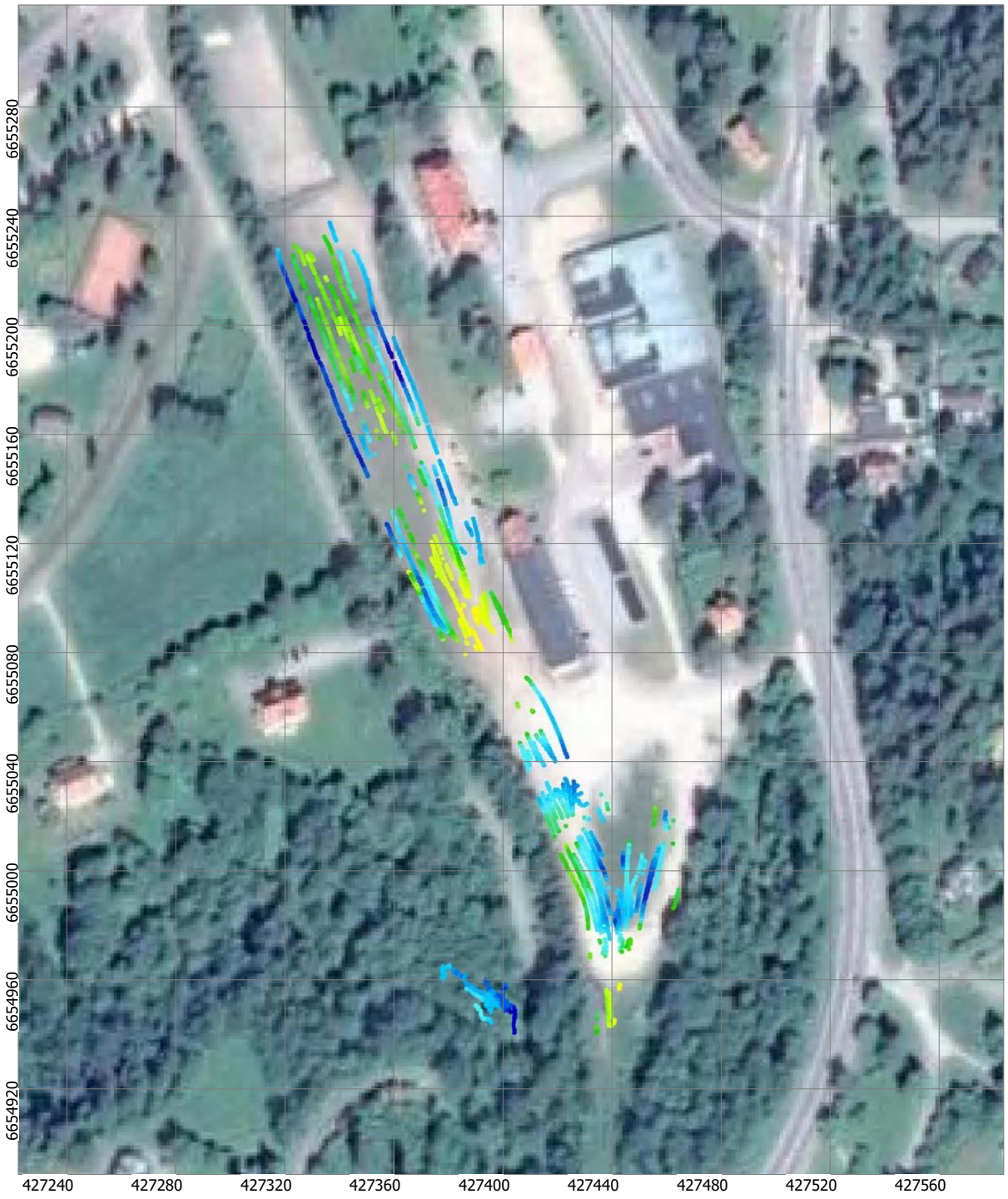

LUND UNIVERSITY
HydroGeophysics Group
AARHUS UNIVERSITY

GCM Hagfors 2017

10 100 1,000 10,000
Resistivity [Ohmm]

Mean Resistivity - Depth, 7-8 m (ohmm)
SCI Smooth Model - Point theme

UTM 33N WGS84
100 m

Vertical profiles of the mean resistivity for different measurement lines are shown below. The lighter color on the profiles indicates that below this depths the received signal is lower than a certain threshold and therefore the data is not used in the interpretation.

Line 1 – North to South

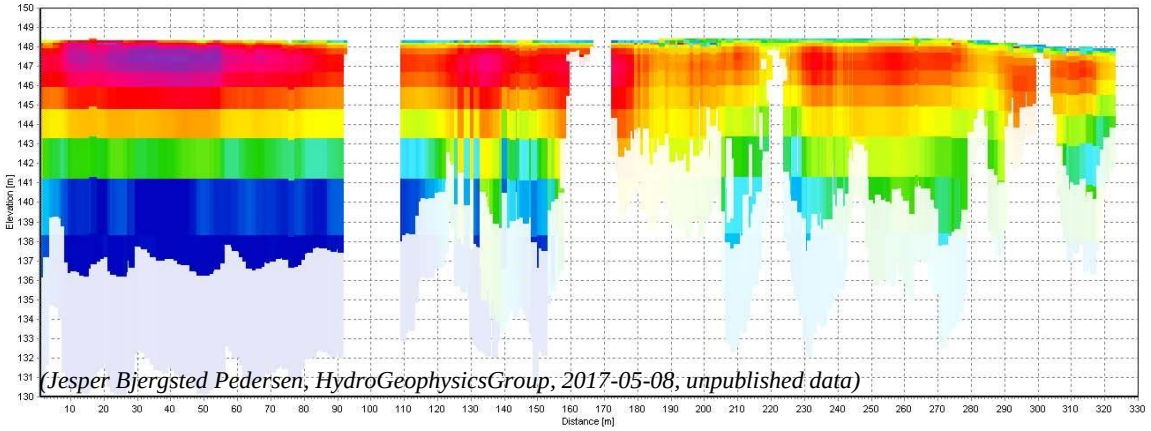

(Jesper Bjergsted Pedersen, HydroGeophysicsGroup, 2017-05-08, unpublished data)

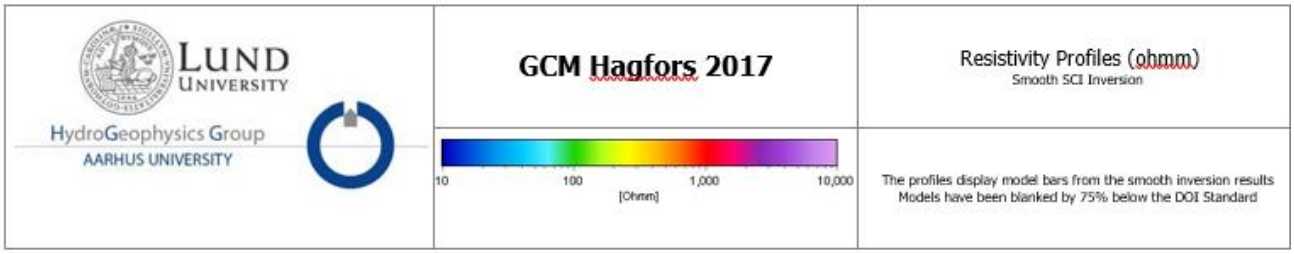

Line 2 – North to south

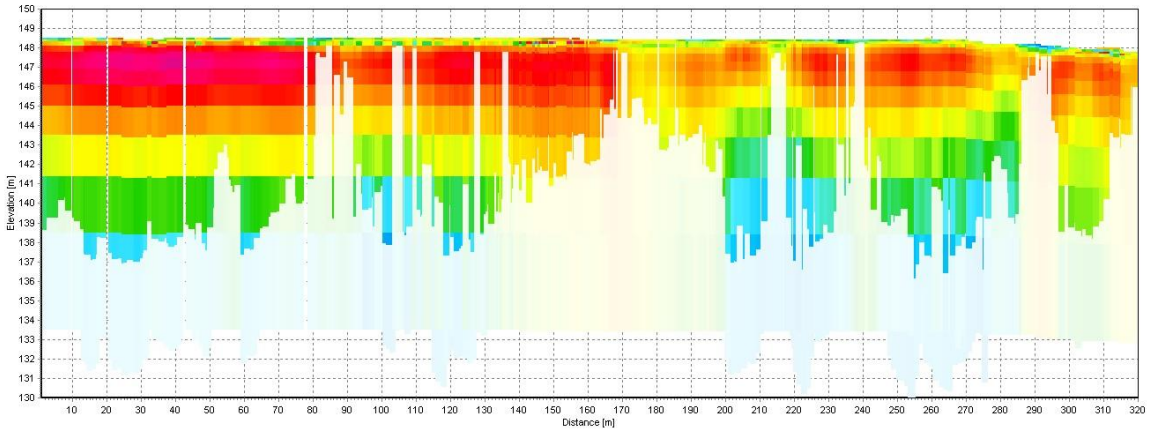

LUND UNIVERSITY
HydroGeophysics Group
AARHUS UNIVERSITY

GCM Hagfors 2017

10 100 1,000 10,000
[Ohmm]

Resistivity Profiles (ohmm)
Smooth SCI Inversion

The profiles display model bars from the smooth inversion results
Models have been blanked by 75% below the DOI Standard

Appendix F – Resistivity and IP profiles

This section contains all the interpreted resistivity and IP profiles collected by multigradient and pole-dipole arrays at Hagforstvätten April 2017. The IP-data collected with pole-dipole for profile 1 has been excluded from the results due to large artefacts created by the inversion. Geological and chemical reference data in the proximity to each profile (< 10 m offset) is presented in Appendix G. The bedrock is shown as a continuous black line in the ERT and IP profiles. In profile 1-4, 6 and 7 the bedrock has been interpolated in GeoScene3D (version 10.0.13.531) using inverse distance weighting (IDW) based on data achieved through NIRAS (Nilsson, 2017, unpublished data). In profile 5 it was possible to interpret the bedrock from the resistivity measurements. Position for geological and chemical reference data is marked in each profile as vertical black lines with offset to profile (meters) within brackets.

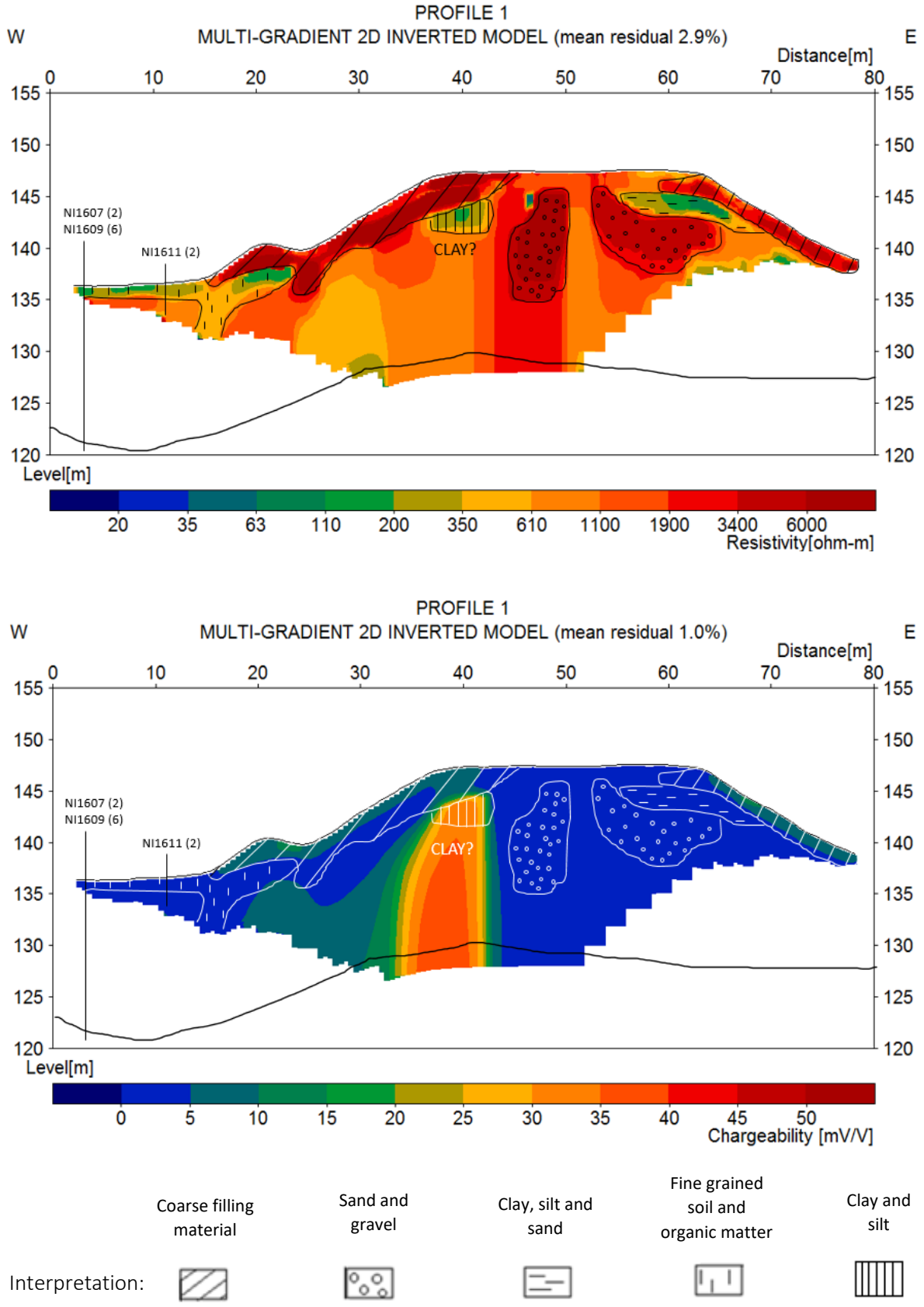

Resistivity and IP result for profile 1 (multi-gradient array). Interpolated bedrock surface shown as continuous black line and interpreted geology marked according to system underneath the profile. Position for geological and chemical reference data marked as vertical black lines with offset to profile (meters) within brackets.

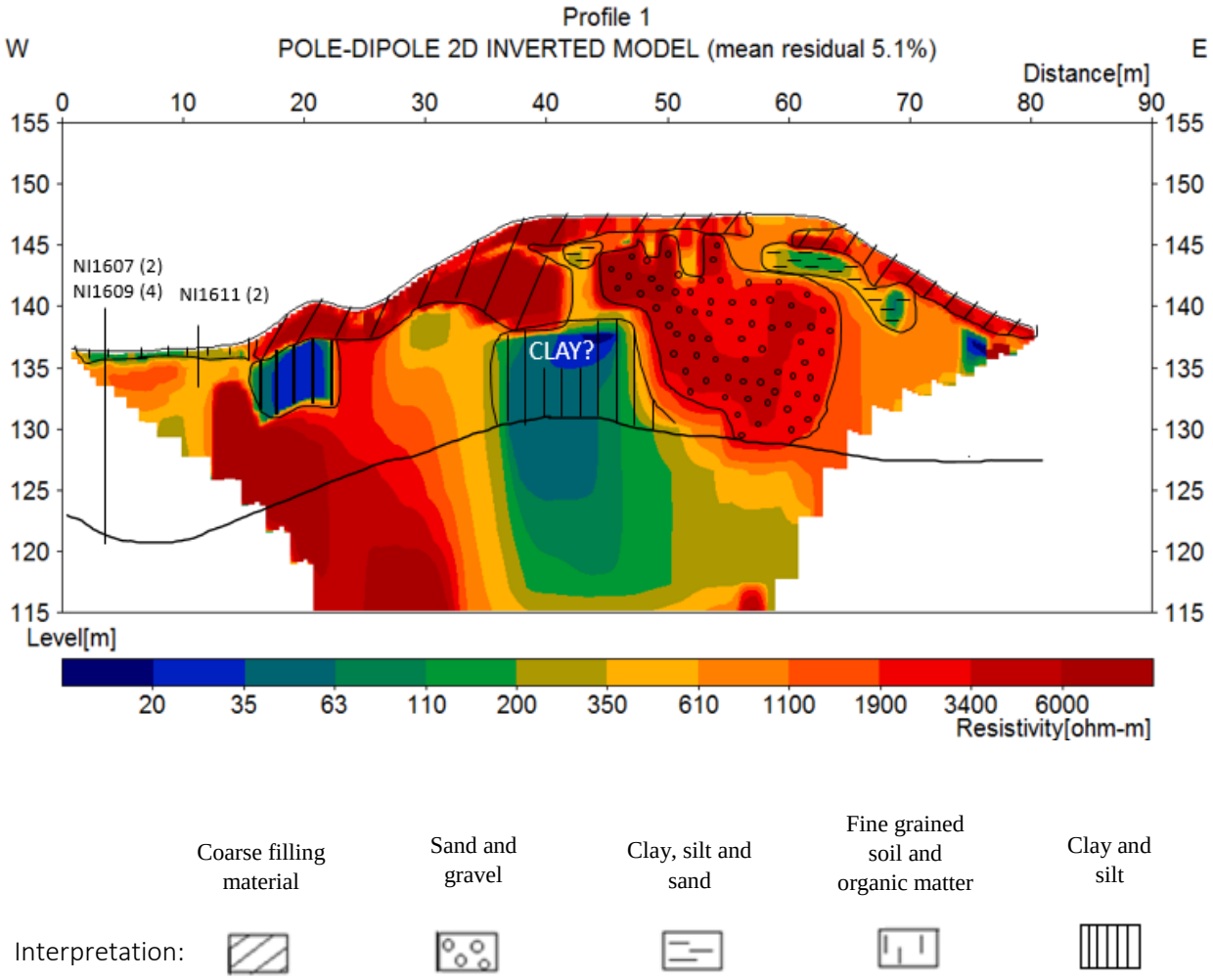

Resistivity result for profile 1 (pole-dipole array). Interpolated bedrock surface shown as continuous black line and interpreted geology marked according to system underneath the profile. Position for geological and chemical reference data marked as vertical black lines with offset to profile (meters) within brackets. IP-data collected with pole-dipole array has been excluded from the results due to large artefacts created by the inversion.

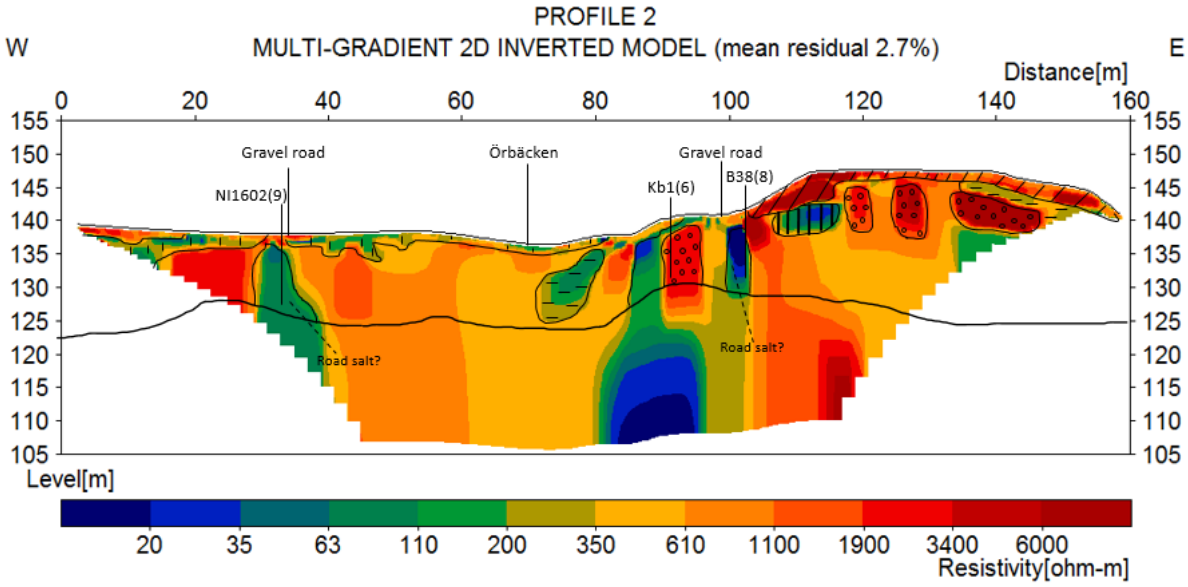

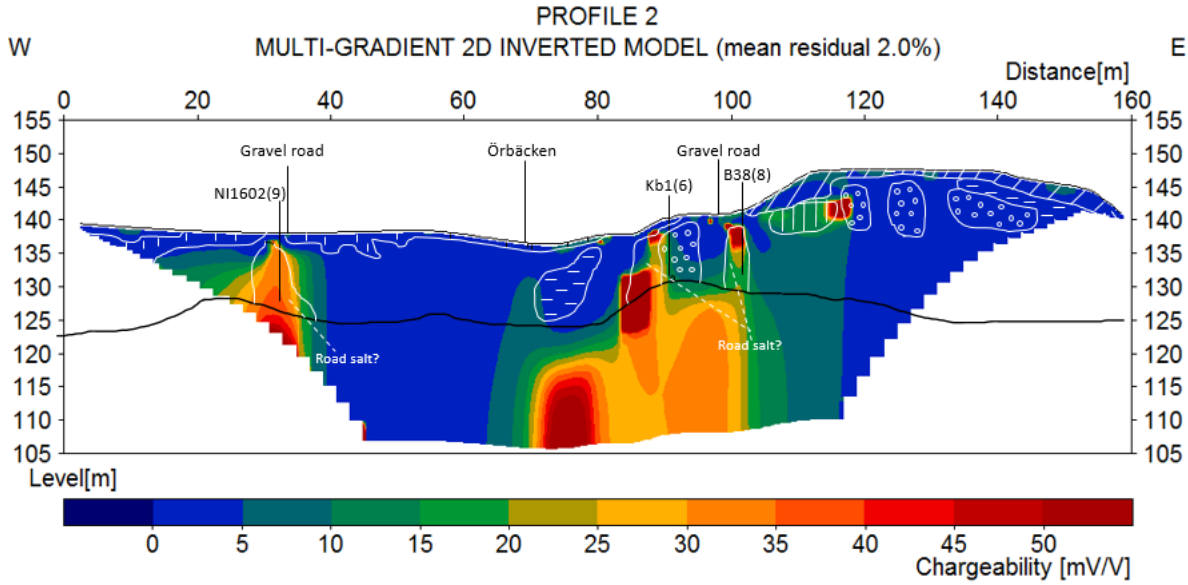

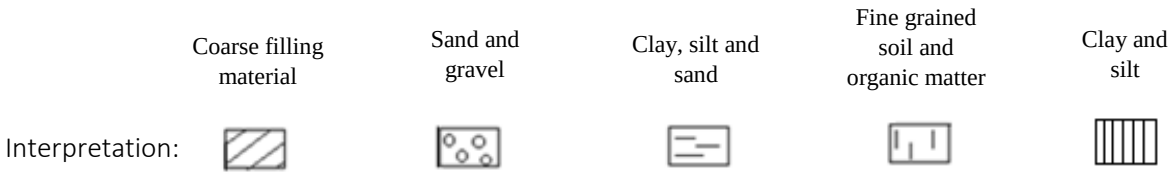

Resistivity and IP result for profile 2 (multi-gradient array). Interpolated bedrock surface shown as continuous black line and interpreted geology marked according to system underneath the profile. Position for geological and chemical reference data marked as vertical black lines with offset to profile (meters) within brackets.

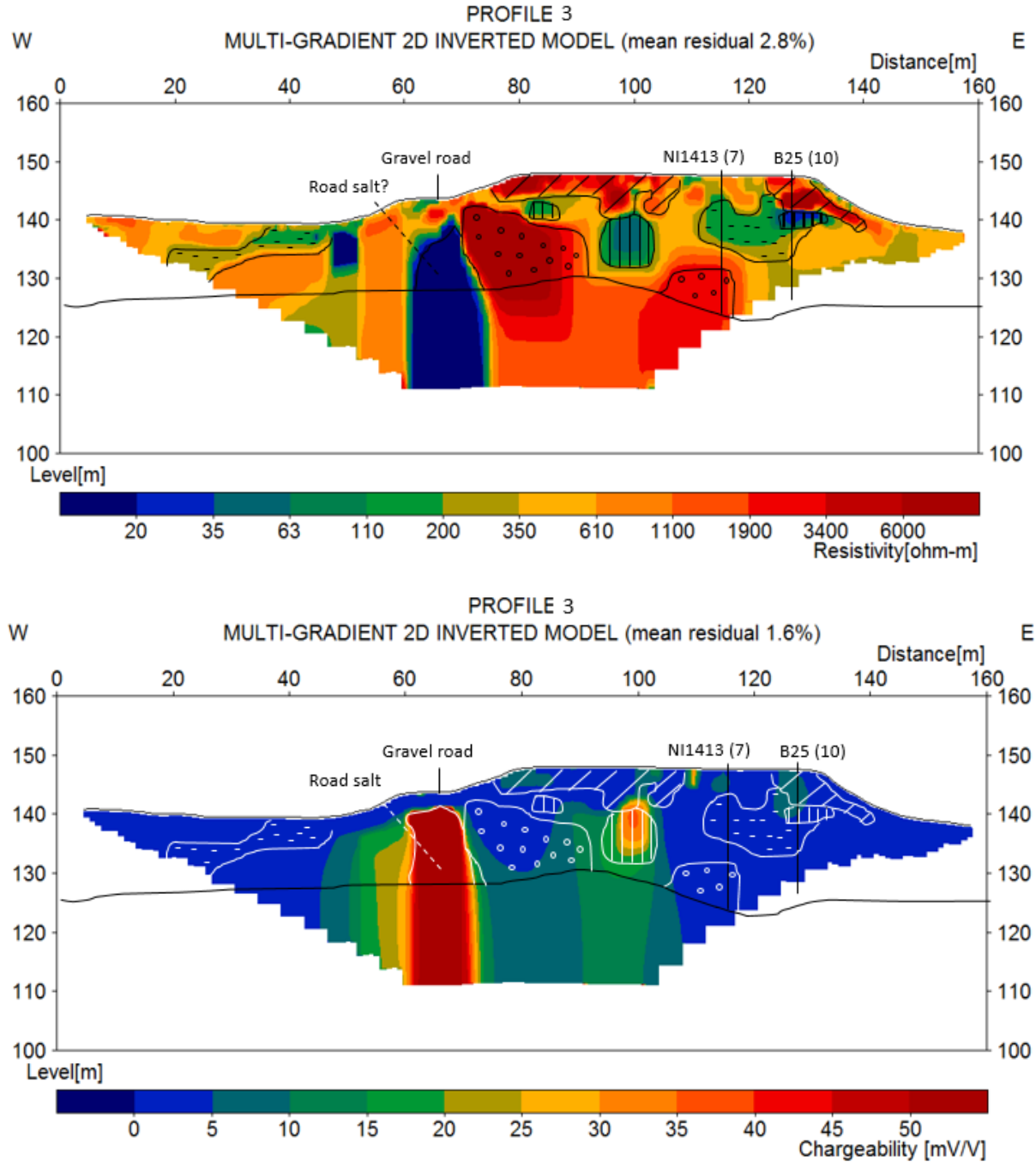

Resistivity and IP result for profile 3 (multi-gradient array). Interpolated bedrock surface shown as continuous black line and interpreted geology marked according to system underneath the profile. Position for geological and chemical reference data marked as vertical black lines with offset to profile (meters) within brackets.

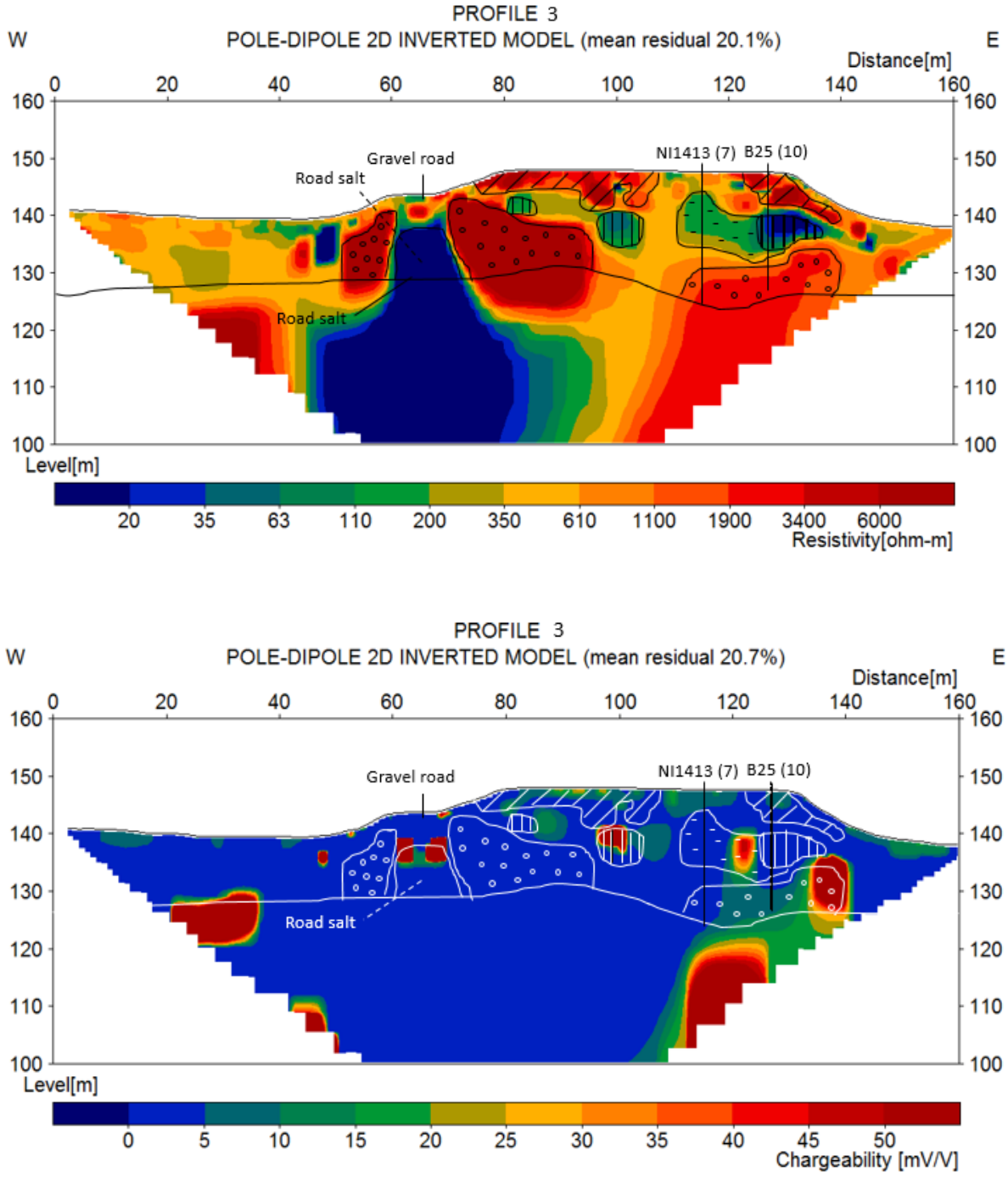

Resistivity and IP result for profile 3 (pole-dipole array). Interpolated bedrock surface shown as continuous black line and interpreted geology marked according to system underneath the profile. Position for geological and chemical reference data marked as vertical black lines with offset to profile (meters) within brackets.

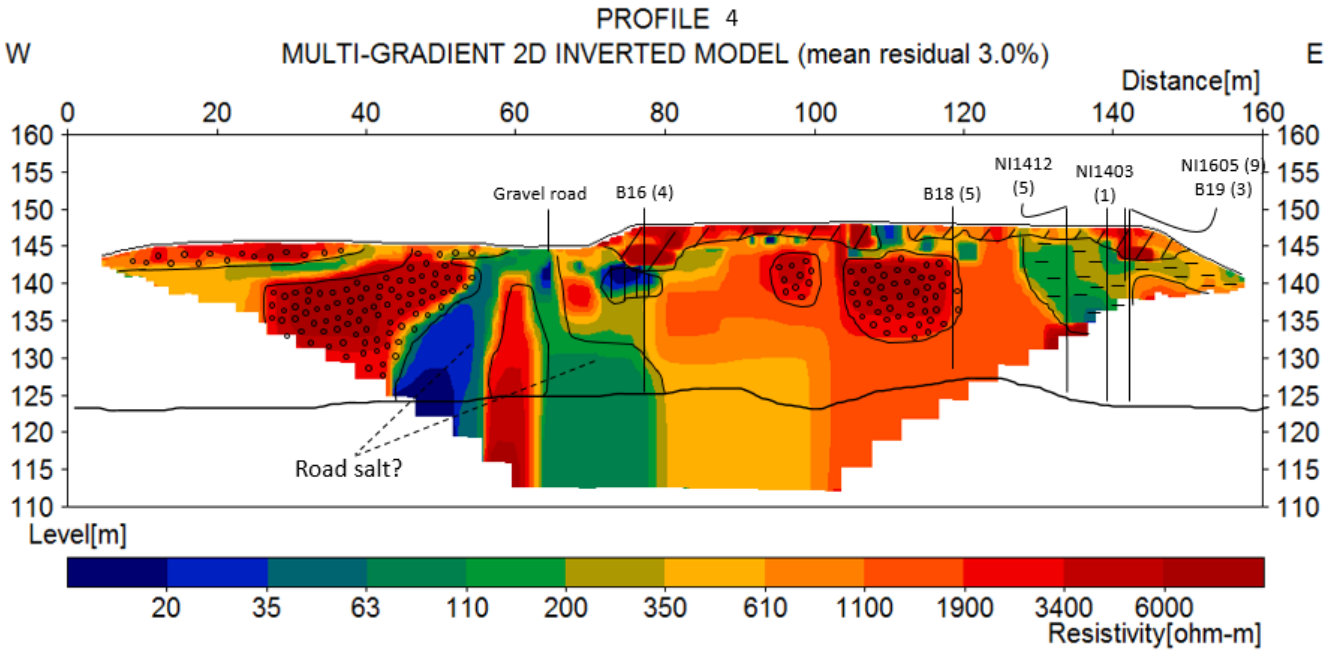

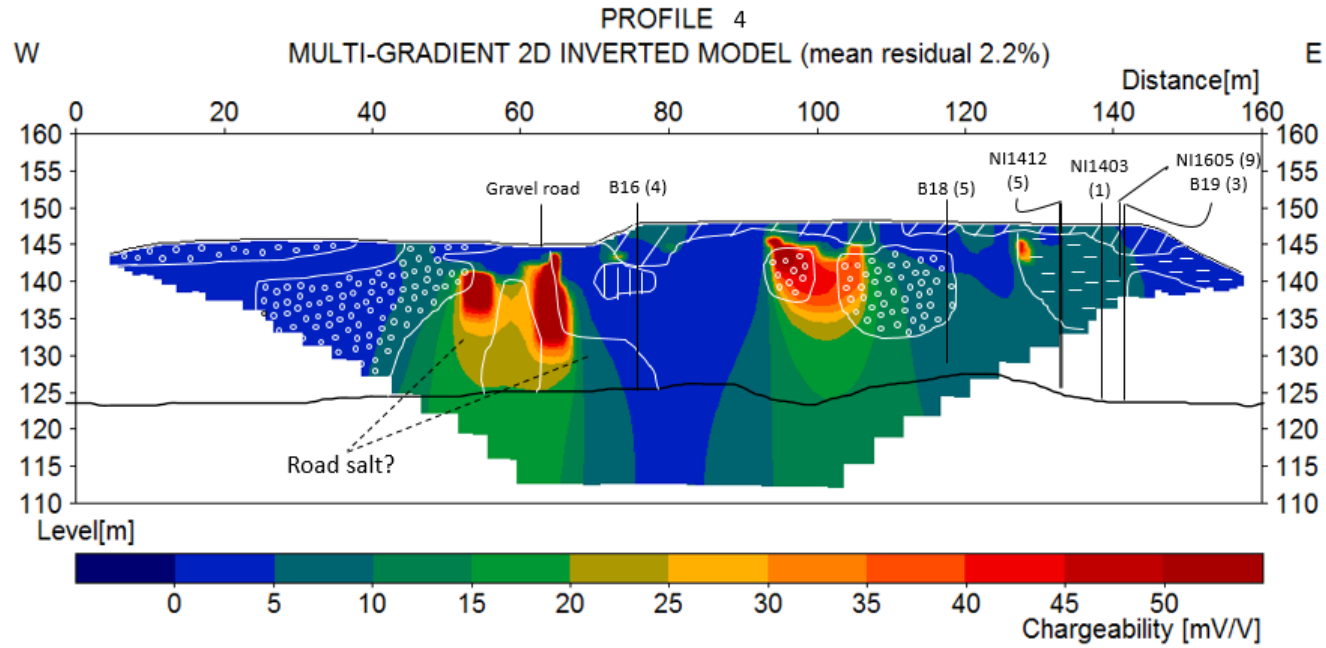

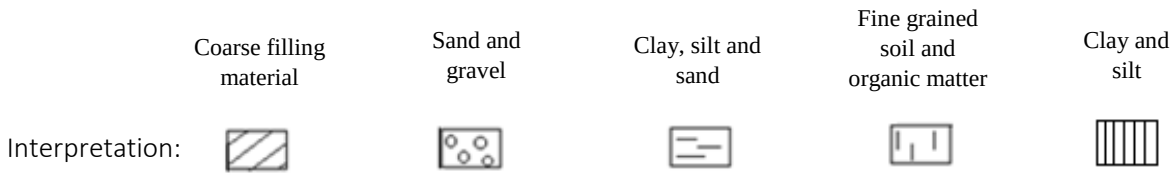

Resistivity and IP result for profile 4 (multi-gradient array). Interpolated bedrock surface shown as continuous black line and interpreted geology marked according to system underneath the profile. Position for geological and chemical reference data marked as vertical black lines with offset to profile (meters) within brackets.

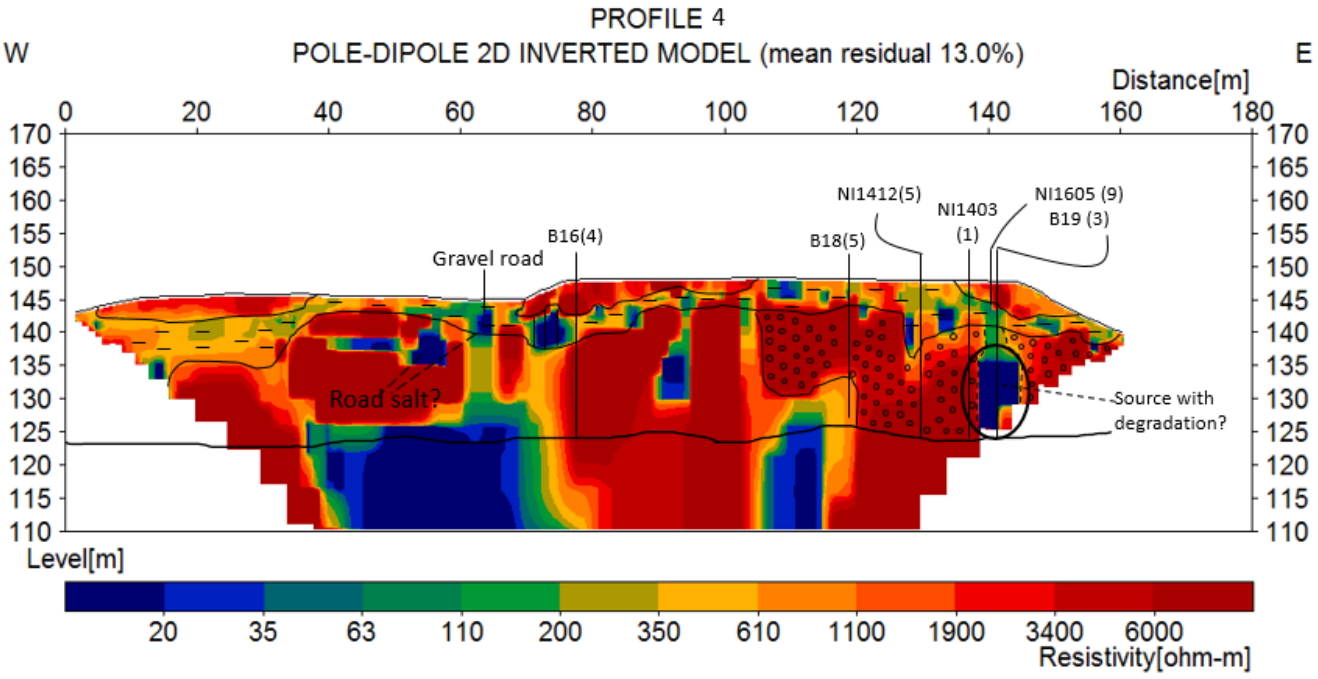

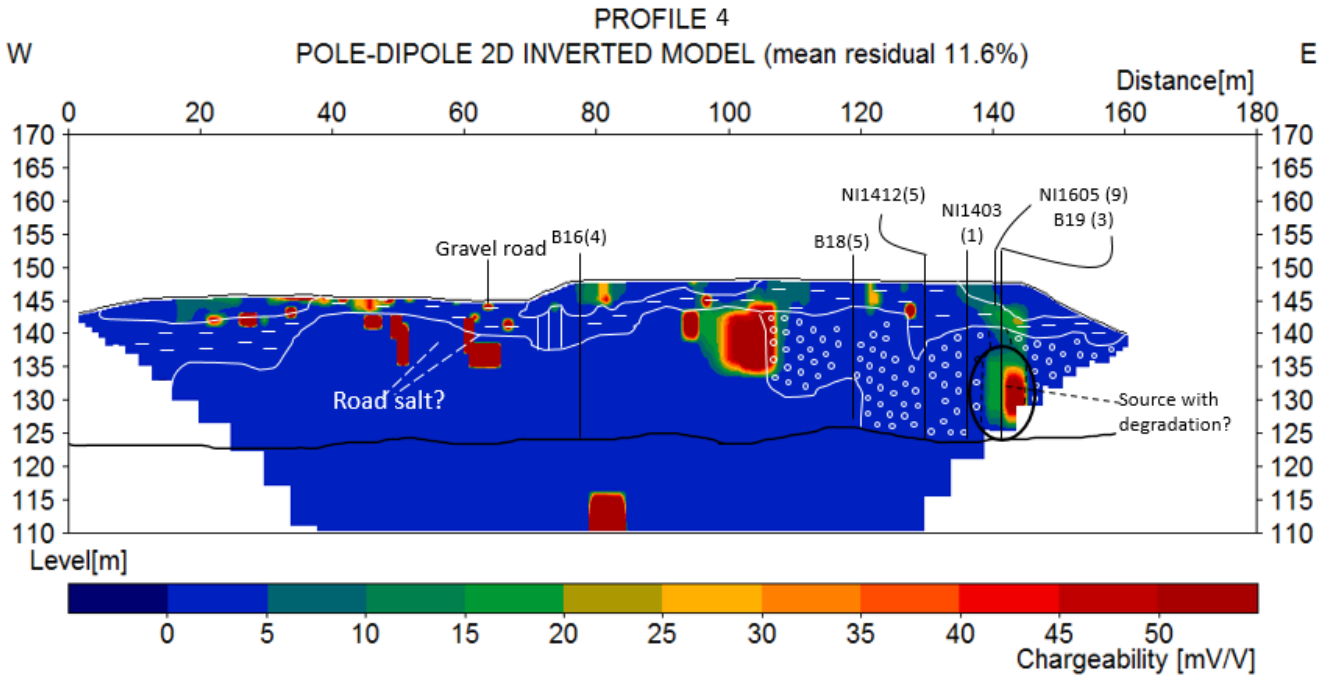

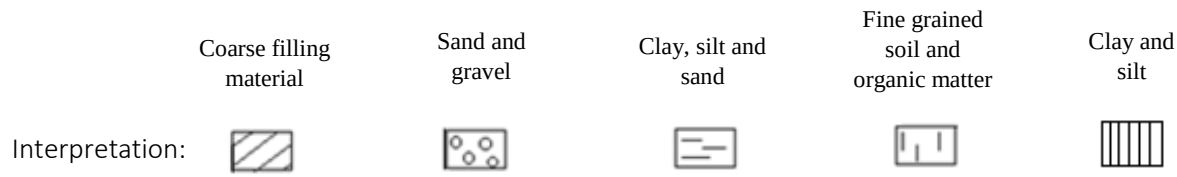

Resistivity and IP result for profile 4 (pole-dipole array). Interpolated bedrock surface shown as continuous black line and interpreted geology marked according to system underneath the profile. Position for geological and chemical reference data marked as vertical black lines with offset to profile (meters) within brackets.

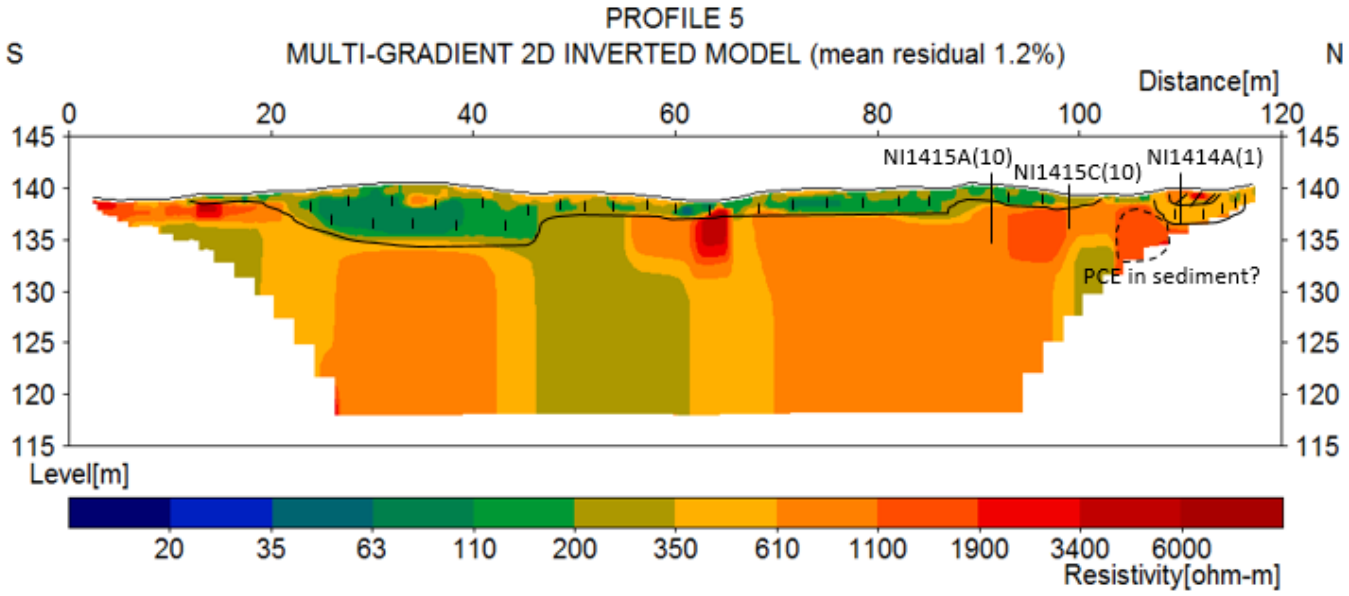

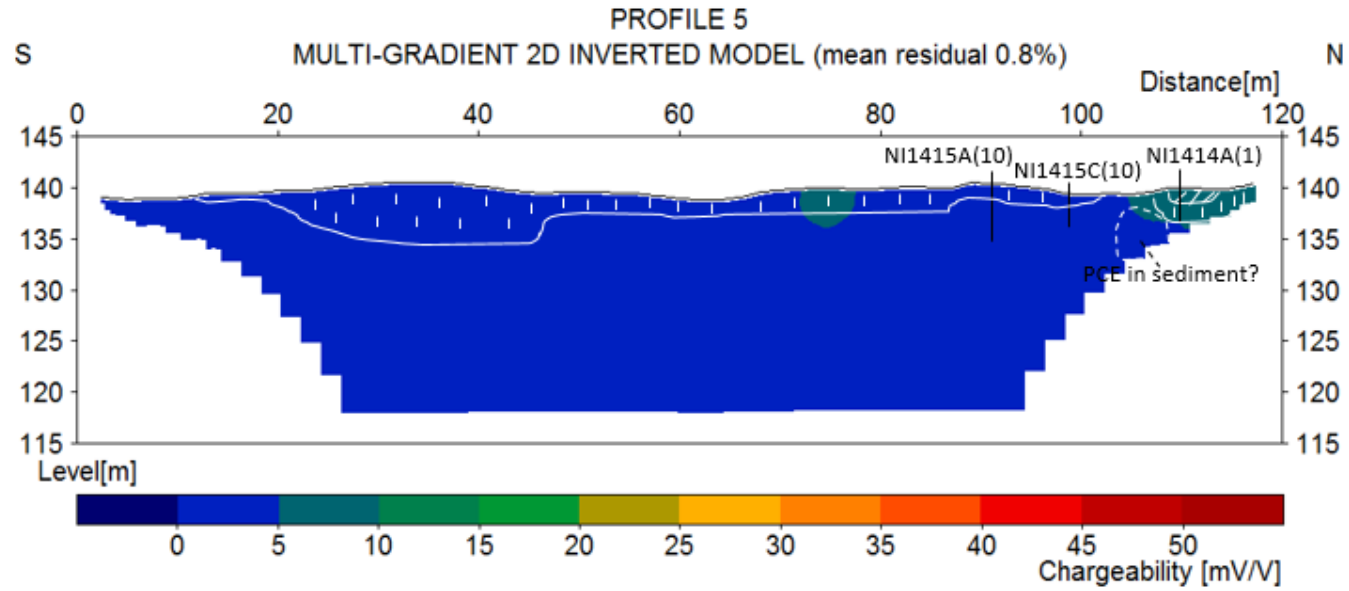

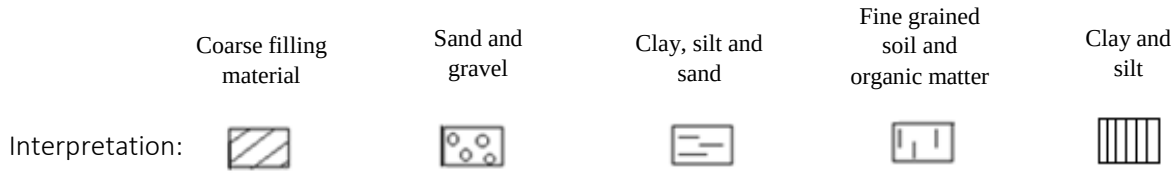

Resistivity and IP result for profile 5 (multi-gradient array). Interpreted geology marked according to system underneath the profile. Position for geological and chemical reference data marked as vertical black lines with offset to profile (meters) within brackets.

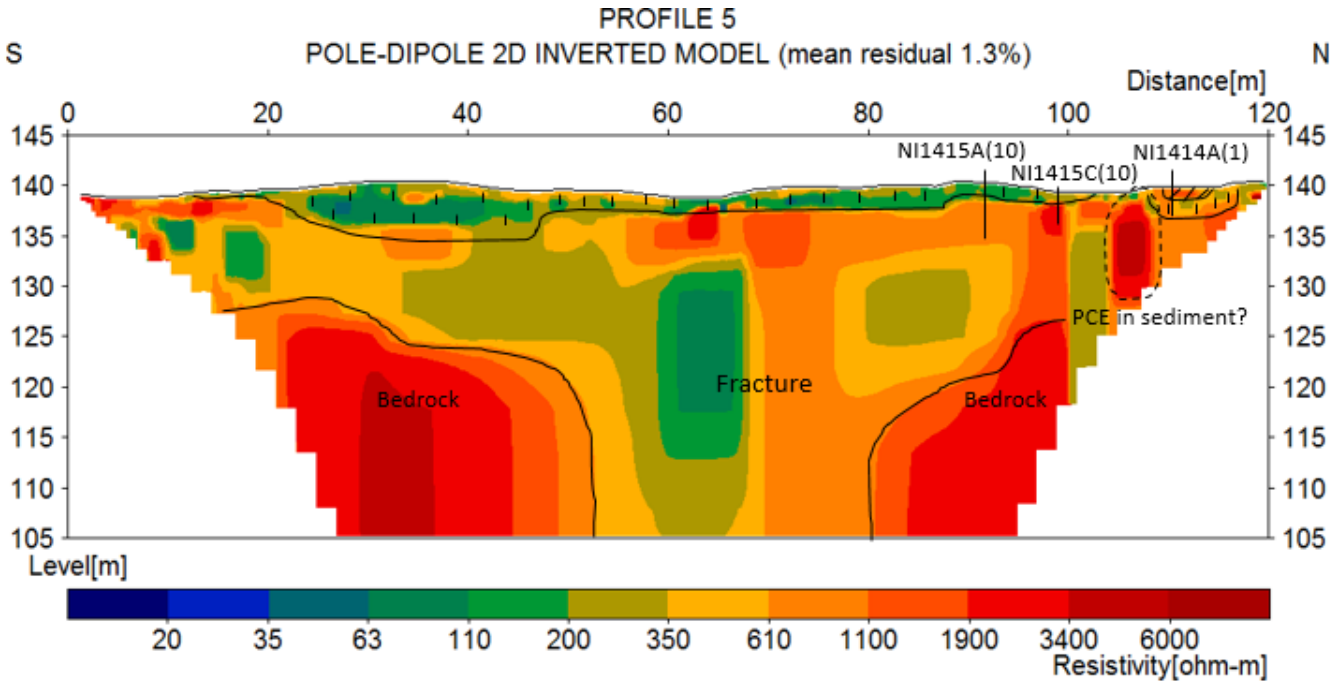

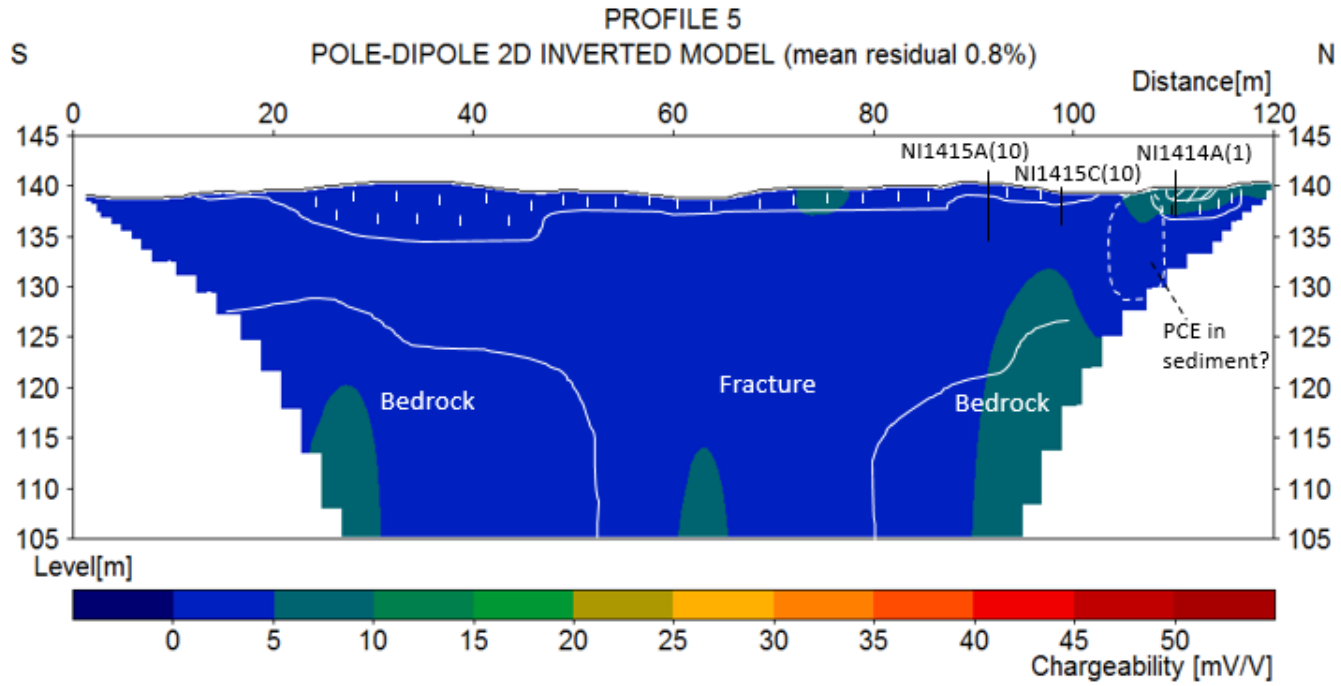

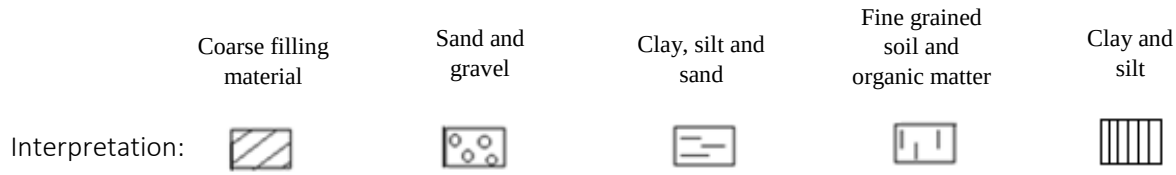

Resistivity and IP result for profile 5 (pole-dipole array). Interpreted geology marked according to system underneath the profile. Bedrock has been interpreted from resistivity measurements. Position for geological and chemical reference data marked as vertical black lines with offset to profile (meters) within brackets.

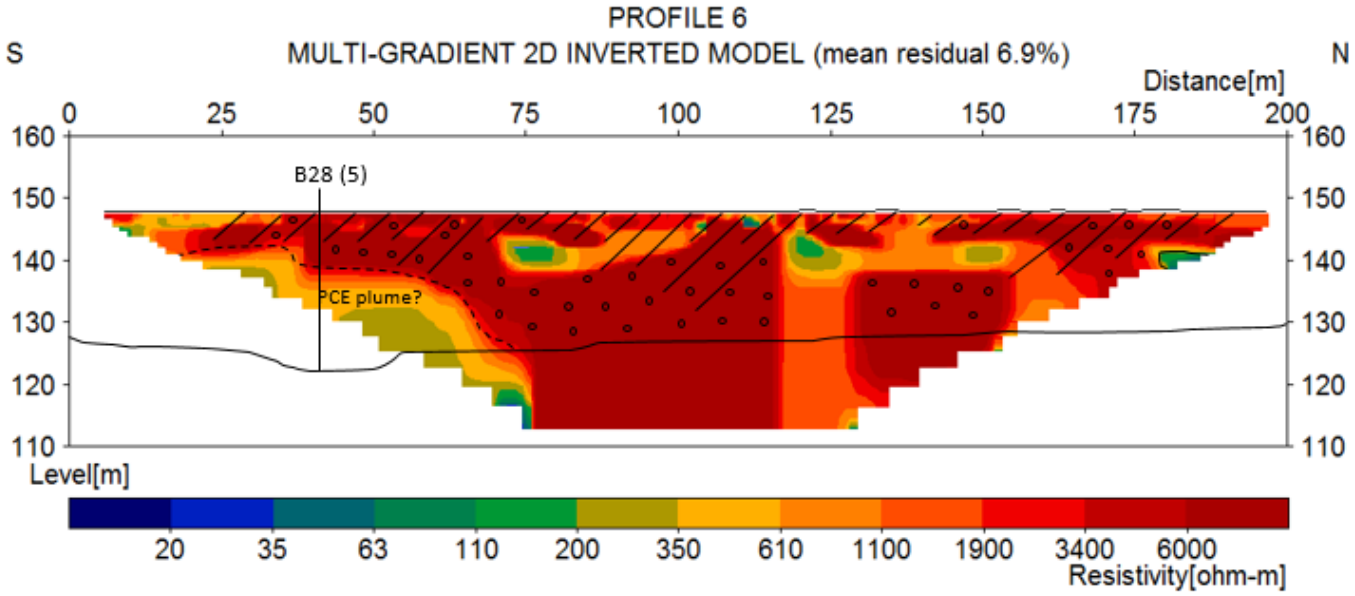

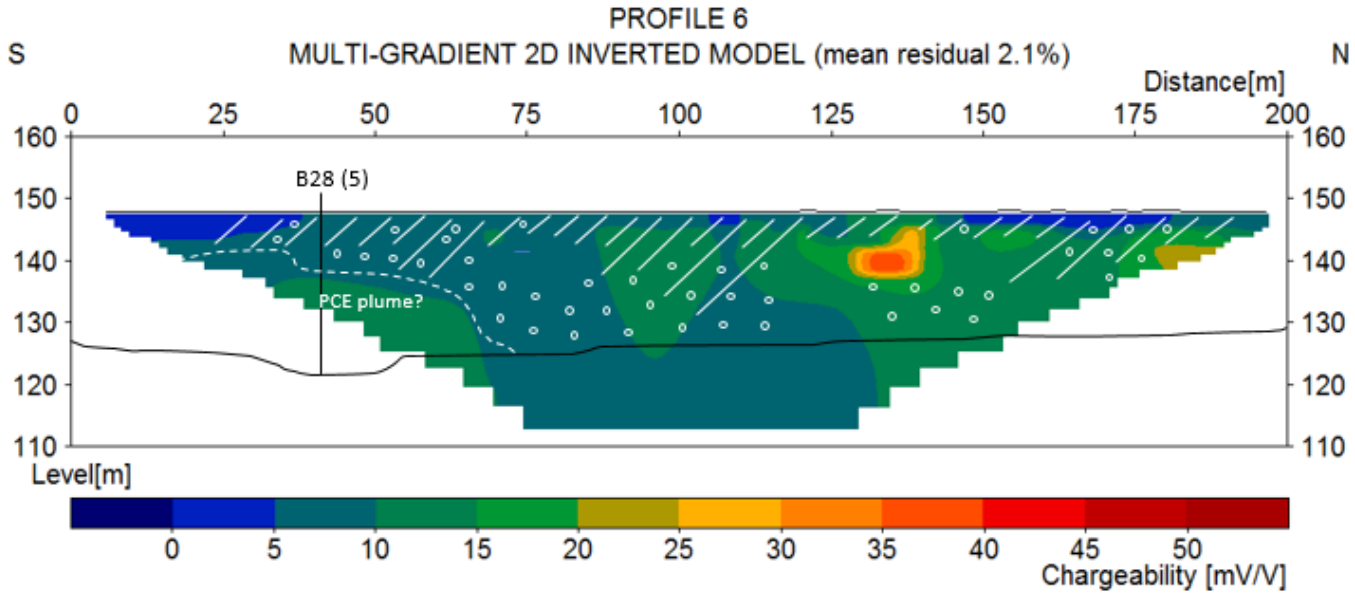

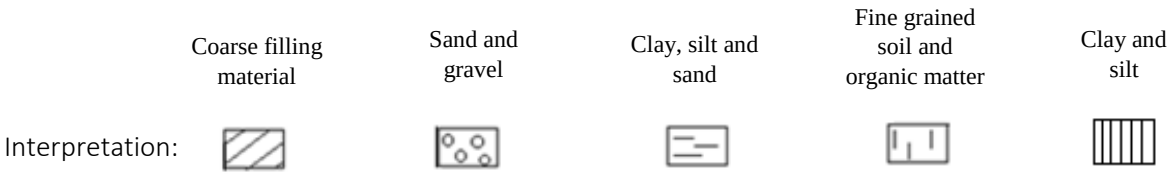

Resistivity and IP result for profile 6 (multi-gradient array). Interpolated bedrock surface shown as continuous black line and interpreted geology marked according to system underneath the profile. Position for geological and chemical reference data marked as vertical black lines with offset to profile (meters) within brackets.

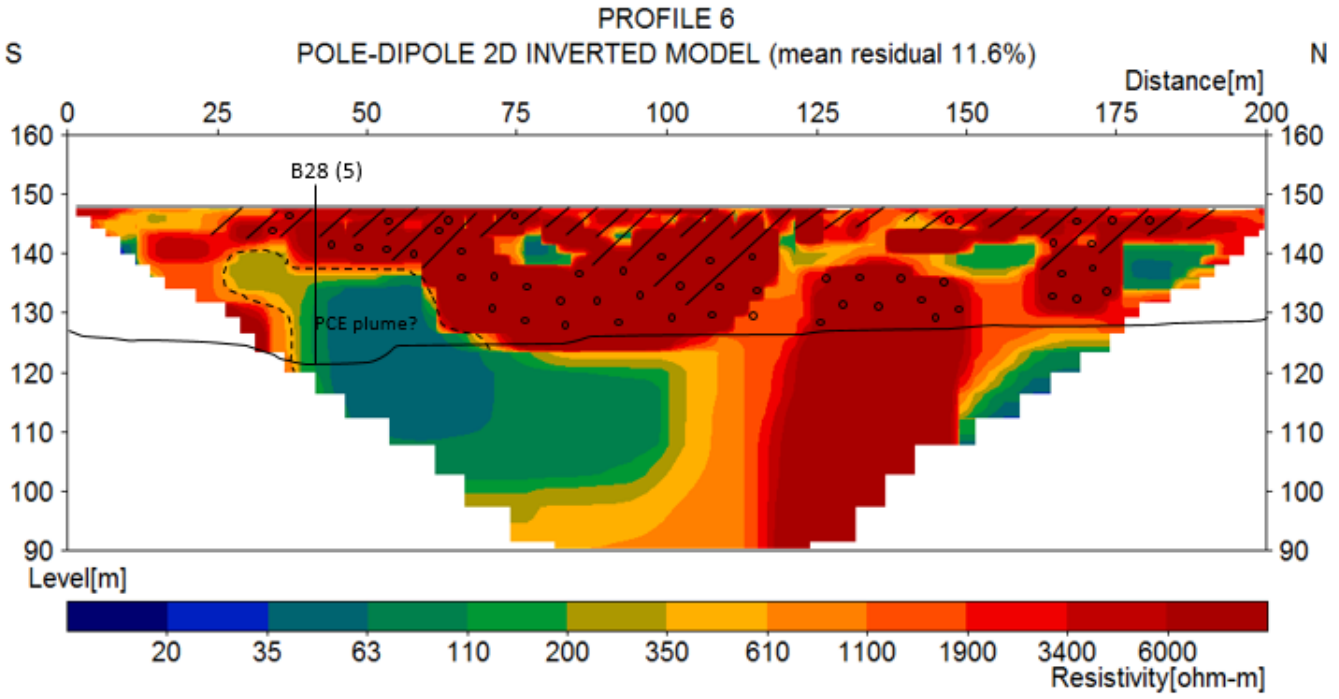

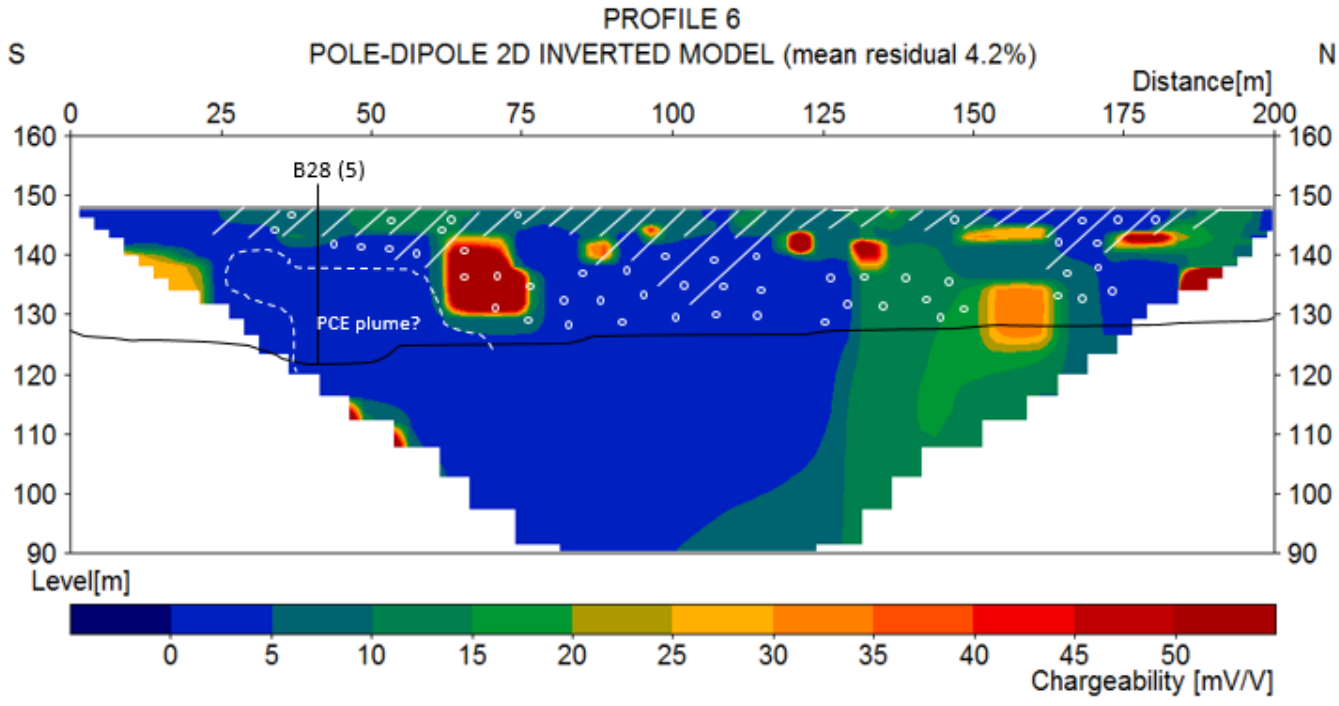

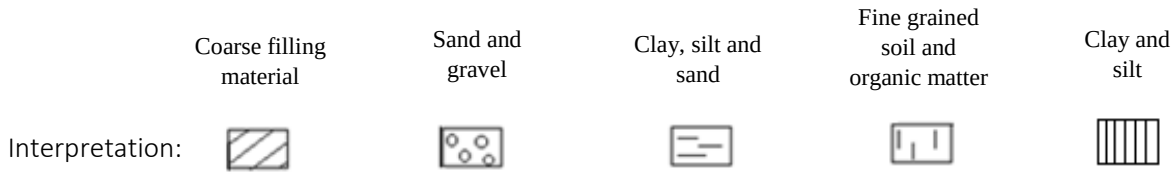

Resistivity and IP result for profile 6 (pole-dipole array). Interpolated bedrock surface shown as continuous black line and interpreted geology marked according to system underneath the profile. Position for geological and chemical reference data marked as vertical black lines with offset to profile (meters) within brackets.

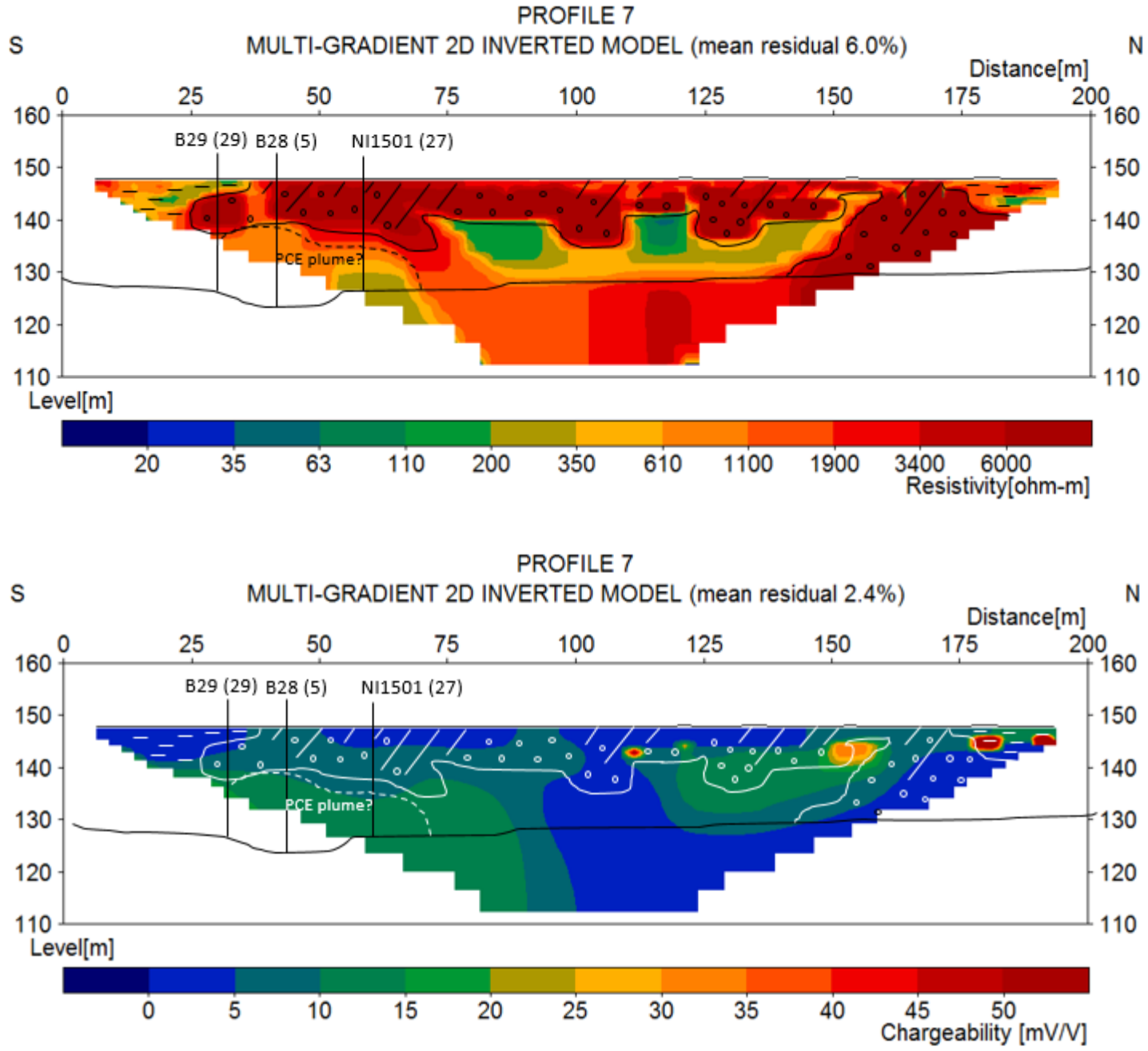

Resistivity and IP result for profile 7 (multi-gradient array). Interpolated bedrock surface shown as continuous black line and interpreted geology marked according to system underneath the profile. Position for geological and chemical reference data marked as vertical black lines with offset to profile (meters) within brackets.

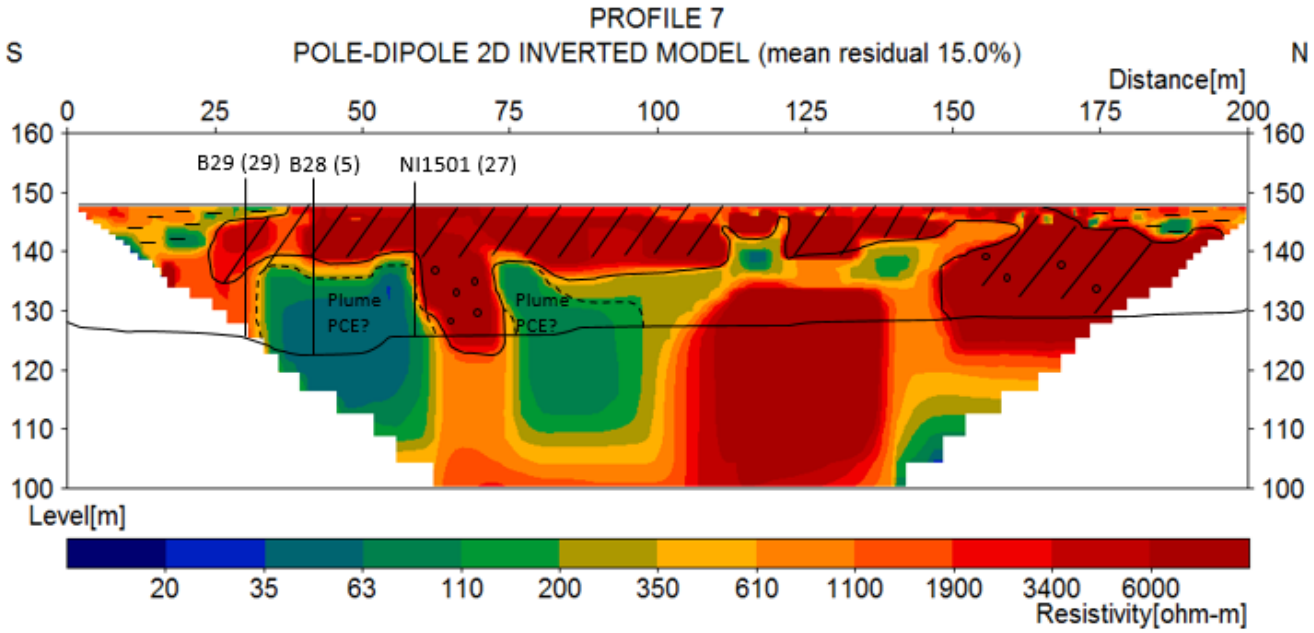

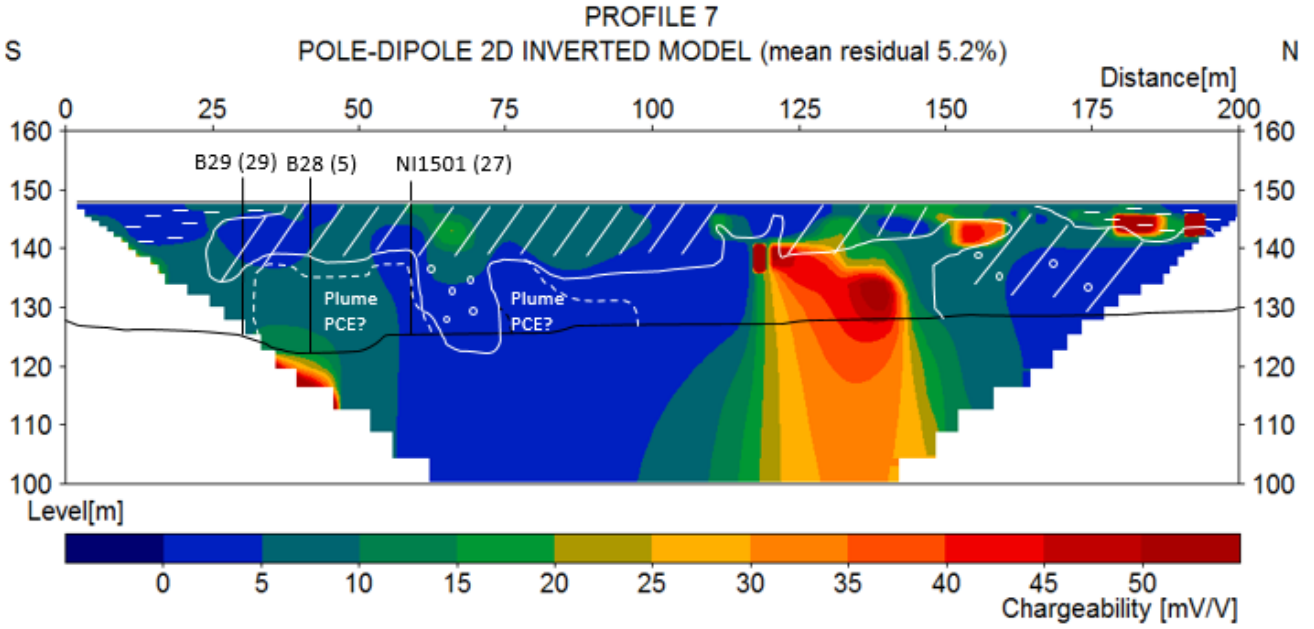

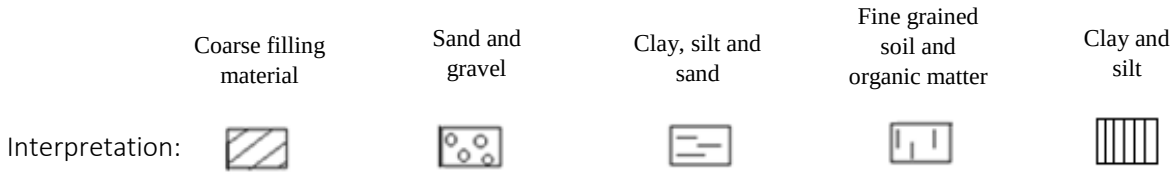

Resistivity and IP result for profile 7 (pole-dipole array). Interpolated bedrock surface shown as continuous black line and interpreted geology marked according to system underneath the profile. Position for geological and chemical reference data marked as vertical black lines with offset to profile (meters) within brackets.

Appendix G – Geological and chemical reference data

Geological and chemical reference data in the proximity to each profile (< 10 m offset). Based on previous drillings and samplings at the contaminated site (Nilsson, 2017, unpublished data).

PROFILE 1

NI1607, NI1609, NI1611

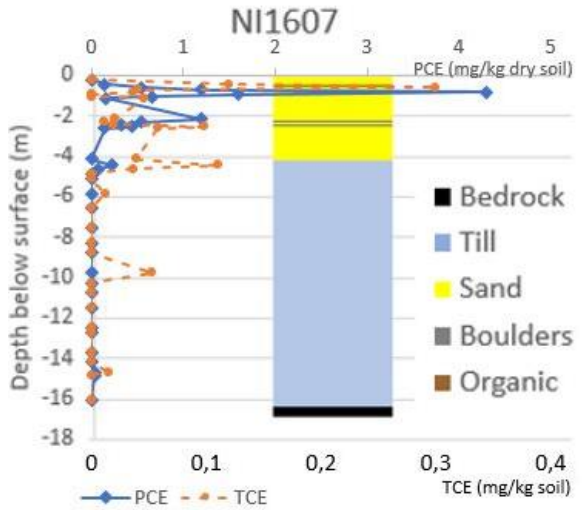

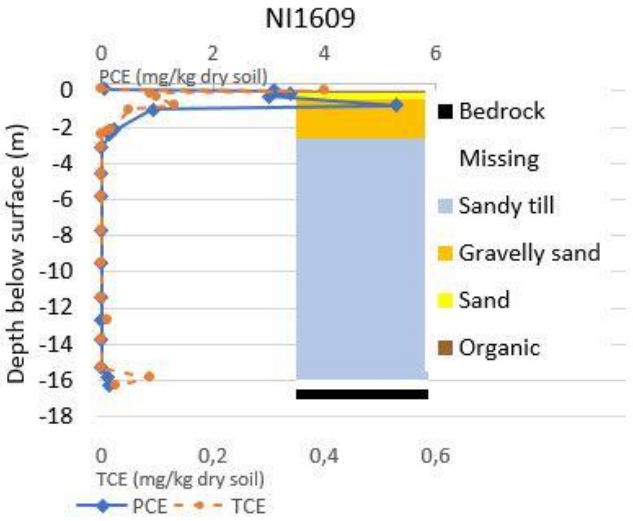

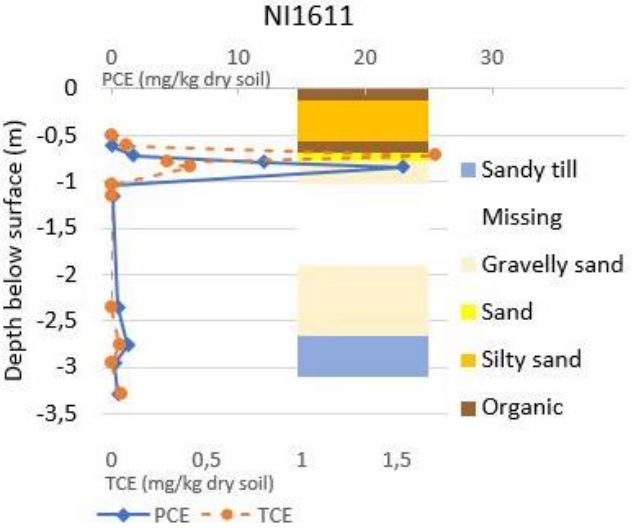

PROFILE 2

NI1602, Kb1, B38

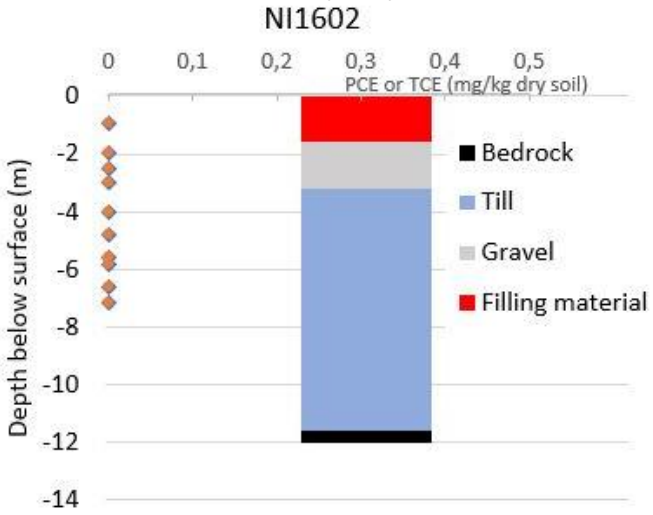

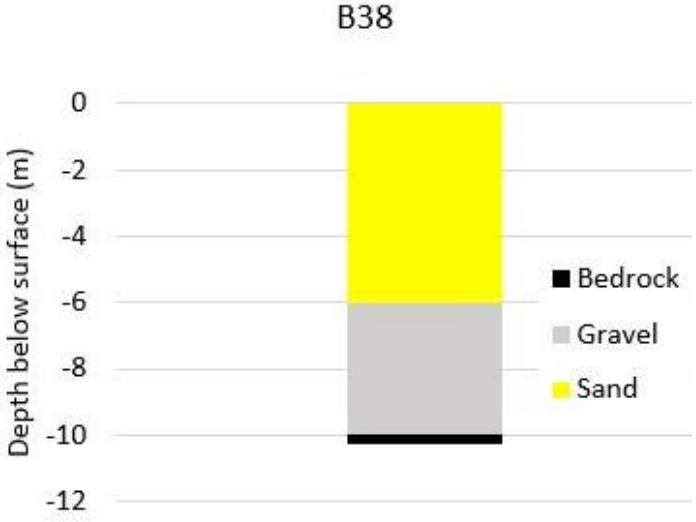

PROFILE 3

NI1413, B25

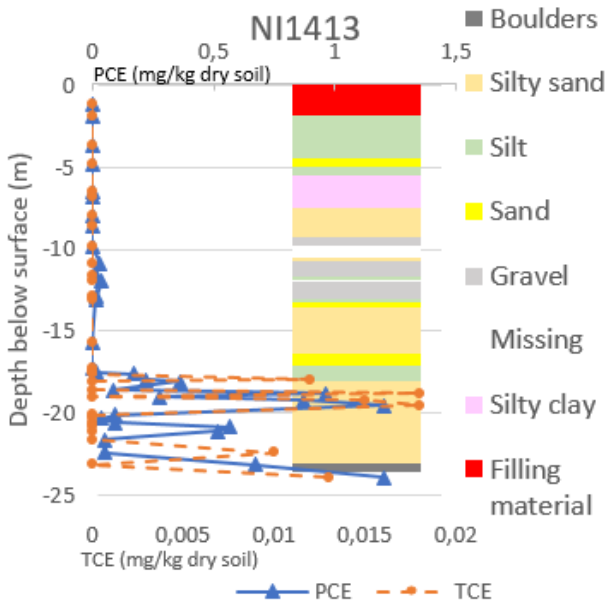

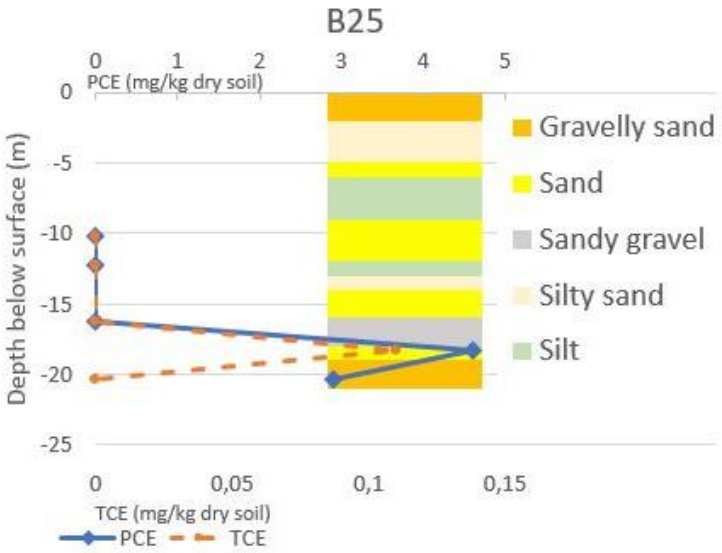

PROFILE 5

NI1415A, NI1415C, NI1414A

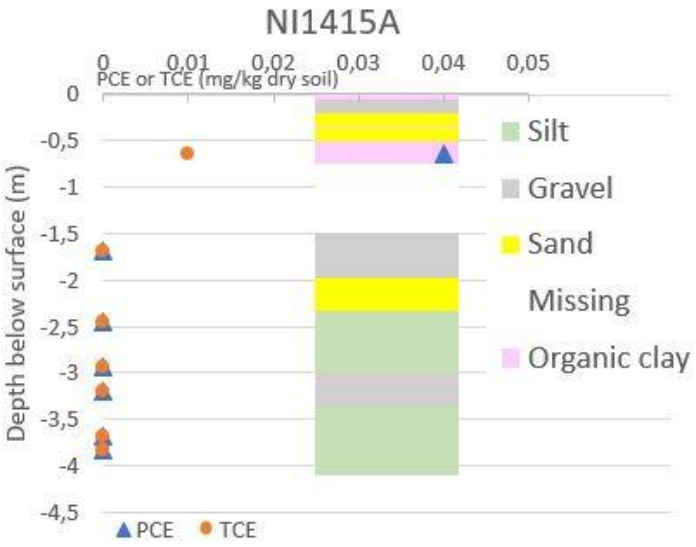

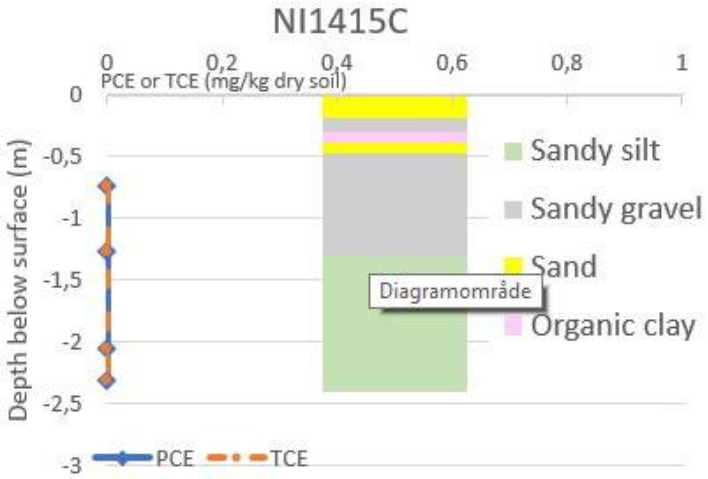

PROFILE 6 and 7

B28

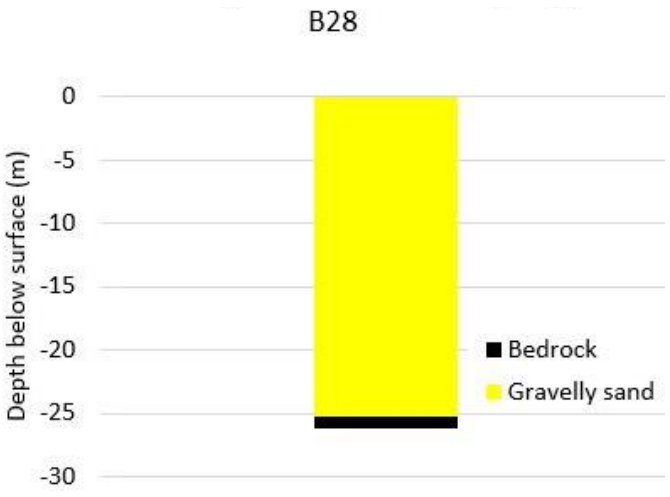

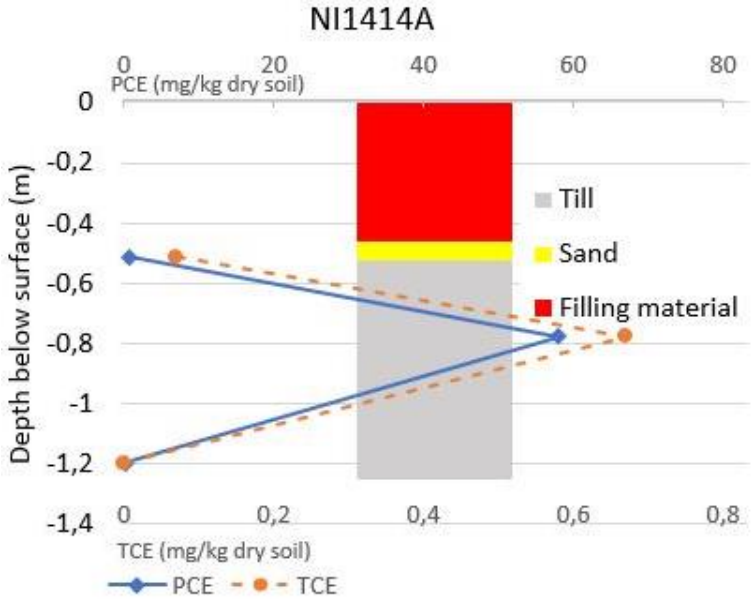

PROFILE 4

B16, B18, NI1412, NI1403, NI1605, B19

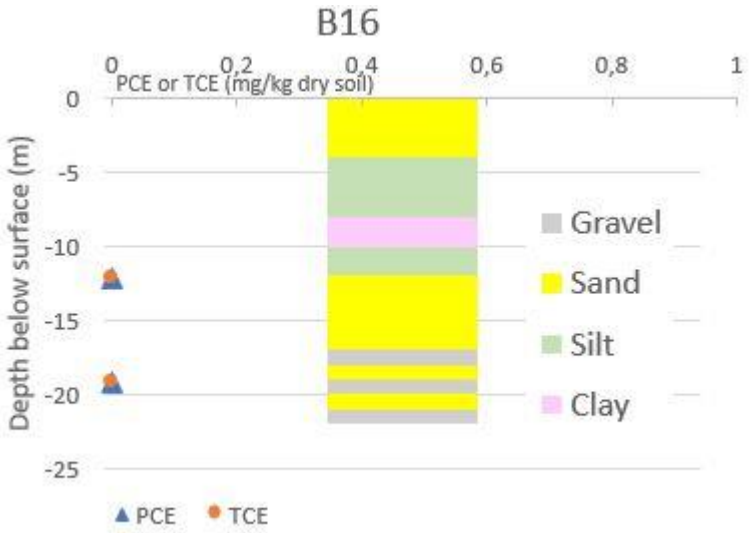

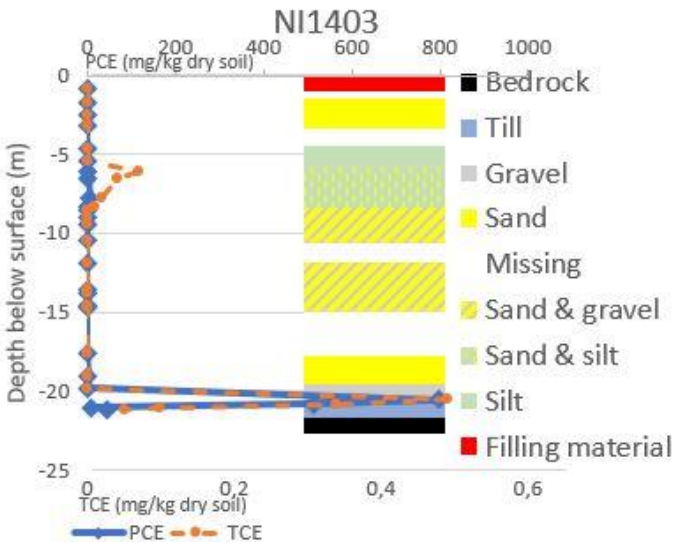

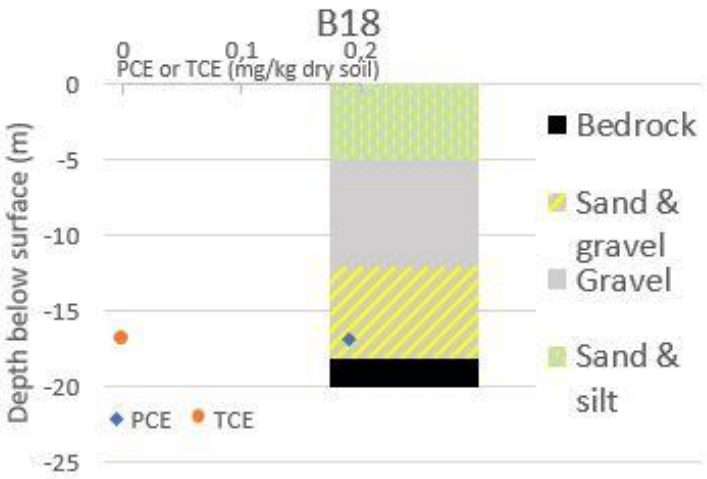

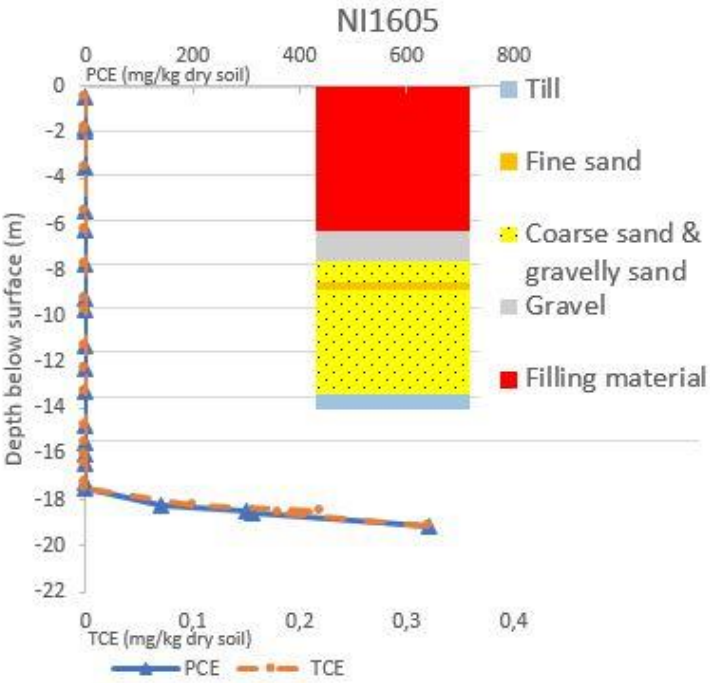

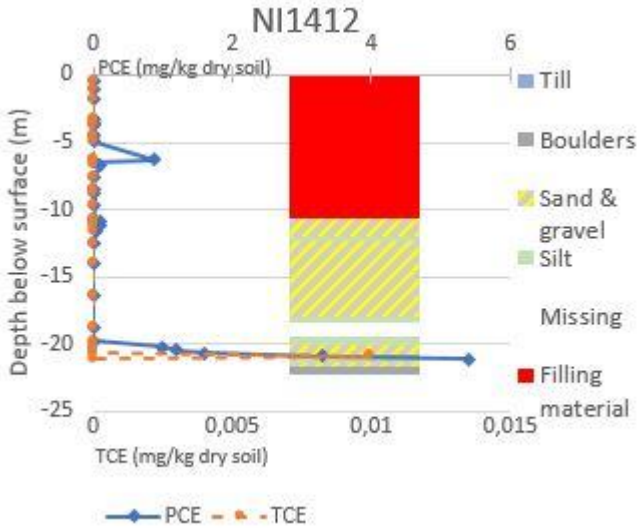

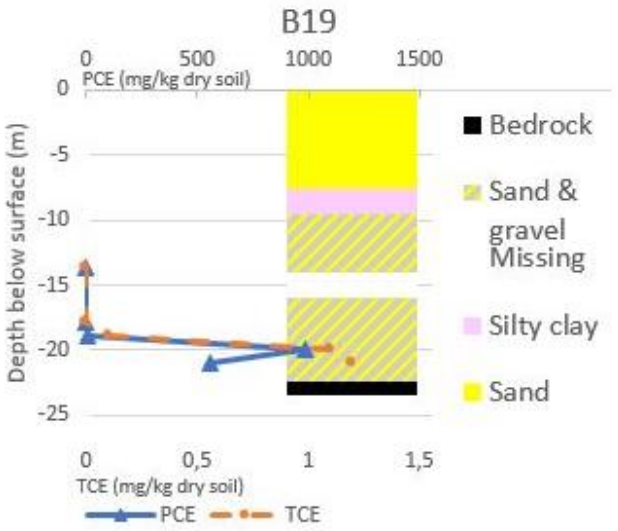

Appendix H – GPR-profiles

GPR-profiles showing a reflective surface about 6-7 meters below surface marked with red arrows. The profiles are running in south-north direction and positions of the sections are seen in figure 5.2a in chapter 5.1 *Background survey*. The top profile is coinciding with ERT-profile 6 (figure 5.3 in chapter 5.2 *ERT and IP survey*)

S N

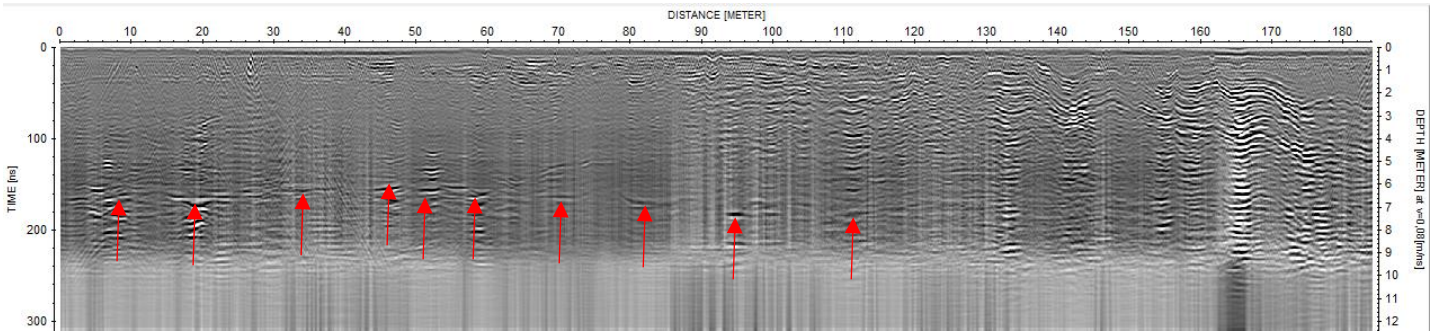

N S

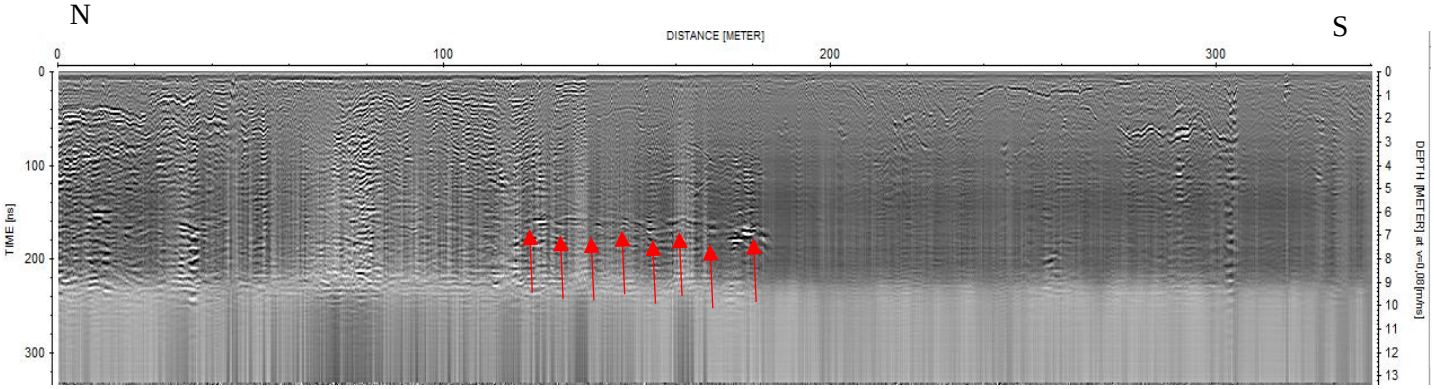

S N